Influence of Driving Patterns and Optimal Robust Powertrain Combined Design and Control on Plug-in Vehicle Cost, Life Cycle Emissions, Component Sizing, and Battery Stress

Submitted in partial fulfillment of the requirements for

the degree of

Doctor of Philosophy

in

Mechanical Engineering

Orkun Karabasoglu

M.S., Carnegie Mellon University, Pittsburgh, US
M.S., Sabanci University, Istanbul, Turkey
B.S., Bochum University of Applied Sciences, Bochum, Germany
B.S., Kocaeli University, Kocaeli, Turkey

Carnegie Mellon University
Pittsburgh, Pennsylvania

April 2013

ACKNOWLEDGEMENTS

I want to thank to Prof. Jeremy J. Michalek for giving me this unique opportunity to study at Carnegie Mellon University and to work with him on challenging research projects. Not only has he been an excellent advisor, but also a great role model. The way he works with students reflects on his excellent communication and leadership skills. I had the privilege to witness how he approaches to problems and comes up with creative solutions. I can honestly say that I have learned a lot working with him and I am in his debt for helping me with my academic and personal endeavors. This dissertation could not be completed without the support and advice from my committee members, Prof. Chris Atkeson, Prof. Jonathan Cagan and Prof. Illah Nourbakhsh. Taking Prof. Atkeson's course on Dynamic Optimization clearly shaped the way I think about algorithms and taught me how to use them in engineering. It especially helped me formulate my own research problem. Also his unique and fun style of linking all these concepts to everyday life made me enjoy the subject even more. Prof. Cagan played an important role in helping me quantify the uncertainty in my results. His encouragement to run many sensitivity scenarios and evaluate results accordingly improved the quality of my work considerably. Prof. Nourbakhsh`s supercapacitor work at ChargeCar is the inspiration behind the fourth chapter. His public contest to develop the best control strategy paved the way for me to work on supercapacitor-battery control. His insight and suggestions are greatly appreciated. I thank all of my committee members for their valuable feedback and friendly support. They have greatly influenced the way I think and approach to problems.

I want to thank the faculty and students in the Design Decisions Laboratory, xEV Group, and ChargeCar Group. Special thanks to Burak Yuksel, Guo Li, Paul Kimball and Lu Pan for

their help with the work presented in this thesis and papers, and making my graduate life more collaborative, enjoyable and fun; Dr. Elizabeth Traut for her valuable critique and NHTS data; Prof. Bill Messner, Dr. Dan Opila, Dr. Norman Shiau, Nikhil Kaushal, Osman Khajawa, Alex Styler, Andrew Finlayson, Rebecca Stabile, Paul Yoon, Julian Ramos, Apurba Sakti, Tugce Yuksel, Grace Heckman, John Helveston, Aida Khajavirad, Varun Krishnakumar, Camilo Resende, Allison Weis for their valuable feedback and discussions. I enjoyed learning from each other very much.

I would like to thank to my MS advisor, Prof. Gullu Kiziltas, and my other professors and mentors at Sabanci University and Kocaeli University for supporting and believing in me. I also owe thanks to my family for their never ending support: my father Zafer Karabasoglu, my mother Fatma Karabasoglu, and my sister Ebru Karabasoglu. I also thank to anyone else that I might have forgotten to mention here.

This research was supported in part by the National Science Foundation CAREER Award, and grants from Ford Motor Company and Toyota Motor Corporation. The support from these programs is highly appreciated.

ABSTRACT

Influence of Driving Patterns and Optimal Robust Powertrain Combined Design and Control on Plug-in Vehicle Cost, Life Cycle Emissions, Component Sizing, and Battery Stress

by

Orkun Karabasoglu

Chair: Jeremy J. Michalek

Plug-in Hybrid Electric Vehicle (PHEV) powertrain design and control is a challenging task for a few reasons: (1) their efficient powertrain architectures with multiple energy sources and regenerative braking capabilities introduce multiple degrees of freedom for design and energy management (control) decisions, which are coupled. Vehicle design includes multiple coupled decisions in itself, such as battery, motor, and engine sizing, while controllers are developed to achieve efficiency. Design and control is usually done sequentially which lead to suboptimal results. (2) Powertrain components are sized to follow driving patterns which dictates the road demand however they vary significantly from driver and driver, day to day and trip to trip. Still the vehicle should be designed robustly for the market. (3) Each design and control decision introduces a cost component which is a nonlinear function of the vehicle life so all design and control decisions should be evaluated from life cycle perspective (For example, energy storage systems are expensive but allows for the use of potentially cheap electricity).

The first goal of this thesis is to determine the impact of driving patterns on the life cycle benefits of plug-in hybrid electric vehicles. For this purpose, I design different powertrains similar to the ones in the vehicle market and simulate them under different driving patterns. Then

I build a quantitative framework to model life cycle cost and emissions of vehicles. Using the proposed framework, I compare conventional, hybrid, plug-in hybrid vehicles with different battery sizes, and battery electric vehicles under various scenarios. This goal aims to answer the questions: *How much do driving patterns affect the life cycle benefits of PHEVs? Which powertrain does perform better under which driving pattern? How much does the vehicles all-electric range change due to driving patterns?* Results indicate that under the urban NYC driving cycle, hybrid and plug-in vehicles can cut life cycle emissions by 60% and reduce costs up to 20% relative to conventional vehicles (CVs). In contrast, under highway test conditions (HWFET) electrified vehicles offer only marginal emissions reductions at higher costs. NYC conditions with frequent stops triple life cycle emissions and increase costs of conventional vehicles by 30%, while aggressive driving (US06) reduces the all-electric range of plug-in vehicles by up to 45% compared to milder test cycles like HWFET. Hybrid vehicles are more robust to the variation in driving patterns. I discuss policy implications.

The second goal of this thesis is to create a holistic framework for the optimal design and control of energy systems, accounting for the interactions between design and control, and making each design and control decision to achieve the maximum benefits for the entire life cycle of the system. Having determined the impact of driving patterns for PHEVs from the first goal, the aforementioned framework is applied to the co-design of PHEV powertrains for the minimum life cycle cost for a real world driving cycle. Firstly, a quasi-static backward looking parallel PHEV model is developed with its dynamic model counterpart for the performance computing which is the acceleration time from 0-60 mph. We account for design and control interactions by performing a parametric study over the vehicle design space, optimizing the controller for each design. The vehicle design space - consisting of engine, motor and battery

size variables - is discretized and searched exhaustively using an iteratively refined grid resolution to minimize lifetime cost. Ultimately, the system is optimized to determine the optimal vehicle designs that minimize life cycle cost. Intelligent system level control of the powertrain has the potential to downsize the expensive powertrain components such as battery, motor and engine. This goal aims to answer the questions: *How to account for the design and control interactions during vehicle powertrain design? What is the life cycle cost-minimizing PHEV parallel powertrain design? How important is system level control? What are the implications of intelligent control on powertrain design and cost?* Results indicate that using optimal control with perfect information (dynamic programming) provides a 5% smaller battery pack than using a simultaneously optimized rule-based controller for a particular 22-mile real-world driving cycle, creating an upper bound for the potential benefits of predictive controllers.

The third goal of this thesis is to study the effects of intelligent system level combined with supercapacitors to reduce battery stress and extend battery life thus reducing lifetime cost. For this purpose I integrate energy-dense batteries with power-dense supercapacitors in battery electric vehicles(BEVs) to reduce battery stress and increase battery life for the variation of real world driving patterns and elevation profiles I have discussed in the first research question. We globally optimize the energy management strategy of supercapacitor-battery systems in EVs for real world driving conditions. We minimize battery current squared as a degradation factor as peak-leveling and Joule heating accelerate battery degradation in EVs. This goal aims to answer the questions: *Can I reduce battery stress to extend its life with supercapacitors and smart control for real world driving conditions? Can I reduce battery peak power requirement which might lead to smaller batteries.* Results indicate that by integrating a 50 Wh supercapacitor and

an optimal controller, we achieve over 60% reduction in battery current-squared losses using dynamic programming. Improved efficiency and reduced battery size can help to make plug-in vehicles more competitive, while reduced battery use can improve battery life, reducing life cycle cost and environmental issues associated with battery production.

This research develops a robust co-design framework for energy systems with applications on PHEV powertrains by integrating vehicle design, control and economics, identifies optimal vehicle powertrain designs under a distribution of driving patterns, examines the potential component downsizing due to intelligent system level control, compares different powertrain technologies over various driving patterns for life cycle cost and emissions, and models the integration of supercapacitors with batteries to extend battery life and reduce battery stress, battery size, and lifetime cost.

TABLE OF CONTENTS

LIST OF TABLES

LIST OF FIGURES

1 INTRODUCTION

Equipped with a motor, battery, and gasoline engine, plug-in hybrid electric vehicles (PHEVs) offer a viable solution to reduce gasoline consumption and potentially reduce emissions and ownership costs since they operate partly on inexpensive electricity that can be obtained from local, renewable, and less emissions-intensive energy sources than gasoline [1] [2] [3].

The fuel economy and emissions of vehicles depend on the way they are driven, including daily driving distance [4] and driving conditions. Official fuel economy ratings are based on standard test driving conditions – called a driving cycle -- but real-world driving patterns can vary substantially from standard test cycles [5][6], leading real-world costs and emissions to deviate from those estimated on window stickers or in life cycle studies. In the literature, vehicle life cycle assessment and design optimization studies are typically conducted using efficiency estimates from federal test cycles, resulting in optimistic results that favor certain powertrains over others. In Chapter 2, I investigate variation in life cycle cost and emission benefits of hybrid and plug-in vehicles under a range of driving conditions with a sensitivity analysis to critical factors such as gasoline prices, vehicle costs and electricity grid mix. Specifically, I compare conventional vehicle (CV), hybrid electric vehicle (HEV), PHEV, and BEV powertrain technologies and identify changes in all-electric range (AER), vehicle efficiency, and battery life, under a variety of driving patterns to determine the most cost effective and lowest GHG-intensive powertrains. Then I discuss the energy policy implications of our findings considering multiple scenarios related to market, vehicle technology, and electricity grid mixture.

Efficient powertrain architectures of PHEVs with multiple energy sources and regenerative braking capabilities introduce multiple degrees of freedom for design and energy management (control) decisions. Vehicle design includes multiple coupled decisions, such as battery, motor, and engine sizing, while controllers are developed to achieve efficiency. Vehicle system level control is responsible for the control of energy flow of components and depends on component capabilities, such as battery capacity and engine and motor efficiency maps and torque capabilities. Yet vehicle performance criteria, such as fuel economy, all electric range, and acceleration depend on the controller [7]. Thus the design and control problems are coupled, and treating them separately can produce suboptimal results [8]. Furthermore, life cycle benefits of PHEVs depend on the driving conditions, including driving style [3] and distance [2] Real world driving conditions vary among drivers and over time, so vehicles optimized for a single test cycle or average driving distance can perform poorly over a range of real driving conditions [9] [10].

The distance that PHEVs can travel using only electricity depends on the size of the battery pack. Large battery packs can extend electric range and lower fuel consumption; however, they are associated with high investment costs, additional production emissions, and extra vehicle mass, which can decrease efficiency [2] [11]. Better energy management and control can improve efficiency and range by determining the best time to draw power from the electrical system vs. the gasoline engine, thus reducing battery requirements and lowering costs. This creates a chance to reduce size of batteries via better control. In Chapter 3, I develop a robust co-design framework and find the impact of intelligent control on downsizing the batteries.

Battery of the electric powertrain is usually sized for energy and the distance needs to be covered with single charge under certain driving conditions and battery cell design is selected to

provide adequate power. During acceleration and deceleration (regenerative braking), current peaks heats up the battery cells which accelerates the battery degradation In Chapter 4, I integrate high power dense supercapacitors with energy dense batteries to reduce the battery stress, increase efficiency, and extend battery life.

Each chapter cites relevant work and references can be found at the end of each chapter.

1.1 Chapter References:

[1] C. Samaras and K. Meisterling, “Life cycle assessment of greenhouse gas emissions from plug-in hybrid vehicles: implications for policy.,” *Environmental science technology*, vol. 42, no. 9, pp. 3170–3176, 2008.

[2] C.-S. N. Shiau, C. Samaras, R. Hauffe, and J. J. Michalek, “Impact of battery weight and charging patterns on the economic and environmental benefits of plug-in hybrid vehicles,” *Energy Policy*, vol. 37, no. 7, pp. 2653–2663, 2009.

[3] O. Karabasoglu and J. Michalek, “Influence of driving patterns on life cycle benefits of hybrid and plug-in electric vehicles,” *in press , Energy Policy*, 2013.

[4] C. N. Shiau, S. B. Peterson, and J. J. Michalek, “Optimal Plug-In Hybrid Vehicle Design and Allocation for Minimum Life Cycle Cost, Petroleum Consumption and Greenhouse Gas,” in *ASME 2010 International Design Engineering Technical Conferences Computers and Information in Engineering Conference IDETCCIE 2010*, 2010, pp. 1–13.

[5] R. Patil, B. Adornato, and Z. Filipi, “Impact of Naturalistic Driving Patterns on PHEV Performance and System Design,” *Society of Automotive Engineers Technical Paper*, pp. 01–2715, 2011.

[6] I. M. Berry, “The Effects of Driving Style and Vehicle Performance on the Real-World Fuel Consumption of U.S. Light-Duty Vehicles,” MS Thesis, Massachusetts Institute of Technology, 2010.

[7] P. Tulpule, V. Marano, and G. Rizzoni, “Effects of Different PHEV Control Strategies on Vehicle Performance,” *Control*, pp. 3950–3955, 2009.

[8] L. Fang and S. Qin, “Concurrent Optimization for Parameters of Powertrain and Control System of Hybrid Electric Vehicle Based on Multi-Objective Genetic Algorithms,” *2006 SICEICASE International Joint Conference*, pp. 2424–2429, 2006.

[9] J. W. Whitefoot, K. Ahn, and P. Y. Papalambros, “The Case for Urban Vehicles: Powertrain Optimization of a Power-Split Hybrid for Fuel Economy on Multiple Drive Cycles,” in *Volume 4: 12th International Conference on Advanced Vehicle and Tire Technologies; 4th International Conference on Micro- and Nanosystems*, 2010, vol. 2010, no. 44120, pp. 197–204.

[10] C.-S. Norman Shiau and J. J. Michalek, “Global Optimization of Plug-In Hybrid Vehicle Design and Allocation to Minimize Life Cycle Greenhouse Gas Emissions,” *Journal of Mechanical Design*, vol. 133, no. 8, p. 084502, 2011.

[11] J. J. Michalek, M. Chester, P. Jaramillo, C. Samaras, C.-S. N. Shiau, and L. B. Lave, “Valuation of plug-in vehicle life-cycle air emissions and oil displacement benefits.,” *Proceedings of the National Academy of Sciences of the United States of America*, vol. 108, no. 40, pp. 16554–8, 2011.

2 INFLUENCE OF DRIVING PATTERNS ON LIFETIME COST AND LIFE CYCLE BENEFITS OF HYBRID AND PLUG-IN ELECTRIC VEHICLE POWERTRAINS

This chapter focuses on the comparison of the potential of hybrid, extended-range plug-in hybrid, and battery electric vehicles to reduce lifetime cost and life cycle greenhouse gas emissions under various scenarios and simulated driving conditions. We find that driving conditions affect economic and environmental benefits of electrified vehicles substantially: Under the urban NYC driving cycle, hybrid and plug-in vehicles can cut life cycle emissions by 60% and reduce costs up to 20% relative to conventional vehicles (CVs). In contrast, under highway test conditions (HWFET) electrified vehicles offer lower emissions reductions at higher costs. NYC conditions with frequent stops triple life cycle emissions and increase costs of conventional vehicles by 30%, while aggressive driving (US06) reduces the all-electric range of plug-in vehicles by up to 45% compared to milder test cycles (like HWFET). Vehicle window stickers, fuel economy standards, and life cycle studies using average lab-test vehicle efficiency estimates are therefore incomplete: (1) driver heterogeneity matters, and efforts to encourage adoption of hybrid and plug-in vehicles will have greater impact if targeted to urban drivers vs. highway drivers; and (2) electrified vehicles perform better on some drive cycles than others, so non-representative tests can bias consumer perception and regulation of alternative technologies. We discuss policy implications. Prof. Jeremy Michalek contributed to this work. A version of the work discussed in this chapter has been accepted by Energy Policy Journal and it is currently in press **[*]**. NHTS data is provided by Elizabeth Traut.

[*] O. Karabasoglu and J. Michalek, “Influence of driving patterns on lifetime cost and life cycle benefits of hybrid and plug-in electric vehicle powertrains,” In Press, Energy Policy, 2013.

2.1 Introduction

The Obama Administration`s New Energy for America agenda set a target of achieving 1 million plug-in vehicles on U.S. roads by 2015 [1]. Plug-in vehicles, including plug-in hybrid electric vehicles (PHEVs) and battery electric vehicles (BEVs), may play a key role in cutting national gasoline consumption, addressing global warming, and reducing dependency on foreign oil in the transportation sector. Plug-in vehicles operate partly or entirely on inexpensive electricity that can be potentially obtained from local, renewable, and less carbon-intensive energy sources than gasoline [2,3]. Based on the 2009 National Household Travel Survey (NHTS) [4], approximately 60% of U.S. passenger vehicles that drove on the day surveyed traveled less than 30 miles, a distance that could be powered entirely by electricity using plug-in vehicles. Thus, plug-in vehicles have the potential to offset a substantial amount of gasoline consumption even when charged only once per day.

The fuel economy and emissions of vehicles depend on the way they are driven, including daily driving distance [5, 46-50, 55] and driving conditions. Official fuel economy ratings are based on standard test driving conditions – called a driving cycle -- but real-world driving patterns can vary substantially from standard test cycles [6,7], leading real-world costs and emissions to deviate from those estimated on window stickers or in life cycle studies. In the literature, vehicle life cycle assessment and design optimization studies are typically conducted using efficiency estimates from federal test cycles, with results that favor certain powertrains over others. In this work, we investigate variation in life cycle cost and emission benefits of hybrid and plug-in vehicles under a range of driving conditions with a sensitivity analysis to critical factors such as gasoline prices, vehicle costs and electricity grid mix. Specifically, I

compare conventional vehicle (CV), hybrid electric vehicle (HEV), PHEV, and BEV powertrain technologies and identify changes in all-electric range (AER), vehicle efficiency, and battery life, under a variety of driving patterns to determine the most cost effective and lowest GHG-intensive powertrains. Then we discuss the energy policy implications of our findings considering multiple scenarios related to market, vehicle technology, and electricity grid mix.

2.1.1 Electrified Vehicle Powertrain Alternatives

Electrified powertrains include HEVs, which use a small battery to improve gasoline fuel efficiency but don't plug in; PHEVs, which use both gasoline and electricity; and BEVs, which use only electricity and not gasoline. All three powertrains share an advantage over conventional vehicles: each is capable of regenerative braking. When a conventional car brakes, the vehicle's kinetic energy dissipates mostly as heat. In contrast, an electrified vehicle with regenerative braking capability can capture and store some of this energy in its battery. In addition, HEVs and PHEVs are able to manage engine operating conditions to improve efficiency, turn off the engine at idle, and make use of higher efficiency, lower torque thermodynamic cycles.

Figure 2-1 demonstrates the relationship between the battery and the different operation modes of plug-in vehicles. For safety, reliability, and longevity reasons, electrified vehicle powertrains use only a certain portion of the full energy capacity of its battery, limited by the specified maximum and minimum battery state of charge (SOC) values. Operation of PHEVs can be categorized into two modes as seen in Figure 2-1: charge-depleting (CD) mode refers to the phase where the SOC is above the target SOC and the vehicle receives some or all of its net propulsion energy from the battery pack. Once the battery is depleted to a target SOC, the

vehicle switches to charge-sustaining (CS) mode, in which gasoline is used to provide all net propulsion energy and the electrical system is used only as momentary storage to improve fuel economy, similar to a grid-independent HEV. Some PHEVs operate CD-mode using only electrical energy. Such a configuration, referred to as an all-electric control strategy or an extended-range electric vehicle (EREV), enables short trips to be driven without any gasoline consumption but requires motor and battery designs that can deliver the vehicle's maximum power demands. Other PHEV designs operate CD-mode using a mixture of gasoline and electrical energy. Such a configuration, referred to as a blended control strategy, does not eliminate gasoline consumption even for short trips, but power demands on electrical components are lower, allowing smaller, cheaper components to be used. We focus on EREV PHEVs, since the performance of blended-operation PHEVs varies substantially with control strategy parameters [8-11]. Operation of a BEV is similar to that of a EREV PHEV in CD mode, and operation of an HEV is similar to that of a PHEV in CS mode.

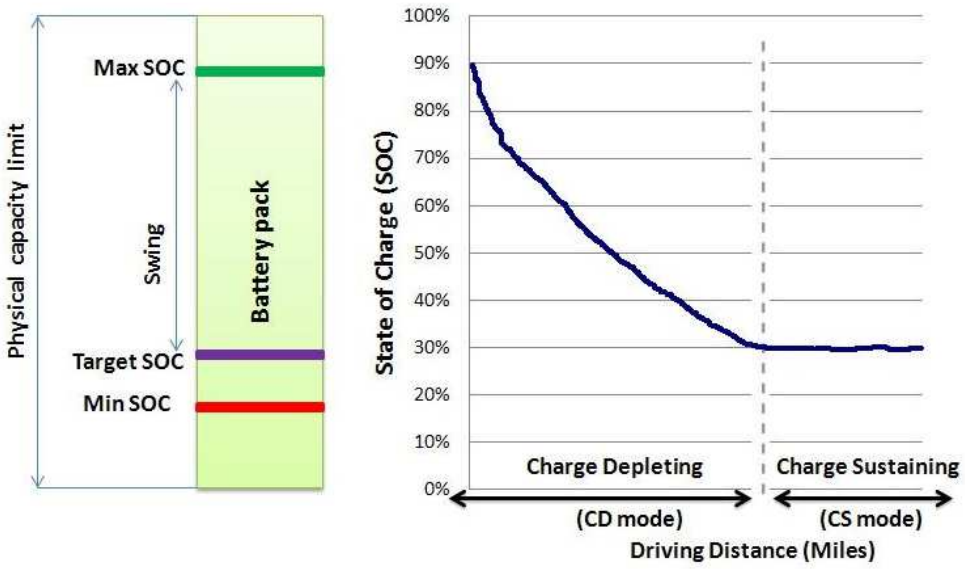

Figure 2-1 Operation modes of a PHEV (figure adapted from Shiau et al [5])

Hybridization can be based on 3 specific powertrain architectures: (1) series, where the engine turns the generator which generates electricity to be used by the electric motor to turn the wheels; (2) parallel, which is capable of transmitting power to the wheels from two different energy sources; and (3) split, which can operate both in series and parallel. For greatest flexibility, we adopt the split powertrain for HEV and PHEV designs, as shown in Figure 2-2, which is currently used in the Toyota Prius HEV and PHEV.

Current gasoline spark-ignition engine technology can typically provide 20% efficiency under urban driving with a maximum of 35% under the most optimal conditions [12]. These low efficiencies suffer even more under real world driving conditions, where closer to 10% of the chemical energy of each gallon of gasoline acts to turn the wheels. The rest of the energy is lost in the form of heat and sound. With the help of a planetary gear-based power-split device, hybridization allows the engine to operate near its most efficient torque and speed values while providing excess power to recharge the battery or drawing remaining power needs from the motor. In this way large amounts of fuel might be saved, depending on the drive cycle. The motor is supplied with the electric energy from the battery, which is partially recharged during regenerative braking in HEV, PHEV and BEV powertrains and can be charged from an electrical outlet for PHEVs and BEVs.

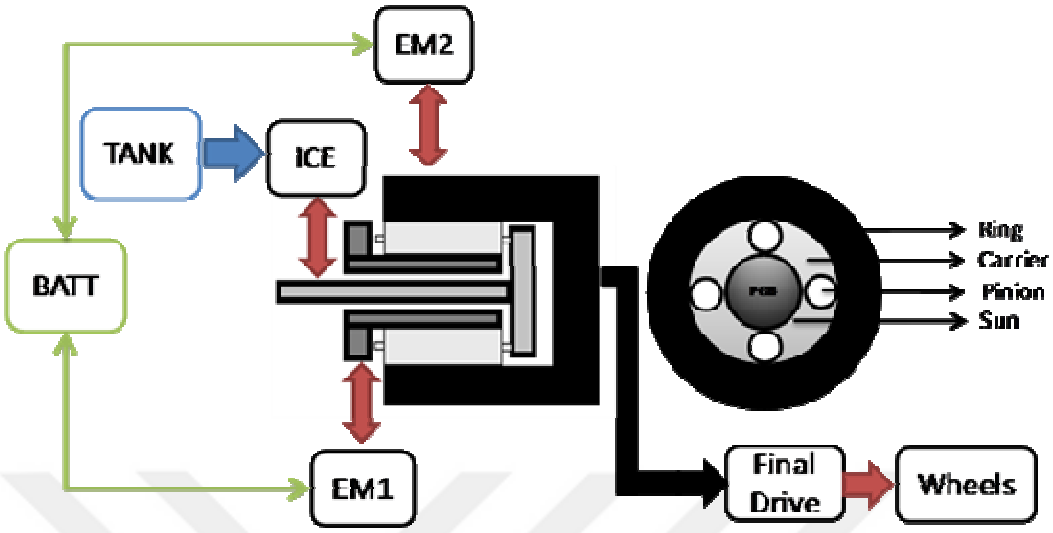

Figure 2-2 Schematic of a split hybrid powertrain

HEV and PHEV vehicle models in this study are based on the Toyota Prius model year 2004 power split configuration (Fig 2). This model has a planetary gear box (PGB), which splits road power demand between the internal combustion engine (ICE) and two electric motor / generators (EM1 and EM2). The EM2 is connected to the wheels over the ring gear, the outer gear of the PGB, and the final drive gear set. The ICE is directly connected to the carrier gear, while the EM1 is connected to the sun gear. The links between sun and ring is the pinion gear, which is set on the carrier gear. The chemical power source, the fuel tank, is attached to the ICE to create chemical and eventually mechanical power to propel the vehicle. The electrical power source, the battery pack, is connected to the electrical motor/generators to propel the vehicle or to be charged. All mechanical and electrical links are presented in Figure 2-2. with thick and thin arrows, respectively. The planetary gear provides an effective continuously variable transmission and allows the power-split PHEV to run both in series and parallel, taking advantage of both configurations. We have used this HEV model to build our PHEV models by increasing the size

of components (battery, engine, and traction motor) as necessary and adopting an EREV control strategy.

2.1.2 Vehicle Comparison Based on Fuel Economy and Emissions

Fuel economy labels (window stickers) tell customers how far a vehicle is likely to travel on a gallon of gasoline under certain conditions. These labels are required by law to give customers the information they need to make informed vehicle purchase decisions. In the past, customers have typically observed lower fuel economy in practice than ratings state because test procedures are more gentle than typical driving conditions. This is in part because some of the fuel economy test procedures were developed under limitations of test equipment capabilities. The EPA updated its fuel economy test procedures in 2006, switching from the prior 2-cycle test to a 5-cycle test to more accurately reflect today`s driving conditions. No single test can account for the different driving patterns of every driver. With new vehicle technologies such as hybrid powertrains now in the vehicle market, comparisons of the benefits of different vehicle technologies have become even more challenging. For example, the benefits of hybrid powertrains over conventional powertrains is more pronounced in aggressive driving and city driving with frequent stops, as we will show in our results.

The EPA working with the Department of Energy (DOE) has recently announced new fuel economy labels for a new generation of vehicles for 2013 and beyond [13]. These labels will inform consumers about the vehicle`s all-electric range (AER), fuel economy, estimated annual fuel cost, GHGs, smog rating, and how they compare to other vehicles. Fuel economy labels help guide consumer purchase decisions, aiming to provide a common ground to compare different

vehicles. Although these new labels provide more information than before, there is also a risk of confusing consumers with too much information. On the other hand, the comparison metrics listed do not account for different representative driving patterns, effects of terrain, weather, changes in fuel price, electricity grid mix, and powertrain degradation, which introduces new costs later during the life of the vehicle (e.g.: reduced fuel efficiency, battery replacement, etc.). These factors have become more important for comparing vehicles as hybrid and plug-in powertrains are introduced. In this work we analyze life cycle economic and environmental implications of conventional, hybrid, and plug-in vehicles under different driving patterns and daily driving distances, and we discuss the sensitivity of our findings to several parameters.

2.2 Literature Review

Prior work has identified driving cycle as a significant factor in vehicle fuel efficiency, and several studies have compared standard driving cycles to regional data collected on vehicle fleets using GPS data. Moawad et al. [14] used GPS data from Kansas drivers to compare the simulated fuel consumption of PHEVs and size vehicle components. They found that significant fuel economy improvements are achieved with HEVs compared to CVs; however these gains were lower than those usually estimated using standard drive cycles. Sharer et al. [15] compared CVs and HEVs under a range of driving cycles and found that HEVs are more sensitive to aggressive driving. Fontaras et al. [16] analyzed HEVs with European and real world driving cycles and found that under urban driving conditions, fuel consumption of HEVs are 40-60% lower than conventional vehicles. This benefit is even greater for low-average-speed driving with many stops, while at speeds over 95km/h HEV fuel consumption is similar to that of CVs. Tate et al. [17] used GPS driving data from southern California [18], which consists of 621 samples, to study PHEV performance. The associated power and speed values of the driving samples are

found to be higher than those associated with the UDDS driving cycle. The study also compares average energy consumption per unit distance to that of UDDS and HWFET drive cycles and finds that 94% of vehicles function at higher energy consumption under real-world driving conditions than they do under UDDS and HWFET cycles. A 2001 report [19] states that impact of aggressive driving in city conditions varies greatly depending on the type of vehicle: Powerful vehicles are robust, but low power vehicles show 6% reduction in efficiency compared to standard drive cycles. However in highway conditions, characterized by high speeds, impact of aggressive driving was much higher: 33% penalty for the average car, and 28% for the powerful car. Berry and Heywood [7] analyzed the effect of driving patterns on the fuel economy of CVs and found that the sensitivity of vehicle fuel economy to aggressive driving is a function of how wheel work and efficiency vary with driving patterns. Whitefoot et al. [20] optimized HEVs under different driving cycles for minimal fuel consumption, finding that vehicles designed for one driving cycle show significantly lower performance on other drive cycles. Patil et al. [21] optimized a series PHEV for naturalistic drive cycles and showed that the higher energy demands of real world cycles require larger batteries to meet AER targets. The required optimal battery size changed nonlinearly with desired AER. Fellah et al. [22] found that if batteries of PHEVs are sized for the UDDS cycle, only 22% of 363 trips from Kansas City can be driven in all electric mode due to power limitations.

Despite the fact that standard cycles are not representative of real driving patterns, some of them can span a wide range. Patil et al. [6] investigated the impact of real world driving cycles on PHEV component sizing using GPS data from southeastern Michigan. Simulations using the GPS driving data indicate that about 90% of the trips in the data are higher fuel-consuming per mile than the UDDS and HWFET standard cycles, while about 90% of the trips are lower fuel-

consuming per mile than the US06 cycle. Similarly after examining the Southern California regional travel data [18], Tate et al. [17] found that the vast majority of the energy demanded by the drive cycles of the dataset is bounded by the energy levels required by US06, a reasonable upper limit, and UDDS, a fair lower limit. Thus both studies agree that UDDS and US06 appear to provide reasonable bounds to characterize the effect of driving cycle variation over a population of drivers. The authors also emphasize the need for larger electrical components when real world driving is considered. All of these prior driving cycle studies focus on vehicle performance and efficiency but do not assess the full lifetime cost and life cycle implications of different powertrain technologies.

Life cycle assessment studies have shown that vehicle electrification has the potential to reduce GHGs; however, potential benefits depend on the source of electricity used to charge the vehicle. In 2009, the U.S. grid mix consisted of 45% coal, 23% natural gas, 20% nuclear, 7% hydroelectric, 4% other renewable, 1% petroleum, and 0.6% other [23]. Lipman and Delucchi provide a recent review of studies [24]. Weber et al. [25] show that determining regional grid mix is nontrivial, and dispatch studies such as Sioshansi and Denholm [26] highlight that the mix associated with marginal demand for electricity varies widely depending on charge timing. Samaras and Meisterling [27] find that under a high carbon-intensity electricity generation scenario life cycle GHGs of PHEVs are 9-18% higher than HEVs, while GHGs are 30-47% lower under a low-carbon scenario. The Electric Power Research Institute (EPRI) together with the National Resources Defense Council (NRDC) [28] analyzed the GHG impacts of PHEVs over the 2010 to 2050 timeframe for several scenarios including different levels of CO_2 intensity in the electricity sector and fleet penetration of PHEVs. Some of the assumptions include

projections of vehicle time-of-day charging, plant dispatch, plant retirement and construction, and public policy. Each of the EPRI scenarios showed significant GHG reductions, and PHEV adoption reduces petroleum consumption significantly. Argonne`s well-to-wheels report [30] states that PHEVs charging from the US average grid-mix produce 20% to 25% lower GHGs than CVs but 10% to 20% higher GHGs than gasoline HEVs. They suggest that to receive significant reductions in emissions, PHEVs and BEVs must recharge from a grid-mix which consists of largely non-fossil sources. According to their study, electric range decreases with real world driving. Michalek et al. [31] estimate the economic value of life cycle oil consumption and air emissions externalities from conventional, hybrid and plug-in vehicles, finding that HEVs and PHEVs with smaller battery packs provide the greatest benefits per dollar spent. Hawkins et. al. [51] provide a life cycle inventory of CVs and BEVs and find that BEVs decrease global warming potential by 10-24% under a European grid mix.

A few studies have examined the role of driving patterns on life cycle implications, primarily assessing the importance of variation in driving distance. Shiau et al. [29] constructed an optimization model to find the optimal allocation of CVs, HEVs, and PHEVs to drivers based on driving distance to minimize life cycle GHG emissions, finding that optimal allocation based on distance is a second order effect. Traut et. al. [46] extended Shiau's study to include BEVs and workplace charging infrastructure while accounting for day to day driving variability. They identify gasoline and battery prices needed for plug-in vehicles to enter the cost-minimizing solution. Neubauer et. al. [48, 55] investigated the sensitivity of PHEV and BEV to driving distance and charging patterns, accounting for factors such as battery degradation and the need for a backup vehicle for BEVs when taking long trips. They find that changing the drive pattern can increase the PHEV-to-CV cost ration by a factor of up to 1.6, and the cost of backup vehicles

for BEVs can be substantial. Kelly et al. [47] used NHTS data and examined the effects of charging location, time, rate, and battery size. Finally, Raykin et al. [49, 50] analyzed the effect of driving patterns on tank-to-wheel energy use of PHEVs, using an estimated relationship between driving distance and drive cycle based on a travel demand model and vehicle driving simulation. They find that PHEVs result in greater GHG reductions relative to CVs in city rather than highway conditions.

With the exception of Raykin et al. [49, 50], those studies that investigate variations in drive cycle focus on the effects on performance or efficiency without examining the larger system (e.g.: full life cycle), and those studies that investigate life cycle implications of electrified vehicles either ignore variation in driving conditions or confine scope to examining variation in driving distance and charge timing. Raykin et al. examine both drive cycle and distance in a study of the greater Toronto area, concluding that both matter in estimating life cycle implications. We build on this finding by examining a range of drive cycles and distribution of driving distances for the United States and estimating effects on life cycle emissions, gasoline consumption, lifetime ownership cost, battery degradation, and AER for CVs, HEVs, BEVs, and PHEVs of varying battery capacity.

2.3 Proposed Methodology

We use the Powertrain Systems Analysis Toolkit (PSAT) SP1 Version 6.2, developed by Argonne National Laboratory [32], to model conventional, hybrid, plug-in hybrid, and battery electric vehicles with identical body characteristics, comparable control strategies, and comparable performance characteristics, and we simulate each vehicle over a range of drive cycles to compare vehicle efficiency and life cycle implications (Fig 3). We account for battery degradation, different daily driving distances and different scenarios for costs, vehicle

technology and electricity grid. In this section we explain each model and their interactions in detail. First, we discuss the choice and characteristics of driving cycles and travel patterns. Then we describe engineering, battery degradation, cost, and environmental models.

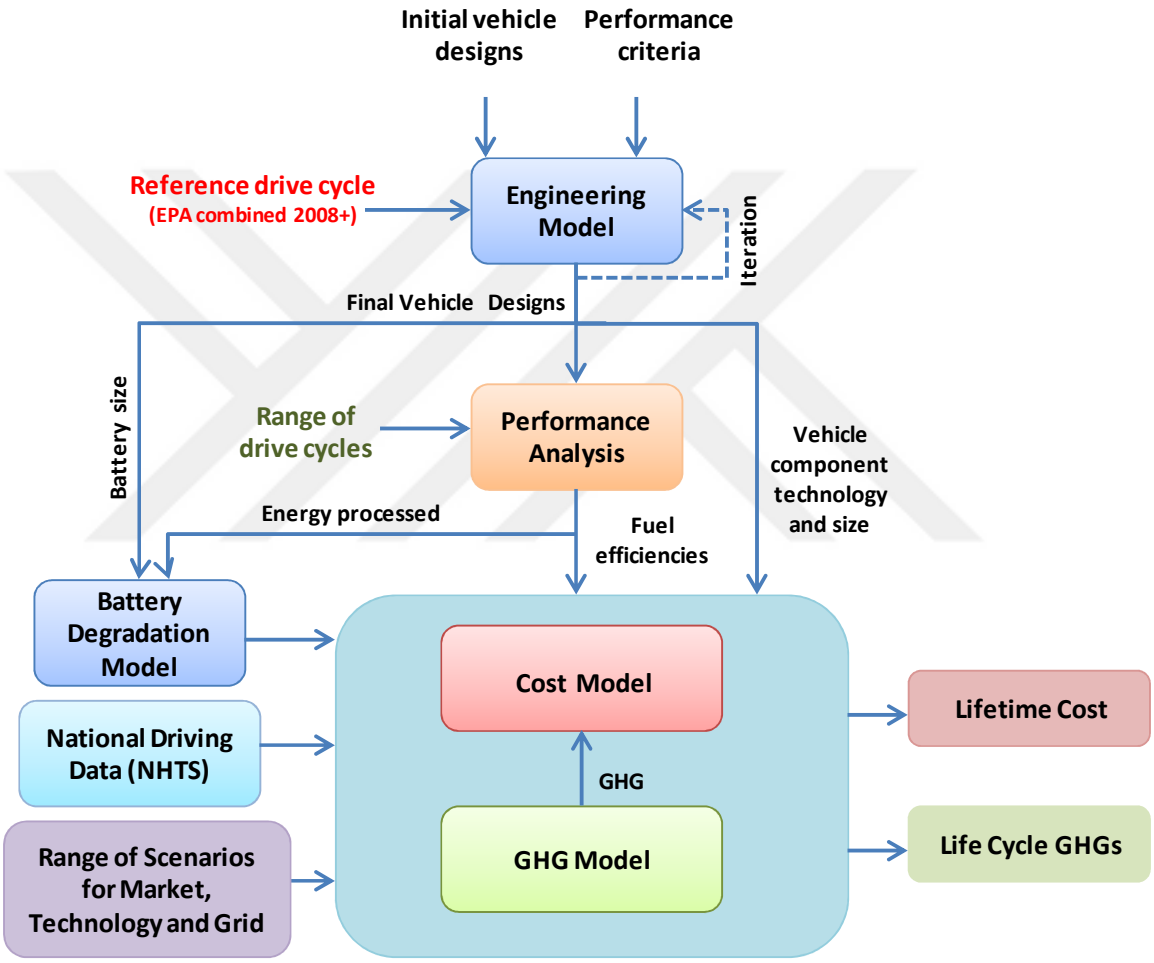

Figure 2-3 Framework of vehicle life cycle benefit comparison for different driving patterns

2.3.1 Driving Cycles

Efforts to assess and improve the fuel economy and emissions of vehicles are typically not conducted under real-world driving, since multiple noise factors such as various driving patterns, traffic conditions, weather, and terrain might affect the results. Instead, tests are done in a laboratory under controlled and repeatable conditions so that even small fuel economy improvements are not lost due to the noise in the environment. This enables designers, analysts and regulators to compare different vehicle designs to each other on a common basis. A chassis dynamometer is the device used to simulate driving in laboratory conditions: the wheels are placed on rollers that simulate the road load by matching the inertia of the car so that the propulsion system of the vehicle needs to work to rotate the wheels at a certain reference speeds. The speed reference used in this test is taken from a given drive cycle (test cycle) in the form of a series of target vehicle speed values over time. During the test a driver tries to match the vehicle`s speed to the reference speed at each moment in time using a visual feedback by a computer screen. An emission analyzer is connected to the exhaust pipe of the vehicle to track emissions and estimate fuel consumption. Different driving cycles used during this test result in different performance demands and thus different fuel consumption and emissions. The performance of some powertrain designs may be more sensitive to driving cycle than others. EPA has been using standard driving cycles (FTP and HWFET) to report the fuel consumption and emissions of vehicles. When these test cycles were designed, chassis dynamometer technology was not capable of simulating high acceleration and deceleration [33], and the test cycles were constrained to conditions less aggressive than observed in practice. Also because traffic patterns have changed since the 1960s and 1970s, when the FTP and HWFET drive cycles were created, they may fail to represent typical driving conditions today. In 2006, EPA announced a new

method to measure fuel economy based on a five-cycle testing method in an effort to better reflect real world performance. According to this method, vehicles are tested on aggressive (US06), air conditioning on (SC03) and cold weather (Cold FTP) drive cycles in addition to city (FTP) and highway (HWFET). Characteristics of these drive cycles are given in Table 2-1 [7]. Weighted combinations of these test results are used to calculate the city and the highway fuel economy values [34]. Alternatively, automakers could use unadjusted FTP and HWFET test results in some regression equations to approximate the 5-cycle city and highway fuel economies, with some restrictions during 2008-2010 period. [34]:

$$\text{Five-cycle city fuel economy} = \frac{1}{0.003259 + \frac{1.1805}{\text{FTP fuel economy}}} \tag{2-1}$$

$$\text{Five-cycle highway fuel economy} = \frac{1}{0.001376 + \frac{1.3466}{\text{HWFET fuel economy}}} \tag{2-2}$$

$$\text{EPA combined MPG[2008+]} = \frac{1}{\frac{0.43}{\text{5-cycle city MPG}} + \frac{0.57}{\text{5-cycle highway MPG}}} \tag{2-3}$$

For MY2011 and beyond, the 5-cycle fuel economy method is required to be used; however, if the five-cycle city and highway fuel economy results of a test vehicle group are within 4% and 5% of the regression line, respectively, then the automaker is permitted to continue using the regression estimates. These regression equations may be optimistic or pessimistic estimates of measured 5-cycle fuel economy, depending on vehicle and powertrain design. The equations

were developed for gasoline vehicles; however, we also apply them to estimate reductions in electrical efficiency of plug-in vehicles for the 5-cycle fuel economy estimates.

DRIVE CYCLE	FTP	HWET	US06	SC03	C-FTP
Description	Urban/City	Free-Flow Traffic on Highway	Aggressive Driving on Highway	AC on, Hot Ambient Temp.	City, Cold Ambient Temp.
Regulatory Use (2010)	CAFE & Label	CAFE & Label	Label	Label	Label
Data Collection Method	Instrumented Vehicles / Specific Route	Chase-Car / Naturalistic Driving	Instrumented Vehicles / Naturalistic	Instrumented Vehicles / Naturalistic	Instrumented Vehicles / Specific Route
Year of Data Collection	1969	Early 1970s	1992	1992	1969
Top Speed	90 kph (56 mph)	97 kph (60 mph)	129 kph (80 mph)	88 kph (54 mph)	90 kph (56 mph)
Avg. Velocity	32 kph (20 mph)	77 kph (48 mph)	77 kph (48 mph)	35 kph (22 mph)	32 kph (20 mph)
Max. Accel.	1.48 m/s^2	1.43 m/s^2	3.78 m/s^2	2.28 m/s^2	1.48 m/s^2
Distance	17 miles (11 km)	16 miles (10 km)	13 miles (8 km)	5.8 miles (3.6 km)	18 miles (11 km)
Time (min)	31 min	12.5 min	10 min	9.9 min	31 min
Stops	23	None	4	5	23
Idling Time	18 %	None	7 %	19 %	18 %
Engine Start	Cold	Warm	Warm	Warm	Cold
Lab. Temp.	68-86 °F	68-86 °F	68-86 °F	95 °F	20 °F
Air Conditioning	Off	Off	Off	On	Off

Table 2-1 Characteristics of U.S. certification drive cycles [7]

While the new standards offer an improvement in estimating real-world fuel economy, test estimates can still differ from real-world driving, favoring certain vehicle designs and powertrains over others and representing some driver habits and driving conditions better than others. We can understand the effects of different driving styles by considering approximate upper and lower bounds on those styles. To evaluate how the relative benefits of different vehicle technologies change with respect to driving cycles, we examine five different driving cycles plus the EPA combined estimate: (1) the Urban Dynamometer Driving Schedule (UDDS) represents city driving conditions for light duty vehicles which are characterized by relatively slow speed. UDDS is also called LA4, FTP72 and FUDS and is related to the FTP cycle; (2) the Highway

Fuel Economy Test (HWFET) which represents highway driving conditions under 60 mph; (3) the US06 cycle is an aggressive driving cycle with high acceleration and high engine loads; (4) the NYC cycle represents low speed urban driving with frequent stops; (5) the LA92 cycle is an aggressive driving cycle in city conditions; and (6) the combined MPG computed by the EPA by weighting city and highway efficiency. We use regression equations Eq(1-3) to adjust fuel and electrical efficiency values of FTP, HWFET, and combined fuel economy. Table 2-1 and

Statistics	Units	UDDS	HWFET	US06	NYC	LA92
Distance	mi	7.45	10.27	8.01	1.17	9.82
Max. speed	mi/h	56.70	59.90	80.29	27.53	67.20
Avg. speed	mi/h	19.58	48.28	47.96	7.05	24.61
Avg. acceleration	m/s^2	0.50	0.19	0.67	0.62	0.67
Avg. deceleration	m/s^2	-0.58	-0.22	-0.73	-0.60	-0.75
Time stopped (%)	%	18.92	0.65	7.5	35.12	16.31
Stop freq. (#/mi)	1/mi	2.28	0.10	0.62	15.38	1.63

Table 2-2 summarize the characteristics of these driving cycles for comparison, and Figure 2-4 shows the statistics normalized to unadjusted UDDS, which is adopted by several life cycle and optimization studies in the literature. We will summarize the adjusted and unadjusted efficiencies of vehicles in Table 5.

Statistics	Units	UDDS	HWFET	US06	NYC	LA92
Distance	mi	7.45	10.27	8.01	1.17	9.82
Max. speed	mi/h	56.70	59.90	80.29	27.53	67.20
Avg. speed	mi/h	19.58	48.28	47.96	7.05	24.61
Avg. acceleration	m/s^2	0.50	0.19	0.67	0.62	0.67
Avg. deceleration	m/s^2	-0.58	-0.22	-0.73	-0.60	-0.75
Time stopped (%)	%	18.92	0.65	7.5	35.12	16.31
Stop freq. (#/mi)	1/mi	2.28	0.10	0.62	15.38	1.63

Table 2-2 Driving Cycle Characteristics [32]

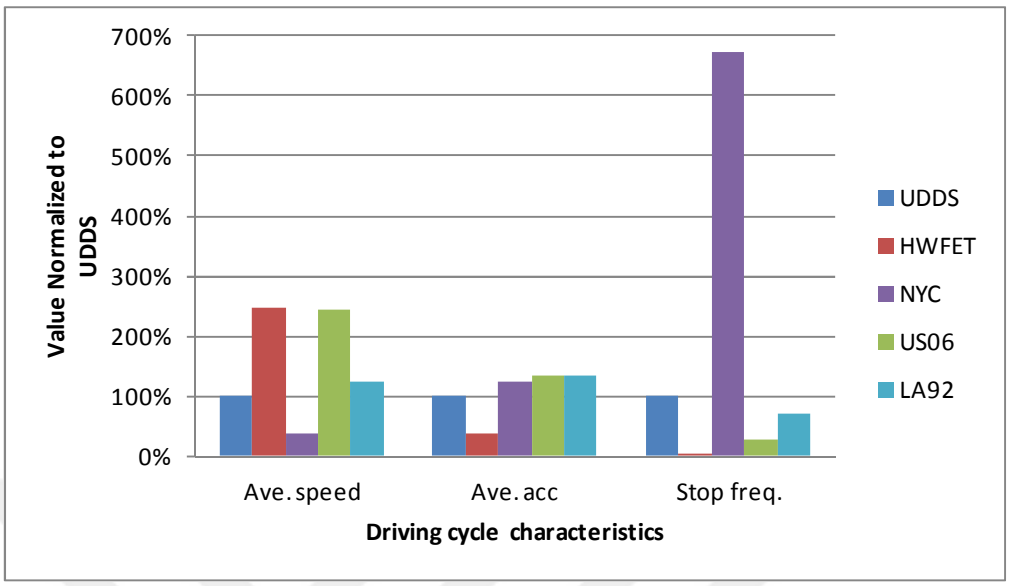

Figure 2-4 Driving cycle characteristics

Patil et al. [6] find that the US06 is more fuel-consuming than 90% of real-world GPS cycles collected in southeast Michigan. The NYC cycle is low speed with frequent stops and relatively high acceleration and deceleration, serving as a reasonable bound on urban driving conditions. LA92 represents somewhat more aggressive and higher speed driving in city conditions. A recent study by Rousseau et al. [35] claims that this cycle is closer to real-world driving than the standard test cycles, partially due to the fact that it was designed using data collected in 1992, after dynamometer technology had improved.

2.3.2 Distribution of daily distance driven

Daily driving distance is an important factor in estimating the real benefits of electrified vehicles since EREV PHEVs have the potential to power daily trips entirely on electricity if the distance between charge points is shorter than the AER of the PHEV. If daily distance driven is longer than the AER, there will be additional gasoline consumption.

The second implication of daily driving distance is that vehicle life depends on use. Typical vehicle life is assumed to be approximately 150,000 miles [36]. Daily driving distance determines the life of the vehicle and the amount of time over which the purchase cost is spread, which is important for computing net present value of lifetime vehicle ownership.

The average daily distance driven by US drivers is estimated using data from the 2009 National Household Travel Survey (NHTS) [4]. Data is collected on daily trips taken in a 24-hour period by over 150,000 interviewed households and 300,000 people. The dataset provides information about the characteristics of the trips such as length, duration, and the type of the vehicles used. Figure 2-5 shows the weighted daily driving distance distribution for automobiles.

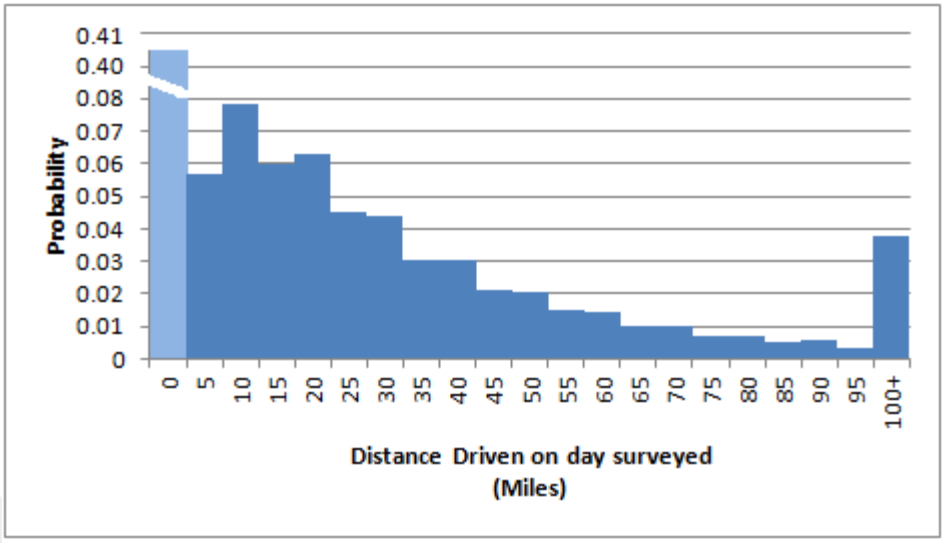

Figure 2-5 NHTS Distribution of daily distance driven

These data were obtained from the post-processed NHTS 2009 dataset of 294,407 automobiles which only include cars, vans, SUVs, and pickup trucks, where 14 data points were removed since the daily distance reported was not plausible. Considering only the vehicles which drive that day, average daily distance driven is found to be 37.1 miles, implying an average annual distance of 13,500 miles per vehicle. When we include the vehicles that did not drive, the average distance driven that day is found to be 22.0 miles, implying an average annual distance of 8,050 miles, lower than EPA estimates.

2.3.3 Engineering Model

Vehicle designs and performance analysis takes place in the engineering model of the proposed framework (Fig. 3). PHEVs have several important performance characteristics that affect their economic and environmental benefits. One of them is the distance the vehicle can be driven using only electricity, s_{AER}. Change in driving patterns results in change in s_{AER}. We calculate s_{AER} as:

$$\begin{aligned} s_{AER} &= Zk\eta_{CD} \quad \text{(miles)} \\ k &= \frac{C_{BAT}V_{BAT}K_{BAT}}{1000} \quad \text{(kWh)} \end{aligned} \tag{2-4}$$

where Z is the battery swing window (%) shown in Figure 2-1, k is the total battery energy capacity (kWh), η_{CD} is the vehicle fuel efficiency in CD mode (mi/kWh), C_{BAT} is the number of cells in the battery pack, V_{BAT} is the nominal cell voltage and K_{BAT} is the battery capacity (Ah).

For this study, we designed several vehicles including a CV, an HEV, three PHEVs and a BEV. The primary design variables for plug-in vehicles are engine size, motor size, and battery size. Vehicle mass is accounted by adding the mass of each component to the vehicle glider based on their energy and power densities. We assume 1 kg of additional structural weight for each kg of battery cells added to the battery pack for plug-in vehicles [45]. Vehicles are designed for the EPA 5-cycle to meet certain criteria: (1) the desired s_{AER} is satisfied within 1% and (2) the 0-60 mph acceleration time is less than 10.3 seconds (the reference set by the HEV model) in both CS and CD modes. The CV in our study is designed using the PSAT Honda Accord configuration with an altered vehicle body and tires to match Prius MY12 specifications; the HEV is the MY12 Toyota Prius configuration; the PHEVs use the MY12 PHEV configuration

with a switch to a Li-ion battery and increased battery size; and the BEV uses a modified mid-size electric powertrain in PSAT with a Prius body and tires. F/R weight ratio is 06/04, drag coefficient is 0.26, frontal area is 2.25 m^2. Constant power loss due to electric load is the default value of 0.3kW for all vehicles. HEV initial SOC and target SOC are set to 60%. For PHEVs and BEVs, in CD mode the initial SOC is set to 90% and target SOC is set to 30%, and for CS mode the initial and target SOC are set to 30%. Control variables are adjusted from the default to enable regenerative braking when SOC is less than maximum allowable SOC value. Following PSAT defaults, the braking control strategy is set to capture 90% of the braking energy when vehicle deceleration is less than 2 m/s^2 (in practice more or less braking energy may be lost, depending on the brake system design). Argonne's Advanced Powertrain Research Facility has validated the conventional and mild-hybrid vehicles in PSAT within 2% and full hybrid vehicles within 5% for both fuel economy and battery state-of-charge on several driving cycles [37]. Vehicle component sizes are summarized in Table 2-3 and efficiencies are given in Table 2-4. More detail on component specifications and vehicle performance can be found in Appendix and PSAT [32].

Final vehicle designs used in our study, including a CV, an HEV, PHEVs sized for 20, 40, and 60 mile AER, and a BEV sized for 100 mile AER, are summarized in Table 2-3, and fuel economy results are given in Table 2-4. By convention the AER of a plug-in vehicle is indicated with a number x shown as $PHEV_x$ or BEV_x. For example, $PHEV_{20}$ indicates a PHEV with a 20 mile AER under the EPA combined test procedure. Here, vehicle efficiency is a function of drive cycle and will change depending on the vehicles' mass, thus matching the AER of electrified vehicles to the specifications is an iterative process. Also we have sized the components to

satisfy performance constraints both in CD and CS mode. Sizing components for blended control would result in smaller components but an inability to operate as an EREV and greater sensitivity to control strategy parameters. We leave investigation of blended operation PHEVs for future work. Efficiency estimates for each vehicle type could vary for different vehicle and component designs as well as for on-road tests vs. simulation.

Vehicle Type	Engine (kW)	Motor (kW)	Battery (kWh)	Mass (kg)
CV (Corolla engine)	110			1371
HEV (2013 Prius)	73	60	1.3	1424
PHEV20	73	78	9.9	1569
PHEV40	73	88	19.9	1793
PHEV60	73	98	30.2	2027
BEV100		120	54.0	2265

Table 2-3 Vehicle configurations

Vehicle Type			UDDS	HWFET	US06	NYC	LA92	FTP	EPA city (2008+)	EPA highway (2008+)	EPA Combined MPG(2008+)
CV		mi/gal	32.1	52.8	29.8	16.4	28.9	32.8	25.4	37.2	31.0
HEV		mile/gallon	69.5	59.7	43.9	48.0	54.1	67.8	48.4	41.8	44.4
PHEV20	CD eff	mile/kWh	6.2	5.7	3.2	4.2	4.2	6.0	3.3	3.6	3.4
	CD-mpg-eq	mpg-eq	207.9	193.0	108.4	142.0	142.2	202.3	110.0	119.7	115.3
	CS eff	mi/gal	69.4	58.6	41.0	45.7	52.3	67.3	48.1	41.1	43.8
	AER	mile	36.8	34.1	19.2	25.1	25.2	35.8	19.5	21.2	20.4
PHEV40	CD eff	mile/kWh	6.0	5.7	3.2	4.1	4.1	5.8	3.2	3.5	3.4
	CD-mpg-eq	mpg-eq	201.2	192.1	106.9	138.2	138.1	196.2	107.8	119.3	114.0
	CS eff	mi/gal	68.0	58.2	40.2	43.1	50.0	66.0	47.3	40.8	43.4
	AER	mile	71.2	68.0	37.8	48.9	48.9	69.4	38.1	42.2	40.3
PHEV60	CD eff	mile/kWh	5.7	5.6	3.1	3.8	3.9	5.6	3.1	3.5	3.3
	CD-mpg-eq	mile/kWh	192.2	190.0	104.0	129.6	132.2	188.0	104.8	118.1	112.0
	CS eff	mi/gal	65.8	57.8	39.2	40.3	48.0	64.0	46.1	40.5	42.7
	AER	mile	103.5	102.3	56.0	69.8	71.2	101.2	56.4	63.6	60.3
BEV100	CD eff	mile/kWh	4.8	5.2	3.4	3.1	4.1	4.8	2.8	3.3	3.1
	CD-mpg-eq	mile/kWh	162.2	176.4	113.5	103.8	136.9	160.9	94.4	111.0	103.2
	AER	mile	155.9	169.6	109.1	99.8	131.6	154.7	90.7	106.7	99.2

Table 2-4 Efficiency and AER of each vehicle under each driving cycle. The label "2008+" refers to the regression-based adjusted fuel economy calculations used by the EPA between 2008-2011 and beyond 2011 under some specific conditions (Eq(1-3)).

2.3.4 Fuel Consumption

For a distance s driven between charges in a vehicle with a specific s_{AER}, the distance driven in CD mode s_{CD} and CS mode s_{CS}, measured in miles, is calculated as follows:

$$s_E(s) = \begin{cases} s & \text{if } s \le s_{AER} \\ s_{AER} & \text{if } s > s_{AER} \end{cases}$$
$$s_G(s) = \begin{cases} 0 & \text{if } s \le s_{AER} \\ s - s_{AER} & \text{if } s > s_{AER} \end{cases} \quad (2\text{-}5)$$

The NHTS-averaged distance driven on electricity $\bar{s}_E$ and average distance driven on gasoline $\bar{s}_G$ is given by

$$\bar{s}_E = \int_{s=0}^{\infty} s_E f_S(s) ds$$
$$\bar{s}_G = \int_{s=0}^{\infty} s_G f_S(s) ds \quad (2\text{-}6)$$

where $f_S(s)$ is the probability distribution function (PDF) of distance driven for a randomly selected vehicle on a random driving day in the NHTS 2009 data, including those vehicles that were not driven on the day surveyed. We discretize this distribution into 1-mile bins for numerical integration.

Average distance driven per day $\bar{s}$ is given as:

$$\bar{s} = \int_{s=0}^{\infty} s f_S(s)\, ds \tag{2-7}$$

Gasoline consumption $g(s)$, given in gallons, and electricity consumption $e(s)$, given in kWh, on a day with *s* miles of driving is calculated by

$$\begin{aligned} g(s) &= \frac{\max(0, s - s_{\text{AER}})}{\eta_{\text{CS}}} \\ e(s) &= \frac{\min(s, s_{\text{AER}})}{\eta_{\text{CD}}} \end{aligned} \tag{2-8}$$

where η_{CS} and η_{CD} values are fuel efficiencies in CD and CS modes respectively, summarized in Table 2-4.

The average gasoline $\bar{g}$ and electricity $\bar{e}$ consumption in the NHTS data set given as:

$$\begin{aligned} \bar{g} &= \int_{s=0}^{\infty} g(s)\, f_S(s)\, ds \\ \bar{e} &= \int_{s=0}^{\infty} e(s)\, f_S(s)\, ds \end{aligned} \tag{2-9}$$

Typical vehicle life, s_{LIFE} is assumed to be approximately 150,000 miles [36]. *D* is the number of days in the year (365). Vehicle life $T_{\text{VEH}}(s)$ in years is given by:

$$T_{\text{VEH}}(s) = \frac{s_{\text{LIFE}}}{Ds} \tag{2-10}$$

and the NHTS average vehicle life is:

$$\bar{T}_{\mathrm{VEH}} = \frac{s_{\mathrm{LIFE}}}{D\bar{s}} \tag{2-11}$$

2.3.5 Battery Degradation Model

We follow Peterson et al [38] and Shiau et al [5] in modeling battery degradation as a function of energy processed, based on data collected from A123 $LiFePO_4$ cells. Energy processed w_{DRV} in kWh while driving a distance *s* is:

$$w_{\mathrm{DRV}}(s) = \mu_{\mathrm{CD}} s_{\mathrm{E}} + \mu_{\mathrm{CS}} s_{\mathrm{G}} \tag{2-12}$$

where μ_{CD} and μ_{CS} are the energies processed per mile (kWh/mile) in CD and CS modes, respectively. Energy processed, given in kWh, while charging is:

$$w_{\mathrm{CHG}}(s) = s_{\mathrm{E}} \left(\eta_{\mathrm{CD}} \eta_{\mathrm{B}}\right)^{-1} \tag{2-13}$$

where η_B is the battery charging efficiency, assumed to be 95%. The relative energy capacity fade can be calculated as:

$$\mathrm{r}_P(s) = \frac{\alpha_{\mathrm{DRV}} \mathrm{w}_{\mathrm{DRV}} + \alpha_{\mathrm{CHG}} \mathrm{w}_{\mathrm{CHG}}}{k} \tag{2-14}$$

where $\alpha_{\mathrm{DRV}}=3.46\times10^{-5}$ and $\alpha_{\mathrm{CHG}}=3.46\times10^{-5}$ are the relative energy capacity fade coefficients derived from the data set in [38]. We define battery end of life (EOL) as the point when the portion of the remaining energy capacity equals the energy within the swing window under the

original capacity. The relative energy capacity fade r_{EOL} at the EOL becomes the original total capacity minus swing (r_{EOL}=1-Z).

The NHTS average computed battery life, given in years, is found by:

$$\bar{T}_{BAT} = \frac{k(1-Z)}{\left(\alpha_{DRV}\left(\mu_{CD}\bar{s}_E + \mu_{CS}\bar{s}_G\right) + \alpha_{CHG}\bar{s}_E\left(\eta_E\eta_C\right)^{-1}\right)D} \quad (2\text{-}15)$$

We assume that the functional battery life in the vehicle $\bar{\theta}_{BAT}$ is never longer than vehicle life:

$$\bar{\theta}_{BAT} = \min(\bar{T}_{BAT}, \bar{T}_{VEH}) \quad (2\text{-}16)$$

We ignore degradation effects for NiMH cells in the HEV because HEV performance is far less sensitive to capacity fade (effectively an AER of zero); HEV economics are less sensitive to possible battery replacement; and our Li-ion degradation model predicts no replacement for the HEV configuration and use patterns. For Li-ion cells in PHEVs and BEVs we use the battery degradation model described above.

2.3.6 Environmental Model

Life cycle GHG emissions $v(s)$ for a vehicle that travels s miles per day and NHTS-averaged emissions $\bar{v}$ are computed in kg CO_2-equivalent per year:

$$v(s) = v_{\text{VEH}}\left(T_{\text{VEH}}(s)\right)^{-1} + v_{\text{BAT}}k\left(\theta_{\text{BAT}}(s)\right)^{-1} + g(s)v_{\text{G}}D + e(s)\eta_{\text{C}}^{-1}v_{\text{E}}D$$
$$\bar{v} = v_{\text{VEH}}\left(\bar{T}_{\text{VEH}}\right)^{-1} + v_{\text{BAT}}k\left(\bar{\theta}_{\text{BAT}}\right)^{-1} + \bar{g}v_{\text{G}}D + \bar{e}\eta_{\text{C}}^{-1}v_{\text{E}}D \quad (2\text{-}17)$$

where v_{VEH} is the life cycle emissions from producing the base vehicle, v_{BAT} is the life cycle emissions from producing the battery pack (Table 2-5) [3], v_{G} = 11.34 kg-CO_2-eq per gallon is the life cycle emissions per gallon of gasoline consumed [39], v_{E} = 0.752 kg-CO_2-eq per kWh is the life cycle emissions per kWh of electricity consumed [39], and η_{C}=88% for battery charging efficiency [40].

2.3.7 Cost Model

Equivalent annualized cost (EAC) of vehicle ownership is the value of the recurring fixed annual payment whose net present value (NPV) is equal to NPV of vehicle ownership over the vehicle lifetime. This metric makes it possible to compare the ownership cost of vehicles over different lifetimes. The net present value of vehicle ownership includes costs of vehicle production, battery, and vehicle operation plus any carbon price costs, assuming that a carbon tax would be levied equally on all GHG emissions released over the life cycle and that upstream costs would be passed down to the consumer. We define a nominal discount rate r_{N} and inflation rate r_{I}, implying a real discount rate $r_{\text{R}} = (1+r_{\text{N}})/(1+r_{\text{I}}) - 1$ [41]. The capital recovery factor $f_{\text{A|P}}$ for a general discount rate r and time period N in years is given by [41]:

$$f_{\text{A|P}}(r,N) = \left(\sum_{n=1}^{N}\frac{1}{(1+r)^n}\right)^{-1} = \frac{r(1+r)^N}{(1+r)^N - 1}; \quad (2\text{-}18)$$

the annualized cost $c(s)$ for a vehicle that travels s mi/day is:

$$
\begin{aligned}
c(s) = {} & c_{\mathrm{VEH}} f_{\mathrm{A|P}}\left(r_{\mathrm{N}}, T_{\mathrm{VEH}}\right) + c_{\mathrm{BAT}} f_{\mathrm{A|P}}\left(r_{\mathrm{N}}, T_{\mathrm{BAT}}(s)\right) + \\
& p_{\mathrm{GAS}} g(s) D \frac{f_{\mathrm{A|P}}\left(r_{\mathrm{N}}, T_{\mathrm{VEH}}(s)\right)}{f_{\mathrm{A|P}}\left(r_{\mathrm{R}}, T_{\mathrm{VEH}}(s)\right)} + p_{\mathrm{ELEC}} e(s) \eta_{\mathrm{C}}^{-1} D \frac{f_{\mathrm{A|P}}\left(r_{\mathrm{N}}, T_{\mathrm{VEH}}(s)\right)}{f_{\mathrm{A|P}}\left(r_{\mathrm{R}}, T_{\mathrm{VEH}}(s)\right)} + \\
& p_{\mathrm{CO2}} v(s) \frac{f_{\mathrm{A|P}}\left(r_{\mathrm{N}}, T_{\mathrm{VEH}}(s)\right)}{f_{\mathrm{A|P}}\left(r_{\mathrm{R}}, T_{\mathrm{VEH}}(s)\right)} \quad (\$/\text{year})
\end{aligned}
\tag{2-19}
$$

and the NHTS average annualized cost $\bar{c}$ is:

$$
\begin{aligned}
\bar{c} = {} & c_{\mathrm{VEH}} f_{\mathrm{A|P}}\left(r_{\mathrm{N}}, \bar{T}_{\mathrm{VEH}}\right) + c_{\mathrm{BAT}} f_{\mathrm{A|P}}\left(r_{\mathrm{N}}, \bar{T}_{\mathrm{BAT}}\right) + \\
& p_{\mathrm{GAS}} \bar{g} D \frac{f_{\mathrm{A|P}}\left(r_{\mathrm{N}}, \bar{T}_{\mathrm{VEH}}\right)}{f_{\mathrm{A|P}}\left(r_{\mathrm{R}}, \bar{T}_{\mathrm{VEH}}\right)} + p_{\mathrm{ELEC}} \bar{e} \eta_{\mathrm{C}}^{-1} D \frac{f_{\mathrm{A|P}}\left(r_{\mathrm{N}}, \bar{T}_{\mathrm{VEH}}\right)}{f_{\mathrm{A|P}}\left(r_{\mathrm{R}}, \bar{T}_{\mathrm{VEH}}\right)} + \\
& p_{\mathrm{CO2}} \bar{v} \frac{f_{\mathrm{A|P}}\left(r_{\mathrm{N}}, \bar{T}_{\mathrm{VEH}}\right)}{f_{\mathrm{A|P}}\left(r_{\mathrm{R}}, \bar{T}_{\mathrm{VEH}}\right)} \quad (\$/\text{year})
\end{aligned}
\tag{2-20}
$$

where c_{VEH} is the vehicle cost and c_{BAT} is the battery cost specified in Table 2-6 and Table 2-7 for each vehicle and battery type, (cost estimates are taken from [37] and based on 2015 literature review and 2030 DOE program goals to provide a range for sensitivity –battery cost for PHEV20 and 60 have been interpolated), p_{GAS} = \$2.75/gal is the average price of gasoline during 2008-2010 period [42], p_{ELEC} = \$0.114/kWh is the average price of electricity during 2008-2010 period [43], and p_{CO2} is the carbon price, which we vary from \$0- \$100/tCO_2e [44]. The real discount rate r_{R} is used for future commodity purchases under the assumption that prices follow inflation $f_{\mathrm{A|P}}\left(r_{\mathrm{R}}, \bar{T}_{\mathrm{VEH}}\right)^{-1}$ computes NPV of future payments for a commodity whose prices follow inflation, and $f_{\mathrm{A|P}}\left(r_{\mathrm{N}}, \bar{T}_{\mathrm{VEH}}\right)$ converts NPV to EAC). In the next section, we will analyze the results and discuss their engineering and policy implications.

Parameters	Lower	Base case	Upper	Units
Cost of gasoline	$1.59	$2.75	$4.05	per gallon
Cost of electricity	$0.06	$0.114	$0.30	per kW
CO_2 tax	$0	$0	$100	t-CO2-eq
GHGs for electricity emission	0.066	0.73	0.9	kg CO2 eq per kwh
GHGs for gasoline emission	–	11.34	–	kg CO2 eq per gal
Battery charging efficieny	–	0.88	–	%
Vehicle life	–	150000	–	miles
Number of driving days per year	–	365	–	days/year
Nominal discount rate	5	8	15	%
Inflation rate for future fuel prices	–	3	–	%
Real discount rate	–	5	–	%
GHGs for Li-ion battery production	–	120	–	kg CO2 eq
GHGs for NiMH battery production	–	230	–	kg CO2 eq
GHGs for vehicle production	–	8500	–	kg CO2 eq
Battery swing	–	60	–	%

Table 2-5 Parameter levels for base case and sensitivity analysis

	Chemistry	Size(kWh)	2015 LR ($)	2030 PG ($)
HEV	NiMH	1.3	1310	717
PHEV20	Li-ion	6.4	549	171
PHEV40	Li-ion	11.1	500	160
PHEV60	Li-ion	20.0	490	157
BEV100	Li-ion	30.0	472	154

Table 2-6 Battery cost given in $ per kWh for 2015 LR and 2030 PG cases [37]

Vehicle	Battery Size(kWh)	Cost Component	2015 LR	2030 PG
PHEV20	6.4	Vehicle	24369	22598
		Battery	5302	1654
PHEV40	13.0	Vehicle	24369	22598
		Battery	9752	3121
PHEV60	20.0	Vehicle	24369	22598
		Battery	14661	4712
BEV100	30.0	Vehicle	24369	22598
		Battery	21257	6954
HEV	1.3	Vehicle	23546	22206
		Battery	1964	717
CV	0	Vehicle	23340	22088

Table 2-7 Vehicle and battery cost given in $ for 2015 LR and 2030 PG cases

For a new product design problem under short-run competition, there are three sets of decision variables to be determined – new product design variables, new product price, and prices of competitor products. In the following sections, we describe the proposed product design optimization models under Nash and Stackelberg strategies incorporating the FOC equation for unconstrained prices. We then examine the special cases where prices are constrained and develop a Lagrangian extension for this case (the basic concept of the Lagrangian FOC method is described in Appendix A). The major assumptions for the proposed approaches are: (1) Focal firm will design a set of differentiated products that will enter a market with existing products sold by competitors; (2) competitors are Nash price setters for profit maximization with fixed products; (3) competitor product attributes and costs are known; and (4) price is continuous, and each firm's profit function is differentiable with respect to its corresponding price.

2.4 RESULTS AND DISCUSSION

2.4.1 All electric range

Our analysis shows that driving patterns affect AER significantly. An aggressive driving cycle (US06) can reduce AER by 45% relative to a gentle cycle (UDDS) (see Figure 2-6). For example, a PHEV with a split powertrain designed to achieve a 70-mile AER on the FTP drive cycle provides only a 40 mile AER under the NYC drive cycle. Reduced range is particularly important for BEVs, which have no gasoline backup, but reduced range also affects life cycle cost and emissions of PHEVs and can negatively affect customer satisfaction and perception of plug-in vehicle technology. The vehicles components of this study have been sized to satisfy the target AER under the EPA combined mpg(2008+) which adjusts FTP and HWFET test results to estimate outcomes from a 5-cycle test, which results in lower efficiency estimates and thus AER..

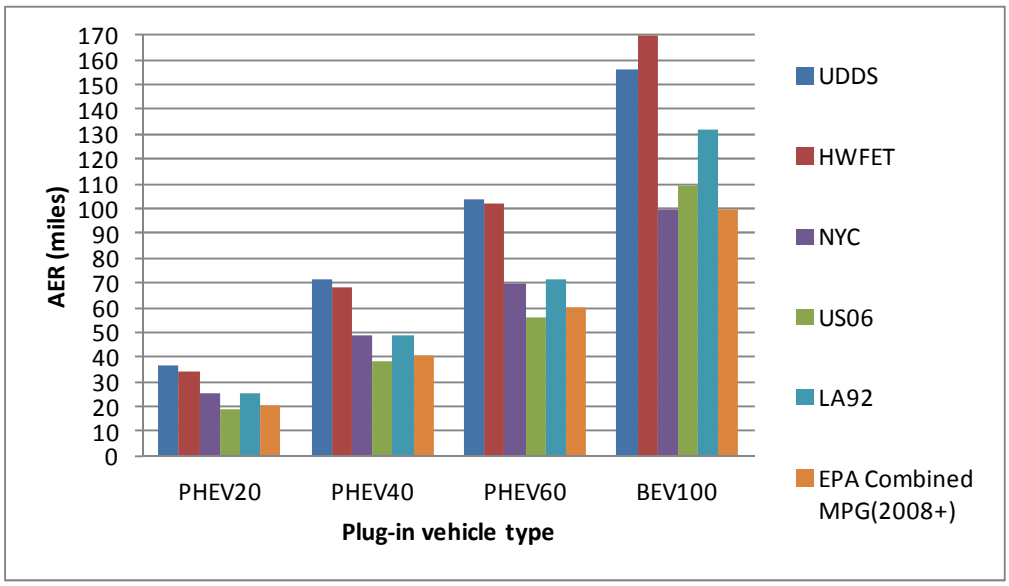

Figure 2-6 All electric range under different driving cycles

2.4.2 Lifecycle Cost

Figure 2-7 summarizes base case equivalent annualized cost for each vehicle type and each driving cycle. 2015 battery price estimates from [37] are used for the base case. Vehicle and battery cost of each vehicles is constant across driving cycles, since vehicle design is given; however gasoline and electricity costs are functions of driving patterns. Under HWFET, US06 and the EPA-5 cycle, the CV is the cost minimum followed closely by the HEV; under the UDDS and NYC driving cycles the HEV minimizes cost. CV is the most sensitive to driving cycle, especially stop-and-go driving and traffic conditions. Electrified vehicles are less sensitive to drive cycle. In the base case, plug-in vehicles are consistently more expensive than HEVs over the life, primarily due to the cost of larger battery packs, and only in NYC conditions is the $PHEV_{20}$ lower cost than the CV.

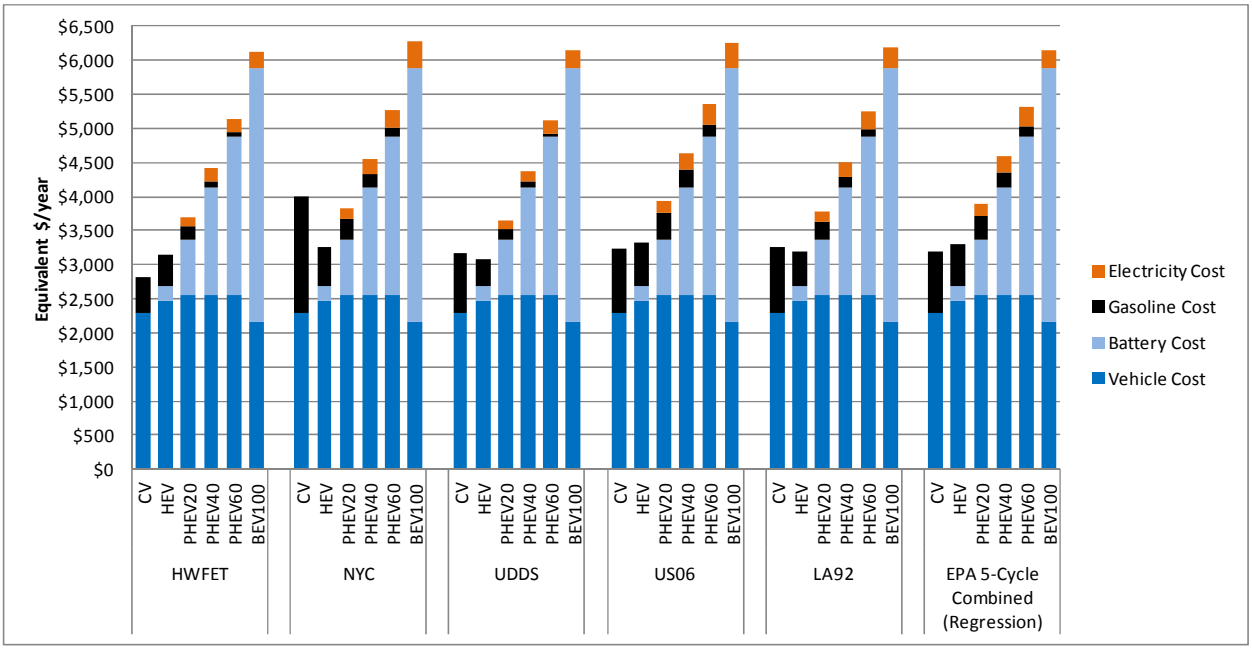

Figure 2-7 NHTS Averaged Annualized Cost Breakdown per Vehicle (Base Case)

The BEV powertrain cost is least sensitive to drive cycle because electricity consumption is a small portion of overall cost, and regenerative braking together with the lack of an idling gasoline engine makes electrified powertrains less sensitive to stopping frequency. The cost associated with CV is 30% higher under NYC conditions than under HWFET conditions.

2.4.3 Lifecycle Greenhouse Gas Emissions

Figure 2-8 shows the breakdown of average annual GHG emissions for each vehicle and driving cycle. Increased battery size results in greater displacement of gasoline with electricity; however, battery production emissions also increase, and vehicle efficiency decreases with vehicle weight. This accounts for the increased GHG emissions of longer-range PHEVs with average U.S. electricity.

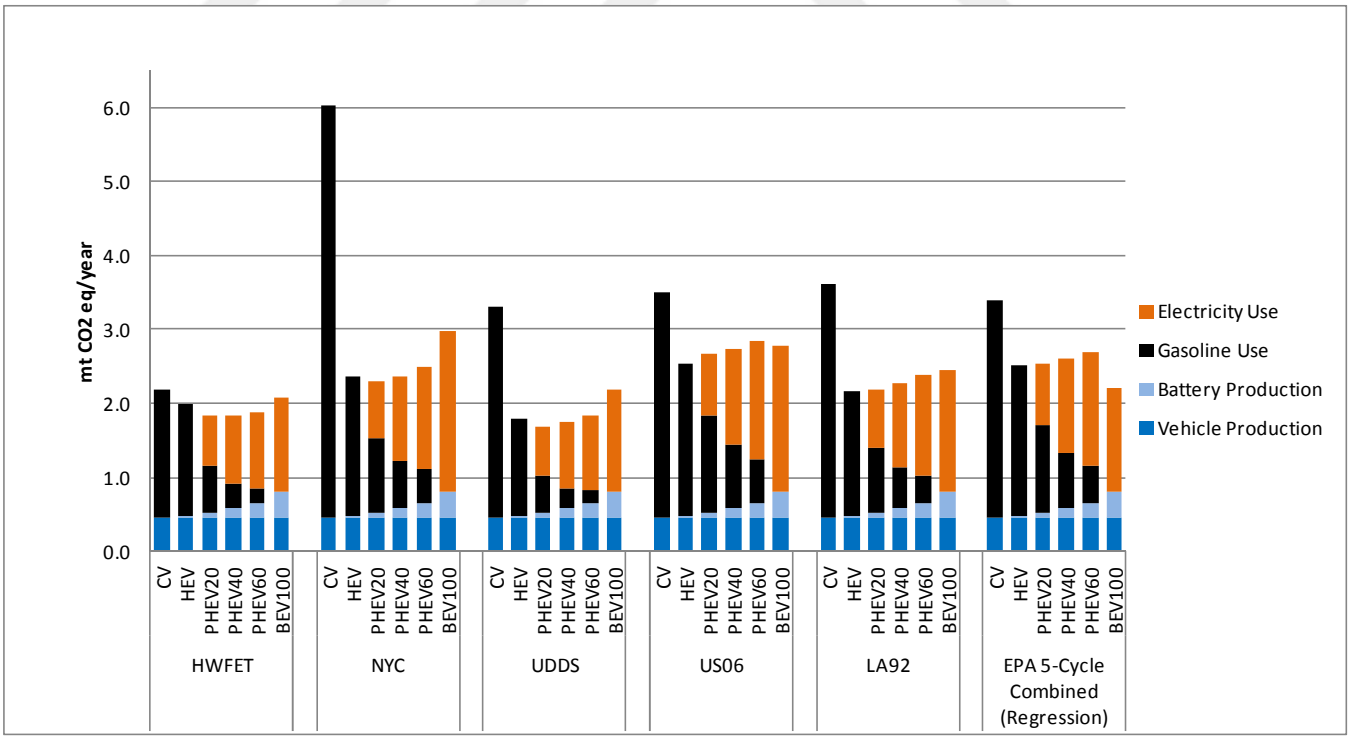

Figure 2-8 NHTS-Averaged Annual GHG Emissions per Vehicle (Base Case)

Under HWFET conditions all powertrains produce comparable life cycle emissions. In all other conditions, electrified vehicles release significantly lower GHGs than CVs -- in particular, HEVs reduce emissions by 60% relative to CV in the NYC cycle. In the base case, plug-in vehicles do not provide substantial GHG reductions relative to HEVs except for the BEV100 in the EPA 5-cycle, which may be optimistic due to application of EPA regression equations to electric operation.

2.4.4 Base case cost and GHG comparison

Figure 2-9 summarizes the life cycle annualized cost and GHG emissions for each vehicle and drive cycle using our base case assumptions. Drive cycles with more aggressive acceleration demands and more stops increase both cost and emissions simultaneously. The CV (diamond) is much more sensitive to drive cycle, whereas the electrified powertrains experience less variation with drive cycle. A move from CV (diamond) to HEV (square) reduces GHG emissions at no cost or at modest cost, depending on the drive cycle. A move from HEV to the plug-in powertrains reduces or increases GHGs, depending on the vehicle and drive cycle, but comes at a substantial increase in costs.

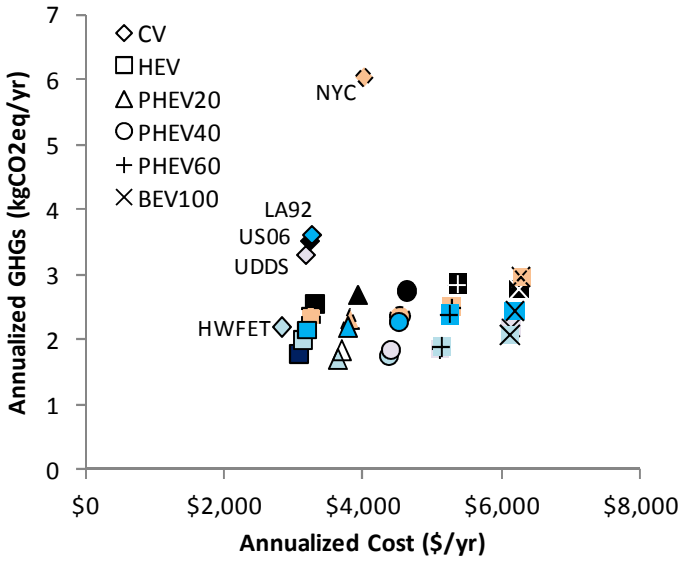

Figure 2-9 Annualized cost vs. annual GHG emissions for various vehicles and drive cycles

2.4.5 Cost and GHGs per mile for different daily driving distances and patterns

Figure 2-10 shows average life cycle GHG emissions per lifetime mile and annualized cost per annual mile traveled as a function of daily distance traveled for the two contrasting driving conditions: HWFET and NYC, assuming one charge per day. GHG emissions per mile vary with daily distance traveled for PHEVs because distance driven between charges affects the portion of travel that can be propelled using electricity in place of gasoline. If a PHEV is driven further than its AER, it will begin to consume gasoline. The resulting trends are similar to the trends identified by Shiau et al [45]: PHEVs with small battery packs have lower emissions when charged frequently and driven primarily in CD mode but may have higher emissions if charged infrequently.

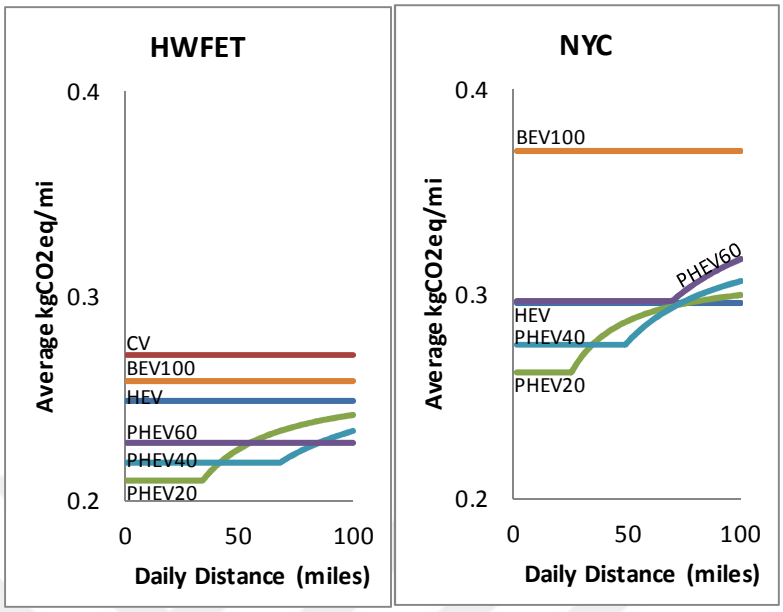

Figure 2-10 Life cycle GHG per mile under HWFET and NYC driving patterns for a variety of daily driving distances (to show detail, y-axis does not cross at zero). The CV has 0.75 $kgCO_2eq/mi$ on the NYC cycle.

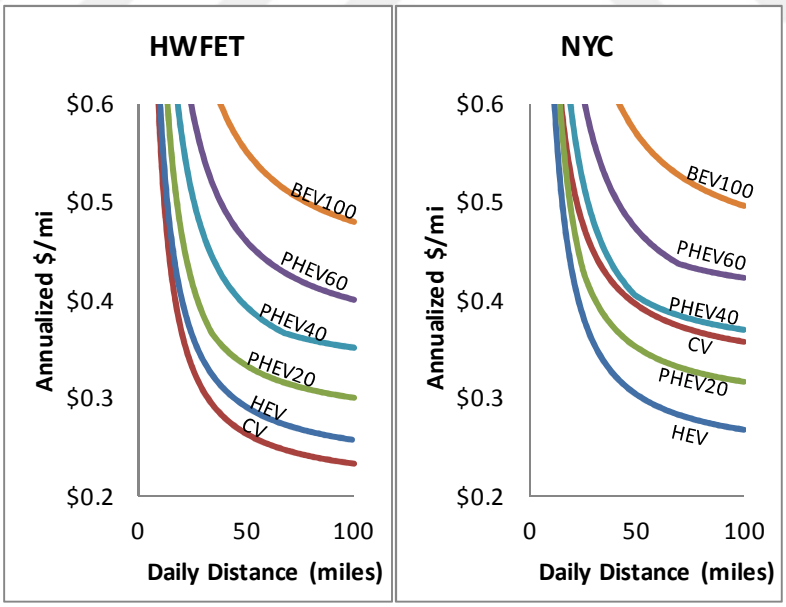

Figure 2-11 The net annualized cost per mile under HWFET and NYC driving patterns for a variety of daily driving distances (to show detail, y-axis does not cross at zero)

The cost curves in Figure 2-11 show a decline of annualized cost/mile with daily driving distance, which results from capital cost of initial vehicle and battery purchase comprising a larger portion of total cost for short daily driving distances, which imply long vehicle life and discounted future fuel costs. The curves have less overlap in this case, and dominant vehicles align with NHTS-averaged estimates in Figure 2-7. Under HWFET conditions the ranking of cost competitive vehicles (CV, HEV, PHEV20, PHEV40, PHEV60, BEV100) follows increasing battery capacity. Under NYC conditions, HEV and PHEV20 are lower cost than CV. In both cases, BEVs increase the costs significantly.

2.4.6 Sensitivity Analysis

Figure 2-12 summarizes sensitivity of annualized cost to gasoline price, electricity price, vehicle and battery price, carbon tax price (GHG value), and discount rate. We focus on comparing two contrasting cases: HWFET which consists of high speed and low acceleration, and NYC which consists of low speed and stop-and-go city driving. Figure 2-10a shows the HWFET and NYC EAC breakdown from the base case (Figure 7). All other cases show the base case as faded bars and display how the results would change under alternative assumptions using error bars. Figure 2-10b shows that increasing gasoline prices affect CV cost most dramatically and makes plug-in technology more cost competitive; however, large battery pack PHEVs remain higher cost. Figure 2-10c shows that electricity price affects the cost of plug-in vehicles with large battery packs most; however, a five-fold increase in electric price has a notably smaller overall effect that does not change ranking. Figure 2-10d emphasizes that vehicle and battery costs have a critical impact on the cost benefits of plug-in vehicles. Near term 2015 vehicle costs estimated by Plotkin and Singh of Argonne National Laboratory (ANL2015)

suggest that plug-in vehicles with large battery packs are more expensive than HEVs regardless of driving cycle, but Department of Energy targets for costs in 2030 (DOE2030), which ANL calls "very optimistic" [37], would result in more comparable costs. Figure 2-10e reveals that while high carbon prices would have non-negligible effects on life cycle costs, they would do little to change the relative costs of the powertrain options except for the relatively large penalty to CVs in NYC conditions. Figure 2-10f examines the effect of varying consumer discount rate. Higher discount rates are less favorable to plug-in vehicles, whose savings are delayed to future years.

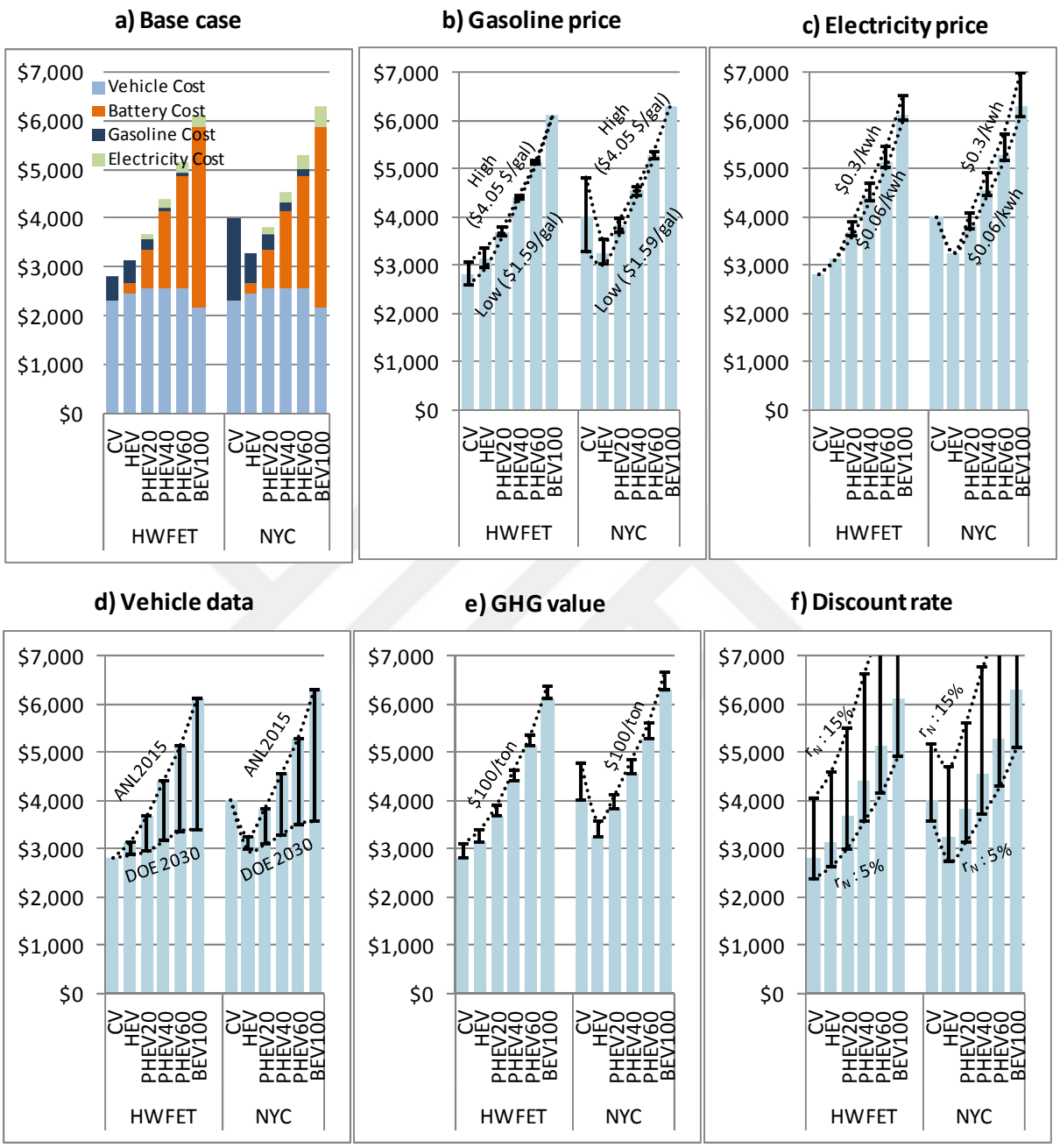

Figure 2-12 Sensitivity analysis for life cycle equivalent annualized cost under HWFET and NYC drive cycles

Figure 2-13 summarizes the effect of electricity source on life cycle GHG emissions. Electricity source varies substantially with location and charge timing [26], is difficult to know

with certainty [25], and is typically not under the consumer's control. Electricity from coal-fired power plants lead to increased emissions from plug-in vehicles, whereas low-carbon electricity sources such as nuclear, wind, hydro, and solar power, result in substantial reductions in life cycle GHG emissions from plug-in vehicles relative to today's U.S. average grid mix. The marginal electricity used to charge plug-in vehicles will typically not be nuclear, which is usually run as base load generation, and use of renewable energy is subject to constraints from the intermittent and variable nature of renewable energy sources, so the zero-emission cases (labeled "Nuclear") serve as lower bounds.

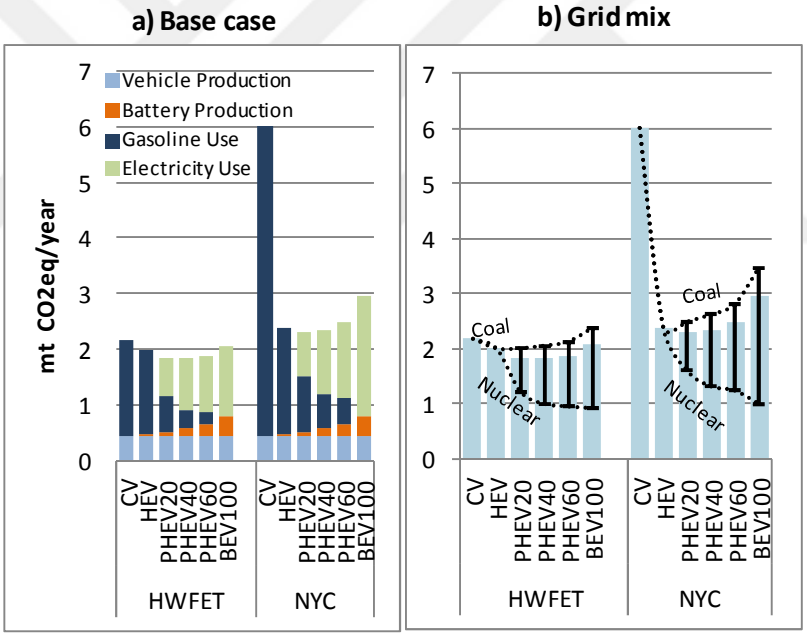

Figure 2-13 Sensitivity analysis for life cycle GHG emissions

2.5 Conclusions

Customer vehicle purchasing decisions are in part guided by EPA fuel economy and AER estimates based on standard laboratory test driving cycles. However, diverse real-world driving conditions can deviate substantially from laboratory conditions, affecting which vehicle technologies are most cost effective at reducing GHG emissions for each driver. As such, the choice of driving cycle for testing necessarily preferences some vehicle designs over others. This effect has become more pronounced with the introduction of hybrid and plug-in powertrains because factors like regenerative braking and engine idling affect the relative importance of aggressive and stop-and-go driving conditions on system efficiency. Compared to cycles like NYC, test drive cycles UDDS and HWFET, used for corporate average fuel economy (CAFE) tests, underestimate relative cost and GHG benefits of hybrid and plug-in vehicles.

With the introduction of hybrid and plug-in vehicles, it has become more important that the right vehicles are targeted to the right drivers. Drivers who travel in NYC conditions could cut lifetime costs by up to 20% and cut GHG emissions 60% by selecting hybrid vehicles instead of conventional vehicles, while for HWFET drivers conventional vehicles provide a lower cost option with a much smaller GHG penalty. CV owners observe more variability in cost and emissions subject to driving conditions, while HEVs offer the most robust, cost effective configuration across the driving patterns tested.

When comparing HEVs to PHEVs under the average U.S. grid mix, it is clear that most of the GHG-reduction benefit of PHEVs comes from hybridization, and relatively little additional benefit can be achieved through plugging in. HEVs provide an optimal or near optimal

economic and environmental choice for any driving cycle. However, given a substantially decarbonized electricity grid plug-in vehicles could reduce life cycle GHG emissions across all driving cycles, and lower battery costs combined with high gasoline prices would make plug-in vehicles more economically competitive.

2.6 Policy Implications

These results have several key policy implications. First, the benefits of plug-in vehicles vary dramatically from driver to driver depending on drive cycle (driving style, traffic, road networks, etc.). While hybrid and plug-in vehicles offer little GHG benefit at higher cost for highway driving (HWFET), they can offer dramatic GHG reductions and cost savings in NYC driving with frequent stops and idling. Electrification will have more positive impact if targeted to drivers who travel primarily in NYC-like conditions rather than HWFET-like conditions. Government could play a role through information campaigns, driver education, as well as modification to fuel economy labels. The new labels already contain a lot of information, but several possibilities could help target the right drivers: First, the label could report several additional characteristic driving cycles besides the city and highway mileage reported now. The label design would need to balance the need to avoid overwhelming the consumer, and more research on this would be needed to determine the best balance. Second, the smartphone QR code available on the new labels currently takes the consumer to a general website that describes the label in more detail. This website could instead offer interactive information for a wider range of driving conditions and even potentially use in-vehicle or smartphone GPS to measure the consumer's driving style, VMT, and local gasoline prices, using this information to give customized estimates for individual drivers. Privacy concerns would need to be addressed in such a system. Adoption by urban drivers may be limited by lower access to dedicated off-street

parking and a higher proportion of renters who lack authority to install charging infrastructure [56-58].

Second, our results suggest that the choice of standardized test used to assess vehicle efficiency for window labels and for CAFE standards can have an important effect on the measured benefit of hybrid and plug-in vehicles relative to conventional vehicles. While choice of testing protocol has always had impact on the relative benefits of vehicles, the unique features of hybrid and electric vehicle powertrains and their importance in certain types of driving amplify this impact and the potential for bias that could systemically underestimate the benefits of hybridization and electrification, influencing adoption rates and corporate strategy for compliance with CAFE standards. Furthermore, vehicles optimized to score well on EPA tests may score less well in real-world driving. Our results suggest that with the presence of hybrid and electric vehicles in the marketplace, the test cycles used to assess fuel efficiency -- while substantially improved from the old tests that are still used for CAFE standards -- should be reexamined to minimize bias. This could be accomplished, for example, using a national collection of representative GPS data to assess a distribution of driving conditions, followed by simulation, testing, and optimization to identify a set of tests that produces fuel efficiency estimates across powertrain types that most closely matches estimates using a representative distribution of on-road GPS data. In particular, CAFE standards are still based on old UDDS and HWFET tests that produce estimates with about 20% lower fuel consumption for CV, 30% lower for HEV, and 40% lower for plug-in vehicles than the EPA 5-cycle regression tests. The CAFE measurement is about 60% lower fuel consuming for CVs and 30% lower for hybrid and electric vehicles than the NYC test. The CAFE tests artificially inflate fuel economy estimates and do so unevenly for different vehicle technologies. Using a common test for CAFE standards and

window labels -- one that is as representative as possible of the resulting efficiency experienced by US drivers across vehicle technologies -- would help reduce bias against certain technologies as well as confusion about why the high fuel efficiency standards cited by politicians fail to match the reality of the vehicle fleet observed by consumers.

Third, as suggested in prior studies [5, 31, 45, 46, 52], HEVs and small-battery PHEVs provide comparable GHG reductions at lower cost than large-battery PHEVs or BEVs with today's electricity grid. This holds true across the driving cycles we tested. In particular, in NYC conditions HEVs show the lowest cost and GHG emissions. This is because hybridization (regenerative braking, efficient engine operation, Atkinson cycle, engine off at idle, etc.) offers most of the GHG benefit, and additional benefits of using electricity rather than gasoline as the energy source are dependent on grid decarbonization. Current federal and state policy favors large battery packs, but this is misaligned with potential for GHG reductions [31]. In fact, given binding CAFE standards plug-in vehicle subsidies may produce no net benefit unless they succeed in stimulating a breakthrough that leads to cost competitive plug-in vehicles and sustainable mainstream adoption that would not have happened otherwise [52, 53]..

Finally, government fleet purchases should account for the anticipated driving conditions of vehicles when selecting powertrain type.

2.7 Limitations and Future Work

There are many factors that may affect the lifetime cost and life cycle emissions of vehicles. In this work we have addressed drive cycle and distance. Climate may also have a substantial effect on vehicle efficiency, range, and battery life due to climate control, battery thermal management, and sensitivity of battery degradation to temperature [59]. Terrain may also affect electrified powertrain designs differently, although all driving cycles presented here are on flat ground.

Vehicle design choices could also influence results. We focus on EREV PHEVs because the broad space of control parameters for defining a blended operation PHEV makes results too dependent on assumptions (each control strategy will perform better on some drive cycles than others). But blended operation PHEVs could be more competitive in some cases, especially for low-range PHEVs. The battery degradation model used in this study is based on laboratory-tested A123 $LiFePO_4$ cells at room temperature. The data ignore temperature variation and calendar fade, they do not account for the higher c-rate implied by more aggressive driving cycles, and they do not examine other chemistries, which can have degradation characteristics more sensitive to state of charge and other factors. Degradation also affects vehicle performance [54], which can prevent the vehicle from satisfy some drive cycles and acceleration tests later in the vehicle's life. In this work, batteries are assumed to have negligible residual value at the end of their life, and they do they need to be replaced during the vehicle life. Even small batteries last more than the life of the vehicles.

We assume a single charge per day for the PHEV simulations, and I ignore range limitations of the BEV100, which in practice can be substantial [48]. Multiple daily charges would increase the benefits of PHEVs and extend the applicability of BEVs. Further, I ignore

differences in maintenance, insurance and charging infrastructure costs across vehicle types and focus only on the split hybrid drivetrain -- results for series and parallel designs and for blended control strategies may vary somewhat. We also ignore any salvage value of the battery pack at end of life as well as opportunities for energy arbitrage in vehicle to grid applications, which are expected to be small [44]. We neglect charging time which might change the electricity source and thus the benefits throughout the day. We have used average grid mix and explored sensitivity scenarios. Variation in benefits might be observed from region to region however when averaged overall, it would converge towards the results presented in this section. PHEVs with small batteries that are charged multiple times during the day might have more benefits than HEVs. One limitation though is that we might not achieve high C-rate with small battery packs. We account only for GHG emissions and ignore other life cycle emissions and impacts, and I assume that CO_2 tax costs are passed through the supply chain to the vehicle customer. Finally, I ignore government subsidies, which reduce costs observed by consumers but transfer these costs to taxpayers rather than eliminating them. With government subsidies, plug-in vehicles are somewhat more attractive purchase options for consumers.

2.8 Chapter References

[1] Barak Obama and Joe Biden, *The Change We Need | New Energy for America*. 2009-04-11.

[2] Bradley, T.H. and A.A. Frank, *Design, demonstrations and sustainability impact assessments for plug-in hybrid electric vehicles.* Renewable and Sustainable Energy Reviews, 2009. **13**(1): p. 115-128.

[3] Samaras, C. and K. Meisterling, *Life Cycle Assessment of Greenhouse Gas Emissions from Plug-in Hybrid Vehicles: Implications for Policy.* Environmental Science & Technology, 2008. **42**(9): p. 3170-3176.

[4] U.S. Department of Transportation, F.H.A., *2009 National Household Travel Survey*. 2009.

[5] Shiau, C-S, N. Kaushal, C.T. Hendrickson, S. Peterson, J. Whitacre and J.J. Michalek, 2010, "Optimal plug-in hybrid electric vehicle design and allocation for minimum life cycle cost, petroleum consumption, and greenhouse gas emissions," *ASME Journal of Mechanical Design, Special Issue on Sustainability*, v132 n9 p091013 1-11.

[6] Rakesh Patil, B.A., and Zoran Filipi, *Impact of Naturalistic Driving Patterns on PHEV Performance and System Design.* SAE 2009 Powertrains Fuels and Lubricants Meeting, 2009.

[7] Irene Michelle Berry, 2010, "*The Effects of Driving Style and Vehicle Performance on the Real-World Fuel Consumption of U.S. Light-Duty Vehicles*", MS Thesis, Massachusetts Institute of Technology

[8] Tulpule, P.; Marano, V.; Rizzoni, G.; , "Effects of different PHEV control strategies on vehicle performance," *American Control Conference, 2009. ACC '09.* , vol., no., pp.3950-3955, 10-12 June 2009 doi: 10.1109/ACC.2009.5160595\

[9] Sciarretta, A.; Back, M.; Guzzella, L.; , "Optimal control of parallel hybrid electric vehicles," *Control Systems Technology, IEEE Transactions on* , vol.12, no.3, pp. 352- 363, May 2004 doi: 10.1109/TCST.2004.824312

[10] Sciarretta, A.; Guzzella, L.; , "Control of hybrid electric vehicles," *Control Systems, IEEE* , vol.27, no.2, pp.60-70, April 2007 doi: 10.1109/MCS.2007.338280

[11] Moura, S.J.; Fathy, H.K.; Callaway, D.S.; Stein, J.L.; , "A Stochastic Optimal Control Approach for Power Management in Plug-In Hybrid Electric Vehicles," *Control Systems Technology, IEEE Transactions on* , vol.19, no.3, pp.545-555, May 2011 doi: 10.1109/TCST.2010.2043736

[12] Heywood, J. B., 2006, Fueling our Transportation Future, *Scientific American*, New York, NY.

[13] US Environmental Protection Agency, 2011, http://www.fueleconomy.gov/feg/label/

[14] Moawad, A., Singh, G., Hagspiel, S., Fellah, M., and Rousseau, A., 2009, "Impact of Real World Drive Cycles on PHEV Fuel Efficiency and Cost for Different Powertrain and Battery Characteristics," The 24th International Electric Vehicle Symposium and Exposition EVS-24, Stavanger, Norway, May 13–1

[15] Sharer, P., Leydier, R., and Rousseau, A., "Impact of Drive Cycle Aggressiveness and Speed on HEVs Fuel Consumption Sensitivity," SAE Technical Paper 2007-01-0281, 2007, doi:10.4271/2007-01-0281.

[16] Fontaras, G., P. Pistikopoulos, and Z. Samaras, *Experimental evaluation of hybrid vehicle fuel economy and pollutant emissions over real-world simulation driving cycles.* Atmospheric Environment, 2008. **42**(18): p. 4023-4035.

[17] Tate, E.D., *The Electrification of the automobile.* 2008.

[18] Southern California Association of Governments; Year 2000 Post-Census Regional Travel Survey, Fall 2003

[19] Energy and Environmental Analysis, Inc, "Owner Related Fuel Economy Improvements," (Arlington, VA: Energy and Environmental Analysis, Inc, December 2001); available at: http://www.fueleconomy.gov/Feg/pdfs/OwnerRelatedFuelEconomyImprovements.pdf

[20] Whitefoot, J.W., K. Ahn, and P.Y. Papalambros, *The Case for Urban Vehicles: Powertrain Optimization of a Power-Split Hybrid for Fuel Economy on Multiple Drive Cycles.* ASME Conference Proceedings, 2010. (44120): p. 197-204.

[21] Patil, R., Adornato, B., and Filipi, Z., 2010,"Design Optimization of a Series Plug-In Hybrid Electric Vehicle for Real-World Driving Conditions", SAE Technical Paper 2010-01-0840

[22] Fellah, M., Signh, G., Rousseau, A., Pagerit, S., Nam, E., and Hoffman, G., 2009, "Impact of Real-World Drive Cycles on PHEV Battery Requirements", SAE Technical Paper 2009-01-1383,

[23] Administration, U.S.E.I. *Annual Energy Review 2009* http://www.eia.gov/cneaf/electricity/epa/figes1.html.

[24] Lipman T, and Delucchi M (2010) Expected greenhouse gas emission reductions by battery, fuel cell, and plug-in hybrid electric vehicles. *Electric and Hybrid Vehicles: Power Sources, Model, Sustainability, Infrastructure and the Market*, ed Pistoia G (Elsevier, Amsterdam), pp 113–153.

[25] Weber, C.L. , Jaramillo, P., Marriott, J. , Samaras, C., 2010, Life cycle assessment and grid electricity: what do we know and what can we know? Environmental Science & Technology http://dx.doi.org/10.1021/es9017909

[26] Sioshansi R, Denholm P (2009) Emissions impacts and benefits of plug-in hybrid electric vehicles and vehicle-to-grid services. Environ Sci Technol 43:1199–1204

[27] Samaras, C. and K.s.w. Meisterling, *Life Cycle Assessment of Greenhouse Gas Emissions from Plug-in Hybrid Vehicles: Implications for Policy*. Environmental Science & Technology, 2008. **42**(9): p. 3170-3176.

[28] Elgowainy, A., Burnham, A., Wang, M., Molburg, J., and Rousseau, A., "Well-to-Wheels Energy Use and Greenhouse Gas Emissions Analysis of Plug-in Hybrid Electric Vehicles," Argonne National Laboratory Report ANL/ESD/09-2, February 2009

[29] Ching-Shin Norman Shiau, Nikhil Kaushal, Chris T. Hendrickson, Scott B. Peterson, Jay F. Whitacre, and Jeremy J. Michalek. Optimal plug-in hybrid Electric Vehicle design and allocation for minimum life cycle cost, petroleum consumption, and Greenhouse gas emissions.
Journal of Mechanical Design, 132:091013—1 — 11, 2010

[30] Laboratory, A.N., *Well-to-Wheels Energy Use and Greenhouse Gas Emissions Analysis of Plug-in Hybrid Electric Vehicles*. 2009.

[31] Michalek, J.J., M. Chester, P. Jaramillo, C. Samaras, C.S. Shiau, and L. Lave (2011) "*Valuation of plug-in vehicle life cycle air emissions and oil displacement benefits*"Proceedings of the National Academy of Sciences, v108 n40 p16554-16558.

[32] Argonne National Laboratory, 2008. Powertrain Systems Analysis Toolkit (PSAT), http://www.transportation.anl.gov/modeling_simulation/PSAT/psat.html

[33] Austin, Thomas C., Francis J. DiGenova, Thomas R. Carlson, Richard W. Joy, Kathryn A. Gianolini, and John M. Lee, "*Characterization of Driving Patterns and Emissions from Light-duty Vehicles in California*," Report No. A932-185 (Sacramento, CA: Sierra Research, Inc., 1993).

[34] EPA, “Fuel Economy Labeling of Motor Vehicles: Revisions To Improve Calculation of Fuel Economy Estimates,” 40 CFR Parts 86 and 600, Federal Register, vol. 71, no. 248 (27 December 2006); available at: http://www.epa.gov/fedrgstr/EPAAIR/2006/December/Day-27/a9749.pdf

[35] Aymeric Rousseau, Mohamed Fellah, Neeraj Shidore, R. “Barney” Carlson, “*Uncertainty Based on Real World Drive Cycles and Impact on Fuel Efficiency*”, International Conference on Li-ion Batteries for Automotive Applications, 2008.

[36] EPA, 2005. Emission Facts: Greenhouse Gas Emissions from a Typical Passenger Vehicle, EPA420-F-05-004, EPA420-F-05-004

[37] Plotkin S, Singh M (2009) Multi-Path Transportation Futures Study: Vehicle Characterization and Scenario Analysis (Argonne National Lab, US Dept Energy)

[38] Peterson, S. B., Whitacre, J. F., and Apt, J., 2010, “Lithium-Ion Battery Cell Degradation Resulting From Realistic Vehicle and Vehicle-to-Grid Utilization,” J. Power Sources, **195**(8), pp. 2385–2392

[39] Wang, M., Wu, Y., and Elgowainy, A., 2007, “GREET 1.7 Fuel-Cycle Model for Transportation Fuels and Vehicle Technologies,” Argonne National Laboratory, Argonne, IL.

[40] EPRI, 2007, “Environmental Assessment of Plug-in Hybrid Electric Vehicles. Volume 1: Nationwide Greenhouse Gas Emissions,” Electric Power Research Institute

[41] Neufville, R. D., 1990, Applied Systems Analysis: Engineering Planning and Technology Management, McGraw-Hill, New York

[42] Energy Information Administration, 2011, “The U.S. Weekly Retail Gasoline and Diesel Prices,” U.S. Department of Energy

[43] Energy Information Administration, 2011, “Average Retail Price of Electricity to Ultimate Customers: Total by End-Use Sector,” U.S. Department of Energy

[44] Peterson, S. B., Whitacre, J. F., and Apt, J., 2010, “The Economics of Using Plug-in Hybrid Electric Vehicle Battery Packs for Grid Storage,” J. Power Sources, **195**_8_, pp. 2377–2384.

[45] Shiau, C. S. N., Samaras, C., Hauffe, R., and Michalek, J. J., 2009, “Impact of Battery Weight and Charging Patterns on the Economic and Environmental Benefits of Plug-in Hybrid Vehicles,” Energy Policy, 377, pp. 2653–2663.

[46] Traut, E., C. Hendrickson, E. Klampfl, Y. Liu and J.J. Michalek (2012) “Optimal design and allocation of electrified vehicles and dedicated charging infrastructure for minimum life cycle greenhouse gas emissions and cost,” Energy Policy, v51 p524-534.

[47] Kelly, MacDonald and Keoleian “Time-dependent plug-in hybrid electric vehicle charging based on national driving patterns and demographics,” (2012) Energy Policy 94 p395-405

[48] Neubauer, Brooker and Wood (2012) “Sensitivity of battery electric vehicle economics to drive patterns, vehicle range, and charge strategies,” Journal of Power Sources 209 p269-277.

[49] Raykin, MacLean and Roorda (2012) “Implications of driving patterns on well-to-wheels performance of plug-in hybrid electric vehicles,” Environmental Science and Technology 46, 11, p6363-6370.

[50] Raykin, Roorda and MacLean (2012) “Impacts of driving patterns on tank-to-wheel energy use of plug-in hybrid electric vehicles,” Transportation Research Part D: Transport and Environment 17, 3, p243-250.

[51] Hawkins, Singh, Majeau-Bettez, and Stromman (2012) “Comparative environmental life cycle assessment of conventional and electric vehicles,” Journal of Industrial Ecology

[52] Peterson, S. and J.J. Michalek (2013) “Cost effectiveness of plug-in hybrid electric vehicle battery capacity and charging infrastructure investment for reducing US gasoline consumption,” Energy Policy, v52 p429-438.

[53] Congressional Budget Office, (2012). Effects of federal tax credits for the purchase of electric vehicles. In: Proceedings of the Congress of the United States, September 2012.

[54] Markel, Anthony J., and Andrew Simpson (2006), Plug-in hybrid electric vehicle energy storage system design. National Renewable Energy Laboratory.

[55] Neubauer, Brooker and Wood (2013) “Sensitivity of plug-in hybrid electric vehicle economics to drive patterns, electric range, energy management, and charge strategies,” Journal of Power Sources, in press

[56] Traut. E., TW Cherng, C Hendrickson and J. Michalek (2013) “U.S. residential charging potential for plug-in vehicles,” working paper, Department of Mechanical Engineering, Carnegie Mellon University.

[57] Axsen, J., Kurani, K.S., (2012), Who can recharge a plug-in electric vehicle at home? Transportation Research Part D: Transport and Environment 17, 349–353.

[58] Axsen, J., Kurani, K.S., (2012), Characterizing residential recharge potential for plug-in electric vehicles, in: Proceedings of the Transportation Research Board 91st Annual Meeting. Presented at the Transportation Research Board 91st Annual Meeting, Washington, D.C.

[59] Barnitt, R., A. Booker, L. Ramroth, J. Rugh and K. Smith (2010) “Analysis of off-board powered thermal preconditioning in electric drive vehicles,” Proceedings of the 25th World Battery, Hybrid and Fuel Cell Electric Vehicle Symposium and Exposition, Shenzhen, China Nov 5-9, 2010, National Renewable Energy Laboratory report NREL/CP-5400-49252.

3 OPTIMAL CO-DESIGN OF PLUG-IN HYBRID POWERTRAINS AND POTENTIAL OF PREDICTIVE CONTROL STRATEGIES TO DOWNSIZE BATTERIES

In Chapter 2, I investigated the impact of driving patterns on the lifetime cost and life cycle emissions of PHEVs. In this chapter, I focus on developing a combined design and control framework for a real world driving cycle. Then using our proposed framework, I estimate a bound on the potential of predictive control strategies to minimize battery sizing and lifetime cost of plug-in hybrid electric vehicles compared to rule-based control strategies. We account for design and control interactions by performing a parametric study over the vehicle design space, optimizing the controller for each design. We create a backward-looking quasi-static physics model of a parallel Plug-in hybrid powertrain. The vehicle design space - consisting of engine, motor and battery size variables - is discretized and searched exhaustively using an iteratively refined grid resolution to minimize lifetime cost or life cycle greenhouse gas emissions. For rule-based control, I add a rule parameter (engine on-off threshold) to the design space. For predictive control I apply dynamic programming, to identify the optimal controller for each design, providing an upper bound for benefits under perfect information. The optimal co-design of the powertrain has a 7.1 kWh battery, 77.7 kW motor and 46.1 kW engine with a predictive controller. When employed a rule based controller, the co-design has a 7.45kWh battery. For our test drive cycle, based on Kansas City data, the optimal battery size is reduced by 5% with dynamic programming compared to rule-based control and the lifetime cost by 0.4%. These savings are not dramatic, even when the driving patterns and conditions are perfectly known and consistent day-to-day, suggesting that predictive control will not play a major role in making

plug-in vehicles more competitive. However, given the size of the automobile market, predictive powertrain control may nevertheless contribute significant net savings and emission reductions if predictive control can approach the performance of optimal controllers under perfect information. Also results suggests that rule based controllers are good enough to be employed for design studies that optimize the powertrain over a distribution of driving patterns/distances which is computationally expensive using DP. Burak Yuksel, Guo Li, Lu Pan and Prof. Jeremy Michalek contributed to the project discussed here.

3.1 INTRODUCTION

Equipped with a motor, battery, and gasoline engine, plug-in hybrid electric vehicles (PHEVs) offer a viable solution to reduce gasoline consumption and potentially reduce emissions and ownership costs since they operate partly on inexpensive electricity that can be obtained from local, renewable, and less emissions-intensive energy sources than gasoline [1] [2] [3]. Their efficient powertrain architectures with multiple energy sources and regenerative braking capabilities introduce multiple degrees of freedom for design and energy management (control) decisions. Vehicle design includes multiple coupled decisions, such as battery, motor, and engine sizing, while controllers are developed to achieve efficiency. Vehicle system level control is responsible for the control of energy flow of components and depends on component capabilities, such as battery capacity and engine and motor efficiency maps and torque capabilities. Yet vehicle performance criteria, such as fuel economy, all electric range, and acceleration depend on the controller [4]. Thus the design and control problems are coupled, and treating them separately can produce suboptimal results [5].

Furthermore, life cycle benefits of PHEVs depend on the driving conditions, including driving style [3] and distance [2] Real world driving conditions vary among drivers and over time, so vehicles optimized for a single test cycle or average driving distance can perform poorly over a range of real driving conditions [6] [7].

The distance that PHEVs can travel using only electricity depends on the size of the battery pack. Large battery packs can extend electric range and lower fuel consumption; however, they are associated with high investment costs, additional production emissions, and extra vehicle mass, which can decrease efficiency [2] [8]. Better energy management and control can improve efficiency and range by determining the best time to draw power from the electrical system vs. the gasoline engine, thus reducing battery requirements and lowering costs.

Knowing about the road trip, drive cycle, can significantly decrease fuel and electricity consumption of plug-in hybrid vehicles, furthermore increased efficiency might lead to downsized components such as reduced battery and mass. Reduction in component sizes will ultimately lead to overall mass reduction which will further increase efficiency in a compounded effect. Also terrain information could help to effectively make better use of batteries. If it is known that there is an upcoming downhill part of the trip, which can be used for recharging of the battery, then using cheap electricity beforehand and deploying battery to a certain level would be a smart control decision.

We propose an approach to evaluate the impact of predictive control strategies on the optimal sizing and cost of plug-in hybrid powertrains using driving styles and distances informed by GPS and travel survey data. We proceed as follows: Section 3.2 reviews relevant literature and positions our contribution; Section 3.3 defines the methodology and data; Section 3.4 presents results with discussion; and Section 3.5 summarizes conclusions.

3.2 LITERATURE REVIEW

The literature on optimal design and control of electrified vehicles can be categorized into literature on (1) optimal vehicle design, (2) optimal vehicle control, (3) optimal combined vehicle design and control. We review each in turn.

Vehicle design optimization is typically performed to maximize vehicle efficiency under a single driving cycle. Whitefoot et al. [6] compared the optimal power split HEV under different driving cycles for minimal fuel consumption, finding that vehicles designed for one driving cycle show significantly lower performance on other drive cycles (up to 9.8% lower efficiency), and vehicles designed for different drive cycles show variation of up to 41% in electric motor size. Sundstrom et. al [9] analyzed the optimal vehicle hybridization and concluded that full hybridization results in lower fuel consumption for several drive cycles compared to torque assist. Patil et al. [10] optimized a series PHEV for naturalistic drive cycles and showed that the higher energy demands of real world cycles require larger batteries to meet AER targets. Fellah et al. [11] found that if batteries of PHEVs are sized for the UDDS cycle, only 22% of 363 trips from a Kansas City GPS data set can be driven in all electric mode due to power limitations. Shiau et al. [7] and Traut et al. [12]optimized HEV and PHEV design and allocation based on driving distance to minimize life cycle cost and GHG emissions.

Optimal vehicle control is typically performed for a fixed vehicle design to maximize efficiency under a given driving cycle. Dynamic programming (DP) can be used to obtain globally optimal controllers for a given driving cycle in a discretized time and state space, but the resulting controllers are not generalizable to driving conditions different from those it was optimized for. Some researchers have derived general rule-based controllers by manually examining dynamic programming controller results and posing rules that have similar behavior

to DP results. Alternatively, stochastic dynamic programming (SDP) can be used to create generalizable controllers.

Tate and Boyd [13] formulated the efficiency maximization problem as a nonlinear convex problem which later is approximated into a large linear problem. They found the ultimate limit of performance for a series hybrid propulsion employing dynamic programming. They found that by selecting a simple rule-based controller, they could achieve 73% of the DP controller performance.

Lin et al. [14] implemented dynamic programming (DP) to find the optimal energy management of a parallel hybrid electric truck. The study states that by analyzing the dynamics of the powertrain due to DP control actions, near-optimal rules can be obtained, which, unlike DP control signals, are implementable. They have improved the preliminary rule-based strategy by using the insight from DP control policy and reduced its performance gap to the globally optimal (DP) results by 50–70%.

Lin et al. [15] optimized a hybrid vehicle control strategy using stochastic dynamic programming (SDP) and found that SDP controller outperforms the Rule based controllers. Moura et al. [16], [17] used SDP to find optimal energy management of PHEVs and the tradeoff between battery energy capacity and power management. Tate et al.[18] used shortest path stochastic dynamic programming (SP-SDP) for fuel and emission minimization which allows better SOC management and fewer parameters to tune. Opila et al. [19] introduced drivability factors into SP-SDP formulation where the drive cycle is modeled as a Markov Chain. They report having improved the fuel economy by 11% for equivalent drivability compared to baseline controller. Sciarretta et al. [20] introduced a model based for the real time energy management of

parallel hybrid vehicles which minimizes the instantaneous cost function while measuring the vehicle system status online.

A few researchers have examined the combined design and control problem. Fang et al. [5] used a multi-objective genetic algorithm to optimize design and control parameters simultaneously to obtain a Pareto surface of fuel economy, emissions and drivability. Vijayagopal et al. [21] optimized the battery size as well as the engine on-off threshold parameters of the instantaneous control strategy simultaneously for net present value of a series PHEV using the DIRECT algorithm. The study emphasized the need for the reductions in initial investment cost.

Our proposed contribution aims to build on the prior literature in four ways: (1) we follow the literature on combined design and control in order to avoid suboptimal solutions that result from holding design or control parameters fixed or solving them sequentially; (2) we minimize lifetime costs rather than maximize efficiency, since Shiau et al [22] showed that using minimum fuel consumption instead of life cycle cost as an objective yields plug-in vehicles with larger batteries, which are associated with higher lifetime cost; (3) we optimize performance over a representative real world driving cycle with a length of 22 miles which is the average daily trip length National Household Travel Survey (NHTS) reports; and (4) we optimize the controller using dynamic programming to achieve best case results and avoid limiting the controller to a particular rule-based structure, (5) for comparison, we optimize the controller with a rule based controller and compare the results and their implications to that of dynamic programming.

Vijayagopal et al. [21] similarly optimize the joint vehicle design and controller for lifetime costs; however, the vehicle design is limited to battery sizing with a predetermined motor and engine size; their controller architecture is limited to a simple rule-based on/off

threshold parameter; and they use a single fixed daily driving distance, accounting only for the reduction in daily distance driven due to vehicle age. We aim to improve upon this work by generalizing the design to include synergistic engine, motor and battery sizing, by generalizing the controller beyond threshold parameters to a dynamic programming space.

Dynamic programming is a strong approach to find the optimal energy flow management of vehicles with multiple energy sources associated with different costs. Dynamic programming requires exact knowledge of the power demand (road demand, drive cycle, duty cycle) thus it is not directly implementable in real world. However through observation of the optimal system dynamics under various road demand and creation of basic control rules that mimic those behaviors to implement real time. However in his study we shed different light on dynamic programming. We use dynamic programming to find the achievable upper bound of performance by any controller. For example, predictive controllers can approximate to dynamic programming solutions when assisted by GPS, traffic monitoring, a database of driver`s behavior etc. In this study, we show the improvement space for PHEV technology via better control (how much can we improve the design via designing better controllers and treating design and control simultaneously) by comparing the optimal co-designs and their lifetime cost when a predictive controller employed with some information about the trip vs. rule based controller which has no information about the trip, looks at the current vehicle dynamics and makes decisions.

Although we have used a single drive cycle due to the computational burden, when a variety of driving patterns used, vehicle design would be not optimal but also robust since it minimizes the life cycle cost for various driving conditions and distances that the vehicle can be exposed to in real world. During the procedure to find optimal design, we account for variation

and uncertainty in driving patterns, however we assume that once the variation has occurred the vehicle controller knows it to the end of the trip. We base this assumption to the fact that road demand can be fairly approximated. Thus the better the control capability, the closer the optimal design will approach to the their variation

PHEVs have three main powertrain components: an electric motor, a gasoline engine and a battery pack which can be recharged using an external power outlet. Operation modes of PHEVs can be categorized into two.: (1) Charge-Depleting (CD) mode refers to the phase where the battery state of charge (SOC) is above the target SOC, and the vehicle receives some or all of its net propulsion energy from the battery pack. Once the battery is depleted to a target SOC, the vehicle switches to (2) Charge-Sustaining (CS) mode, in which gasoline is used to provide all net propulsion energy and the electrical system is used only as momentary storage to improve fuel economy, similar to a grid-independent HEV. Some PHEVs operate CD-mode using only electrical energy. Such a configuration, referred to as an all-electric control strategy or an extended-range electric vehicle (EREV), enables short trips to be driven without any gasoline consumption but requires motor and battery designs that can deliver the vehicle's maximum power demands. Other PHEV designs operate CD-mode using a mixture of gasoline and electrical energy. Such a configuration, referred to as a blended control strategy, does not eliminate gasoline consumption even for short trips, but power demands on electrical components are lower, allowing smaller, cheaper components to be used. In this work, we work on the blended mode control strategy where the improvement has the potential to downsize components.

Hybridization can be based on 3 specific powertrain architectures: (1) Series, where the engine turns the generator which generates electricity to be used by the electric motor to turn the

wheels; (2) parallel, which is capable of transmitting power to the wheels from two different energy sources; and (3) split, which can operate both in series and parallel. In this study we focus on a parallel architecture.

3.3 METHODOLOGY

3.3.1 Vehicle Co-Design Framework

We modeled a plug-in hybrid electric vehicle based on a parallel powertrain architecture by building on the concepts in [9][23] and using component efficiency maps from the Powertrain Systems Analysis Toolkit (PSAT) [24]. We adopted a quasi-static modeling approach, which neglects higher order terms of the dynamic model, to minimize computational burden, allowing us to identify the globally optimal supervisory control strategy in a reasonable time [23]. Quasi-static fuel economy calculations are reliable enough for control strategy optimization, since the total deviation of the fuel economy estimates from experimental data using hardware in loop simulations has been shown to be below 0.5% in several studies [25][26]. The drawback of the quasi-static method is its 'backward' formulation: the driving profile to be followed must be known a priori. The main components of the PHEV model are an internal combustion engine (ICE), an electric motor (EM) and a battery. The input parameters include the speed-acceleration profile of the drive cycle to be executed. Battery state-of-charge is a state variable.

The optimal design for PHEV component sizing depends on the control strategy used, and the optimal control strategy depends on the vehicle design. We use a nested strategy, described in Figure 3-1, to globally optimize the controller for a given vehicle design using

dynamic programming in an inner loop and globally optimize the design itself in an outer loop for minimum lifetime cost or lifecycle GHGs. We discuss the vehicle optimization and controller optimization formulations in turn.

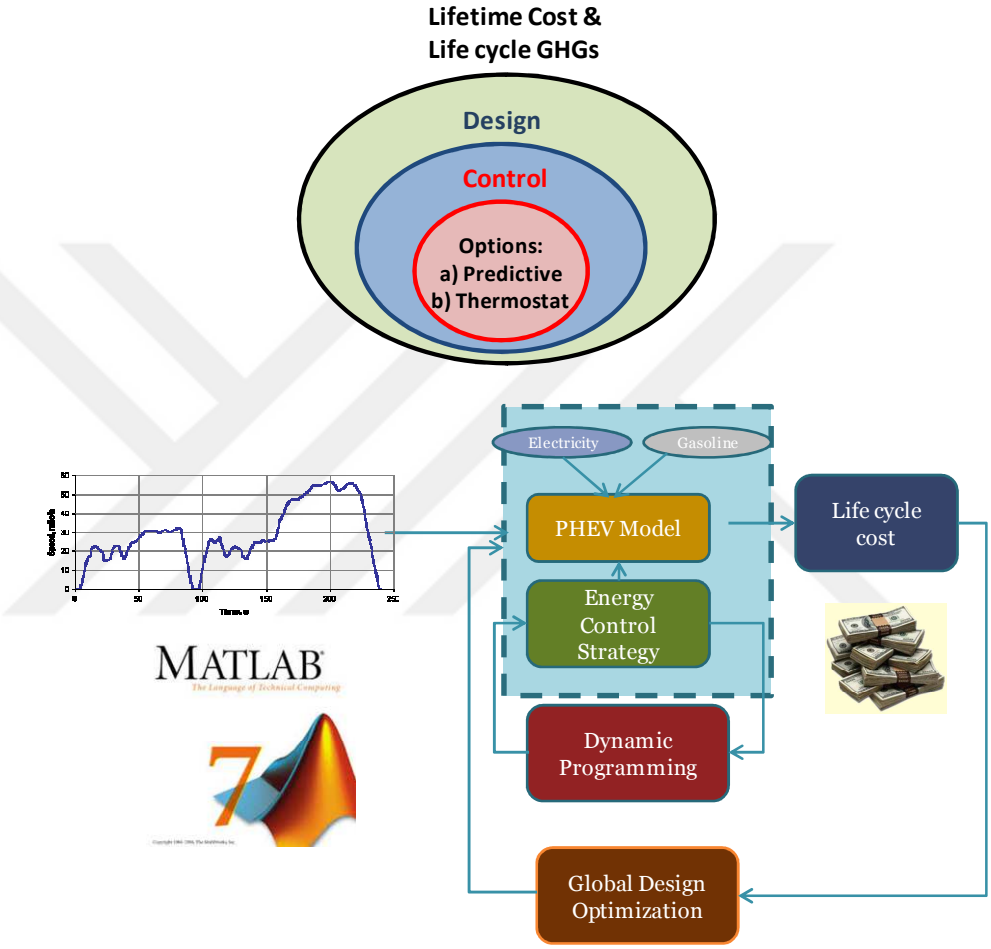

Figure 3-1 Proposed Methodology to determine the potential of intelligent controllers to downsize components and reduce costs.

In the design optimization formulation, **d** is the vehicle design vector containing design variables d_1, d_2, d_3, which stand for battery size in kWh, motor size in kW, and engine size in kW, respectively; c_{LC} is the annualized lifetime cost objective in U.S. dollars per year; c_{ENG}, c_{MOT}, c_{BAT}, and c_{BODY} are the cost of the engine, motor, battery and vehicle body, respectively,

which are given in Figure 3-1; $c_{\mathrm{OP}}^{\mathrm{D}}$ is the operation cost, which is the cost of gasoline and electricity; D = 360 is the driving days per year; $f_{\mathrm{A|P}}$ is the capital recovery factor for a general discount rate r and time period N in years;

(1) Parametric Design Study (Equation 3-1)

$$\text{Select } \mathbf{d}^{*} \text{ that is associated with the minimum } c^{*}_{\mathrm{LC}}(\mathbf{d}) \text{ from the set } S$$

$$S=\left\{\mathbf{d}:\left(\mathbf{d}_{\mathrm{MIN}}\le\mathbf{d}\le\mathbf{d}_{\mathrm{MAX}};\, f_{\mathrm{ACCEL}}(\mathbf{d})\le 11;\, c_{\mathrm{OP}}^{\mathrm{D}}(\mathbf{d})\in\mathbb{R}\right)\right\}$$

where

$$\mathbf{d}=\begin{bmatrix} d_1 & d_2 & d_3 \end{bmatrix}^{\mathrm{T}}$$

$$c_{\mathrm{LC}}(\mathbf{d})=\begin{pmatrix} c_{\mathrm{BODY}}+c_{\mathrm{ENG}}(d_2)+ \\ c_{\mathrm{MOT}}(d_3)+c_{\mathrm{BAT}}(d_1) \end{pmatrix} f_{\mathrm{A|P}}(r_{\mathrm{N}},T_{\mathrm{VEH}}) + Dc_{\mathrm{OP}}^{\mathrm{D}}(\mathbf{d})\frac{f_{\mathrm{A|P}}(r_{\mathrm{N}},T_{\mathrm{VEH}})}{f_{\mathrm{A|P}}(r_{\mathrm{R}},T_{\mathrm{VEH}})}$$

$$\text{and } f_{\mathrm{A|P}}(r,N)=\left(\sum_{n=1}^{N}\frac{1}{(1+r)^{n}}\right)^{-1}=\frac{r(1+r)^{N}}{(1+r)^{N}-1};$$

(2) Control Optimization Formulation (Equation 3-2)

$$c_{\mathrm{OP}}^{\mathrm{D}}(\mathbf{d},s)=\min_{\mathbf{u}\in U_s(\mathbf{d})}\sum_{k=1}^{N_s-1}H_{s,k}(\mathbf{d},u_k)$$

$$H_{s,k}(\mathbf{d},u_k)=c_{\mathrm{G}}\Delta_{s,k}^{\mathrm{GAS}}(\mathbf{d},u_k)+c_{\mathrm{E}}\Delta_{s,k}^{\mathrm{ELEC}}(\mathbf{d},u_k);$$

$$\mathbf{u}=\left[u_1,\ldots,u_k,\ldots,u_{N_s-1}\right]^T;$$

$$U_s(\mathbf{d})=\left\{\begin{array}{c}\mathbf{u}\,|\,\mathbf{u}\in\mathbb{R}^{N_s-1};\ -\mathbf{1}\le\mathbf{u}\le\mathbf{1};\\ \tau_{\mathrm{MIN}}^{\mathrm{M}}(\mathbf{d})\le u_k\tau_{s,k}^{\mathrm{REQ}}\le\tau_{\mathrm{MAX}}^{\mathrm{M}}(\mathbf{d});\\ \tau_{\mathrm{MIN}}^{\mathrm{E}}(\mathbf{d})\le(1-u_k)\tau_{s,k}^{\mathrm{REQ}}\le\tau_{\mathrm{MAX}}^{\mathrm{E}}(\mathbf{d});\\ \omega_{\mathrm{MIN}}^{\mathrm{E}}(\mathbf{d})\le\omega_k^{\mathrm{E}}\le\omega_{\mathrm{MAX}}^{\mathrm{E}}(\mathbf{d});\\ \omega_{\mathrm{MIN}}^{\mathrm{M}}(\mathbf{d})\le\omega_k^{\mathrm{M}}\le\omega_{\mathrm{MAX}}^{\mathrm{M}}(\mathbf{d})\\ x_{\mathrm{MIN}}\le x_k(\mathbf{d},u_k)\le x_{\mathrm{MAX}};\\ x_{k+1}(\mathbf{d})=x_k(\mathbf{d})+f_k^{\mathrm{SIM}}(\mathbf{d},x_k,u_k);\\ P_{\mathrm{MIN}}^{\mathrm{BAT}}(\mathbf{d})\le P_k^{\mathrm{BAT}}(\mathbf{d},u_k)\le P_{\mathrm{MAX}}^{\mathrm{BAT}}(\mathbf{d});\\ \forall k\in\{1,2,...,N_s-1\}\\ (\tau^{\mathrm{E}},\omega_k^{\mathrm{E}})\in M^{\mathrm{E}}\\ (\tau^{\mathrm{M}},\omega_k^{\mathrm{M}})\in M^{\mathrm{M}}\end{array}\right\}$$

T_{VEH} is the vehicle life in years, respectively where they equal to 19 years (for an NHTS average daily driving distance of 22 miles for a vehicle life of 150,000 miles); $\mathbf{d}_{\mathrm{MIN}}$ = [1kWh, 25kW, 25kW]$^{\mathrm{T}}$ and $\mathbf{d}_{\mathrm{MAX}}$ = [15kWh, 120kW, 120kW]$^{\mathrm{T}}$ are the simple bounds on the design variables; and $\mathrm{f}_{\mathrm{ACCEL}}(\mathbf{d})$ is the acceleration time from 0-60 mph computed by a forward looking vehicle simulation model shown in Figure 3-4. ω_{E} and ω_{M} are the angular velocities of the engine and motor and limited by $\omega_{\mathrm{MIN}}^{\mathrm{E}}$, $\omega_{\mathrm{MIN}}^{\mathrm{M}}$ and $\omega_{\mathrm{MAX}}^{\mathrm{E}}(\mathbf{d})$, $\omega_{\mathrm{MAX}}^{\mathrm{M}}(\mathbf{d})$ respectively. $c_{\mathrm{OP}}^{\mathrm{D}}(\mathbf{d})$ is the daily operation cost (depends on the energy management strategy) for design **d** which is found by the summation of single operation costs $c_{\mathrm{OP}}^{\mathrm{P}}(\mathbf{d},s)$ for a driving cycle *s* with a distance of 22 miles which is the average daily driving distance based on NHTS 2009 data

The minimum $c_{\mathrm{OP}}^{\mathrm{P}}(\mathbf{d}, s)$ found via dynamic programming, where k is the time step index, u_k is the control action representing the portion of vehicle torque demand supplied by the electric motor vs. the gasoline engine at time step k; U is the set of feasible control actions; $H_{s,k}(\mathbf{d}, u_k)$ is the cost of control action u_k at time step k for the driving cycle indexed by s (Eq. 28), N_s is the total number of time steps for the driving cycle of length s; c_{G} and c_{E} are the cost of gasoline and electricity in \$/kg and \$/W.s, respectively; $\Delta_{s,k}^{\mathrm{GAS}}(\mathbf{d}, u_k)$ and $\Delta_{s,k}^{\mathrm{ELEC}}(\mathbf{d}, u_k)$ are the gasoline consumption in kg/s and electricity consumption in Ws during the time step k of the drive cycle indexed by s, respectively; $x_k(\mathbf{d})$ is the energy-based battery state of charge (SOC) expressed as a % of capacity at time step k for design $\mathbf{d}$; x_{MIN} and x_{MAX} are the minimum and maximum allowable SOC, respectively; $f_k^{\mathrm{SIM}}(\mathbf{d}, x_k, u_k)$ is the change in state calculated via vehicle simulation, $\tau_{s,k}^{\mathrm{REQ}}$ is the required torque demand to follow the drive cycle (speed profile) at time step k, $\tau_{s,k}^{\mathrm{M}}$ and $\tau_{s,k}^{\mathrm{E}}$ are the portions of torque taken from motor and engine to meet the road demand at time step k for drive cycle indexed by s, $P_{\mathrm{MAX}}^{\mathrm{BAT}}(\mathbf{d})$ and $P_{\mathrm{MIN}}^{\mathrm{BAT}}(\mathbf{d})$ are the charging and discharging power limits for the battery power, $P_k^{\mathrm{BAT}}(\mathbf{d}, u_k)$. Inequality sets constrain the set of admissible state and control region. M^{E} and M^{M} are the sets including the valid domain of the engine and motor maps, respectively. If a determined operation point falls onto outside of the valid component map, then that designs is not valid. If*(2) Control Optimization Formulation* (Equation 3-2*(2) Control Optimization Formulation* (Equation 3-2 has no feasible solution, $c_{\mathrm{OP}}^{\mathrm{D}}(\mathbf{d})$ is undefined and is not considered a valid point in *(1) Parametric Design Study* (Equation 3-1)

The outer loop optimization problem *(1) Parametric Design Study* (Equation 3-1) is a challenging nonconvex problem with potential discontinuities, since the optimal controller $\mathbf{u}^*$ is computed for each candidate design **d** using a dynamic programming routine as an internal loop. This is the reason a parametric study approach has been adopted for the outside design loop to see the design-control interactions. Such an approach is tractable because the design space is low-dimension.

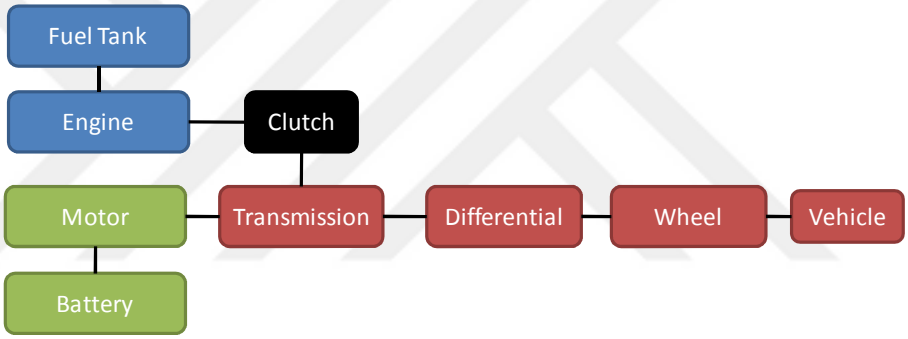

Figure 3-2 Full Parallel PHEV

The vehicle model is full parallel PHEV means that there is a clutch between engine and crankshaft, which can disable the link between them while only the electric motor is operating. Since the torque supplies are engine and the electric motor, the sum of engine and motor torques will give us the total torque.

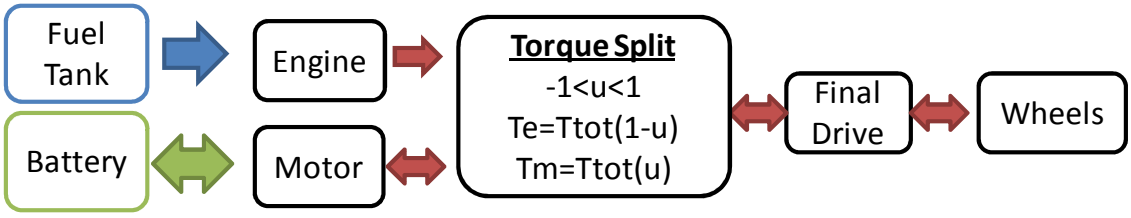

Figure 3-3 Parallel Vehicle Power Flow

3.3.2 Computing Operation Cost with a Globally Optimal Cost-Minimizing Controller

Drive cycle, also called test cycle, duty cycle or speed profile, is a series of target speed values of a vehicle over time. Vehicle system level controller sends control inputs to vehicle components to follow the drive cycle. Fuel economy is estimated by calculating the energy consumed during this process. Federal test cycles are associated with gentle speed profiles, and drivers usually observe higher fuel consumption in real world. We have used a real world drive cycle from Kansas City driving data.

Given the required drive cycle velocity *s* and acceleration a_k at each time step *k*, one can calculate the power, torque, and speed demands for all components in the vehicle at each time step and determine their implications for fuel consumption. In backwards, we begin with road demand characteristics and sequentially compute wheel demand, pre-transmission demand, torque demand split between the engine and motor, fuel consumption from the engine and motor, and finally battery state tracking.

Road demand characteristics:

The wheel variables are defined as speed, acceleration, torque and power values of the vehicle wheel. The angular wheel speed is calculated by

$$\omega_{\mathrm{V}k,s} = \frac{v_{\mathrm{V}k,s}}{r_{\mathrm{W}}} \tag{3-3}$$

where $v_{\mathrm{V}k}$ is the vehicle speed from drive cycle, r_{W} is the wheel radius. The angular wheel acceleration is calculated by,

$$\dot{\omega}_{\mathrm{V}k,s} = \frac{a_{\mathrm{V}k,s}}{r_{\mathrm{W}}} \tag{3-4}$$

where $a_{\mathrm{V}k}$ is the vehicle acceleration from given drive cycle. The demanded torque from the wheels is calculated as follows,

$$\tau_{\mathrm{V}k,s} = \left(F_{\mathrm{R}} + C_{\mathrm{D}} v_{\mathrm{V}k,s}{}^{2} + m_{\mathrm{V}}(\mathbf{d}) a_{\mathrm{V}k,s}\right) r_{\mathrm{W}} \tag{3-5}$$

where F_{R} represents the rolling friction, C_{D} is the aerodynamic coefficient, and m_{v} is the mass of the vehicle where the change in elevation, or non-horizontal movement is neglected; so the force caused by gravity is ignored. m_{V} is a function of design vector $\mathbf{d}$. Change in mass due to fuel consumption are large battery sizes potentially introduce mass to the vehicle and increase road demand.

1) Pre-transmission demand:

The transmission multiplies the wheel variables by constant gear ratios. These series of numbers can be found in [5]. The crankshaft speed is calculated by,

$$\omega_{\mathrm{C}k,s} = \omega_{\mathrm{V}k,s} \mathrm{r}_{\mathrm{G}k,s} \tag{3-6}$$

where r_{Gk} represents the number of teeth of the gear used at time step *k*. We pre-specify the appropriate gear for each time step *k* based on driving cycle demands as follows:

$$\mathrm{r}_{Gk,s} = f(v_{Vk,s}) \tag{3-7}$$

Secondly, the crankshaft acceleration is calculated as,

$$\alpha_{Ck,s} = a_{Vk,s} r_{Gk,s} \tag{3-8}$$

The crankshaft torque is found with following equations,

$$\begin{aligned} \tau_{Ck,s} &= \frac{\tau_{Vk,s}}{r_G \eta_G}, \quad \tau_{Vk,s} > 0 \\ \tau_{Ck,s} &= \frac{\tau_{Vk} \eta_G}{r_{Gk}}, \quad \tau_{Vk,s} \le 0 \end{aligned} \tag{3-9}$$

where η_G is the efficiency of the gearbox, which is taken as a constant value. Since the efficiency means ratio of the output to the input, the direction or sign of the torque value will change the calculation of the crankshaft torque.

2) Torque split between ICE and EM:

The total torque demand of the vehicle is found by the sum of the engine drag torque $\tau^{D}_{Ek,s}$, motor drag torque $\tau^{D}_{Mk,s}$ and the crankshaft torque. The engine drag torque is calculated as in [1],

$$\tau^{\mathrm{D}}_{\mathrm{E}k,s} = \alpha_{\mathrm{C}k,s}\mathrm{I}_{\mathrm{E}k,s} + f(p_{\mathrm{M}}, \omega_{\mathrm{C}k,s}) \tag{3-10}$$

where I_{E} is the engine inertia, and the second term represents the effect of speed $\omega_{\mathrm{C}k,s}$, and drag mean pressure, p_{M} , on the engine drag torque [1], [2]. Motor drag torque is found by,

$$\tau^{\mathrm{D}}_{\mathrm{M}k,s} = \alpha_{\mathrm{C}k,s} I_{\mathrm{M}} \tag{3-11}$$

where I_{M} is the electric motor inertia. The total torque demand must be supplied by the engine and motor, so:

$$\tau_{\mathrm{E}k,s} + \tau_{\mathrm{M}k,s} = \tau^{\mathrm{D}}_{\mathrm{E}k,s} + \tau^{\mathrm{D}}_{\mathrm{M}k,s} + \tau_{\mathrm{C}k,s} \tag{3-12}$$

The optimal splitting ratio $u^{*}_{k,s}$, the control variable of our optimal control problem, determines how much torque to draw from the engine vs. motor:

$$\begin{aligned} \tau_{\mathrm{E}k,s} &= (1-u^{*}_{k,s})\left(\tau^{\mathrm{D}}_{\mathrm{E}k,s} + \tau^{\mathrm{D}}_{\mathrm{M}k,s} + \tau_{\mathrm{C}k,s}\right) \\ \tau_{\mathrm{M}k,s} &= u^{*}_{k,s}\left(\tau^{\mathrm{D}}_{\mathrm{E}k,s} + \tau^{\mathrm{D}}_{\mathrm{M}k,s} + \tau_{\mathrm{C}k,s}\right) \end{aligned} \tag{3-13}$$

When $u_{k,s} = 1$, then the vehicle will be propelled only by motor, and when $u_{k,s} = 0$ the vehicle will be propelled only by the engine.

3) Calculation of fuel consumption and power values of ICE and EM:

So far, the engine torque and crankshaft speed has been found. The fuel mass flow, or the fuel consumption for each time step will be a function of engine power $\tau_{ek}.\omega_{ck}$, engine efficiency η_{E} and the lower heating value as follows Q_{LHV},

$$\Delta_{s,k}^{\mathrm{GAS}}\left(\mathbf{d},u_k\right)=\frac{\tau_{\mathrm{E}k,s}\omega_{\mathrm{C}k,s}}{\eta_{\mathrm{E}}Q_{\mathrm{LHV}}}$$
$$\eta_{\mathrm{E}}=f\left(\omega_{\mathrm{C}k,s},\tau_{\mathrm{E}k,s},d_3\right) \tag{3-14}$$

where d_3 represents the engine size, which scales the engine efficiency. The chemical power produced by the ICE is,

$$P_{\mathrm{E}k,s}^{\mathrm{CH}}=\Delta_{s,k}^{\mathrm{GAS}}\left(\mathbf{d},u_k\right)Q_{\mathrm{LHV}} \tag{3-15}$$

The mechanical power delivered to the crankshaft by the ICE is calculated as,

$$P_{\mathrm{E}k,s}^{\mathrm{MECH}}=\tau_{\mathrm{E}k,s}\omega_{\mathrm{C}k,s}=P_{\mathrm{E}k,s}^{\mathrm{CH}}\eta_{\mathrm{E}} \tag{3-16}$$

The operation cost $H_{s,k}\left(\mathbf{d},u_k\right)$ at time step k is the sum of two terms; gasoline consumption cost and electric consumption cost at time step k. Gasoline cost c_{G} is \$3.3 corresponding to 1.044 \$/kg and electricity cost c_{E} is \$0.11/kWh.

$$H_{s,k}\left(\mathbf{d},u_k\right)=c_{\mathrm{G}}\Delta_{s,k}^{\mathrm{GAS}}\left(\mathbf{d},u_k\right)+c_{\mathrm{E}}\Delta_{s,k}^{\mathrm{ELEC}}\left(\mathbf{d},u_k\right) \tag{3-17}$$

Electric motor of the vehicle has the power equations as follows

$$P_{Mk} = \omega_{Ck}\tau_{Mk}\eta_M, \quad \tau_{Mk} < 0$$
$$P_{Mk} = \frac{\omega_{Ck}\tau_{Mk}}{\eta_M}, \quad \tau_{Mk} \geq 0 \tag{3-18}$$

When $\tau_{Mk} < 0$, then EM is charging the batteries and it is discharging in the case of $\tau_{Mk} \geq 0$. η_M represents the EM efficiency map and it is the function of crankshaft speed and motor torque. This map is being updated by the input of motor size, d_2 for each cycle of inner loop.

$$\eta_M = f(\omega_{Ck}, \tau_{Mk}, d_2) \tag{3-19}$$

The second component of the operation cost results from the electricity consumption $\Delta_{s,k}^{ELEC}(\mathbf{d}, u_k)$ which is basically the motor power P_{Mk} at time step *k*. Electricity cost c_E is 0.11$/kWh and cost of electricity consumption in Ws is given by

$$c_E \Delta_{s,k}^{ELEC}(\mathbf{d}, u_k) \tag{3-20}$$

The total operational cost of PHEV at time step *k* for the deterministic drive cycle in the terms of $ is given below:

$$H_{s,k}(\mathbf{d}, u_k) = c_G \Delta_{s,k}^{GAS}(\mathbf{d}, u_k) + c_E \Delta_{s,k}^{ELEC}(\mathbf{d}, u_k) \tag{3-21}$$

and the total cost during the whole drive cycle can be found by

$$\sum_{k=1}^{N_s-1} H_{s,k}\left(\mathbf{d}, u_k\right) \tag{3-22}$$

1) Electric path and battery equations:

Battery pack of the plug-in vehicle consists of series and parallel battery cells and modeled as a voltage source in series with a resistance. Battery current can be derived as follows [1,2,10,11]

$$I_{\mathrm{B}k} = \eta_{\mathrm{C}} \frac{V_{\mathrm{B}k}(x_k, \mathbf{d}) - \sqrt{V_{\mathrm{B}k}^2(x_k, \mathbf{d}) - 4R_{\mathrm{B}k}(x_k, \mathbf{d})P_{\mathrm{M}k}(x_k, \mathbf{d})}}{2R_{\mathrm{B}k}(x_k, \mathbf{d})} \tag{3-23}$$

where η_{C} is the columbic efficiency, $V_{\mathrm{B}k}(x_k, \mathbf{d})$ is the battery open circuit voltage and $R_{\mathrm{B}k}(x_k, \mathbf{d})$ is the battery inner resistance which are functions of the SOC, number of cells and the modules. The change in SOC level $\Delta x_{k,s}$ is calculated as,

$$\Delta x_{k,s} = -\frac{I_{\mathrm{B}k,s}\eta_B(I_{\mathrm{B}k,s})}{Q_B 3600} \tag{3-24}$$

where Q_B is the battery current capacity and equals to 6.5 Ah. $\eta_B(I_{\mathrm{B}k,s})$ is the battery charging efficiency as a function of the $I_{\mathrm{B}k,s}$.

The aim is to find the battery state of charge (SOC) x_k to keep it between predefined minimum and maximum values during the control optimization process. Battery power output is given by

$$P_{Bk} = V_{OCk} I_{Bk} - I_{Bk}^2 R_B \tag{3-25}$$

where V_{OCk} is the open circuit voltage at step *k*, which is taken account as a function of SOC. Paux = 800 W is a constant auxiliary power demand. Battery discharge resistance decreases and charge resistance increases with SOC.

The power required from battery is given by

$$\begin{aligned} P_{Bk} &= \tau_{Mk} \omega_{Mk} \eta_{Mk}^{-j} - \tau_{Gk} \omega_{Gk} \eta_{Gk}^{j} \\ P_{Bk} &= \tau_{Mk} \omega_{Mk} \eta_{Mk}^{-j} - \tau_{Gk} \omega_{Gk} \eta_{Gk}^{j} \end{aligned} \tag{3-26}$$

where *j*=1 when discharging and *j*=-1when charging.

Quasi-static backward looking model developed above cannot be used for performance simulations. To calculate the accelerations, we have developed a limited forward looking simulink model of the vehicle dynamics, as shown in (3-4). Maximum engine torque $\tau_{MAX}^{E}(\mathbf{d})$ and maximum motor torque $\tau_{MAX}^{M}(\mathbf{d})$ is provided to the powertrain as the inputs and using the transmission traction force is calculated. We subtract this from the load force and propagating the net force through the $1/m_v$ gain block, we calculate acceleration. Taking the integral of the acceleration, we find the velocity which is needed to calculate the vehicle dynamics. Using this

model, we can calculate the acceleration time from 0-60mph and use it in our optimization model to identify feasible design candidates.

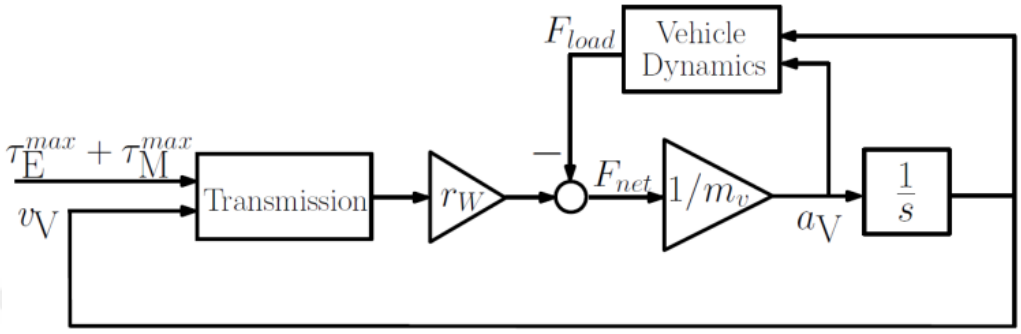

Figure 3-4 Simulink model for the acceleration model

Now that vehicle model is developed, we will optimize the control strategy for blended mode operation where battery state of charge starts from 90% with a target value of 30%. One of the major advantages of blended mode is that vehicle components can be sized smaller such as engine reducing the overall cost. Also blended mode is found to be more efficient compared to CD-CS mode.

3.3.3 Control Parameter Optimization

Dynamic Programming (DP) is a global dynamic optimization algorithm based on Bellman`s Principle [12]. Since we are interested in the globally optimal solutions both for design and control, we adopted DP for the optimal energy control problem of plug-in vehicles.

The discrete time model of the optimal control problem can be expressed by using Euler forward approximation as follows:

$$x_{k+1} = x_k + f_k(x_k, u_k)$$
$$J = \sum_{k=0}^{N-1} H(x_k, u_k, k) \tag{3-27}$$

Dynamic programming (DP) is based on principle of optimality, according to definition of Richard Bellman; whatever current state and decision is, the remaining decisions must constitute an optimal policy w.r.t. the state resulting from the current decision. This definition allows expressing the optimal control problem as a functional recurrence equation, while minimizing the cost function at each step, k ,

$$J^*_k(x_k) = \min_{u_k} \left\{ H(x_k, u_k) + J^*_{k+1}(x^*_{k+1}) \right\} \tag{3-28}$$

Figure 3-5 is a graphical way to explain how DP works. Each grid represents the set of discrete state points (1 state variable in this example), and the arrows are the control decisions. The cost is the effort to go from one discrete point at time k to another feasible point at time $k+1$. We consider only one state variable in our formulation: SOC. Dynamic programming finds all value set of cost functions by looking backwards (Figure 3-6). To find the minimum cost functions and optimal control map, the forward looking to this value set of cost functions has to be implemented. SOC is discretized between 0.3 and 0.9 by 100, and control input is discretized between -engine ratio and 1.

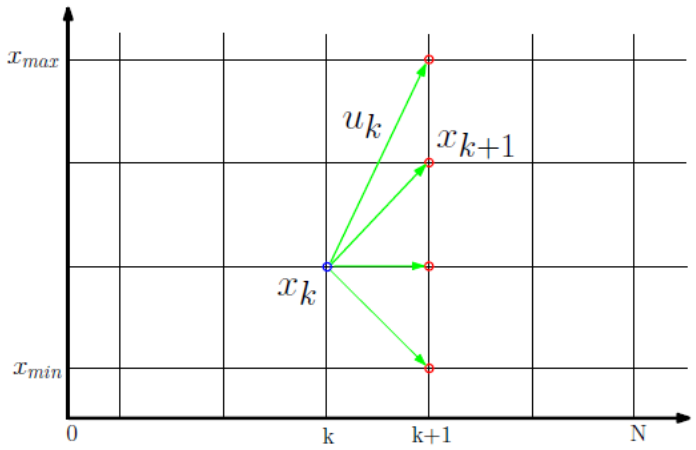

Figure 3-5 ForwardDP

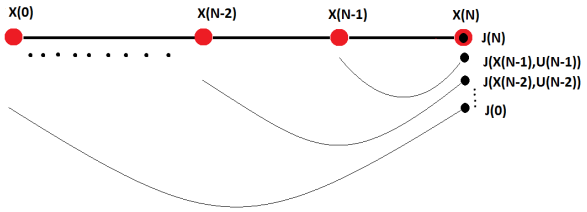

Figure 3-6 Backward DP

The advantage of the dynamic programming approach is using the principle of optimality to reduce the number of calculations required to find the optimal control law, which leads to the global optimum solution. The main difference of this method from direct enumeration of all possible control sequences is its backward calculation. This results a linear relation for dynamic programming between the number of calculations and the size of the problem, while the calculation time increases exponentially with the length of the problem for a global optimal controller based on direct enumeration [12]. Optimal grid size is iteratively found until convergence. In our research we have used the DP function defined in [13].

Since the main object of the inner loop is to find the optimal decision map and to minimize the fuel consumption, the problem to be implemented with DP has to be defined according to this case. First, the state variable is to be chosen as the state of charge (SOC), which is controlled between its predefined boundaries:

As controllers improve with GPS, traffic information, terrain preview, our capability to estimate the speed profiles will increase.

The operation cost function to be minimized is the total consumption of the PHEV:

$$J = \min_{u_k \in U_k} \sum_{k=0}^{N-1} \Delta C_{total\$}(u_k, k) = \min_{u_k \in U_k} \sum_{k=0}^{N-1} \dot{C}_{total\$} \tag{3-29}$$

3.4 Cost Model

Vehicle life is assumed to be 150000 miles which is the U.S. average vehicle life. This number might be optimistic or pessimistic based on the travel patterns of the drivers. Average vehicle life T_{VEH} is found by

$$T_{VEH} = \frac{s_{LIFE}}{Ds} \tag{3-30}$$

where s is denoted daily driving distance. In our case, it corresponds to 19 years for an average daily trip of 22 miles.

Component	2015 LR	2030 PG
Vehicle	24369	22598
Battery ($/kWh)	587	160
Motor ($/kW)	8	4
Engine ($)	$345+2.75d_3+315q$	$360+330q+2.7\ d_3$
Body Cost	24,369	22,597

Table 3-1 Component costs [27]

Table 3-1 shows the cost of components at the factory gate (Suggested factor to find retailer price is reported to be 1.5). We consider two cases for battery cost: 2015 Literature review for upper bound and 2030 Program Goals as lower bound, respectively. The cost estimates are obtained from a recent report from Argonne National Lab. PHEV body cost is assumed to match that of PHEV10 in the report. q is the number of cylinders for the engine.

The real discount rate rR is used for future commodity purchases under the assumption that prices follow inflation $f_{\mathrm{A|P}}\left(r_{\mathrm{R}},\overline{T}_{\mathrm{VEH}}\right)^{-1}$ computes NPV of future payments for a commodity whose prices follow inflation, and $f_{\mathrm{A|P}}\left(r_{\mathrm{N}},\overline{T}_{\mathrm{VEH}}\right)$ converts NPV to EAC).

Parameters	Base case	Units
Cost of gasoline	$2.75	per gallon
Cost of electricity	$0.114	per kW
Number of driving days per year	300	
Battery charging efficieny	0.88	%
Vehicle life	150000	miles
Number of driving days per year	365	days/year
Nominal discount rate	8	%
Inflation rate for future fuel prices	3	%
Real discount rate	5	%

Table 3-2 Parameters for life cycle cost calculation [3]

3.5 Results and discussion

In this section we present the results of this study and discuss the implications.

3.5.1 Co-design Space for intelligent control and rule based control

The co-design space constructed for lifetime cost is given in Figure 3-7 Co-design space with dynamic programming. Infeasible design points which does not satisfy drive cycle, and performance constraints have been removed and the cost minimizing design is chosen from the feasible design points. Energy management of the vehicle is accomplished by dynamic programming algorithm. Lifetime cost is color coded for pdf version.

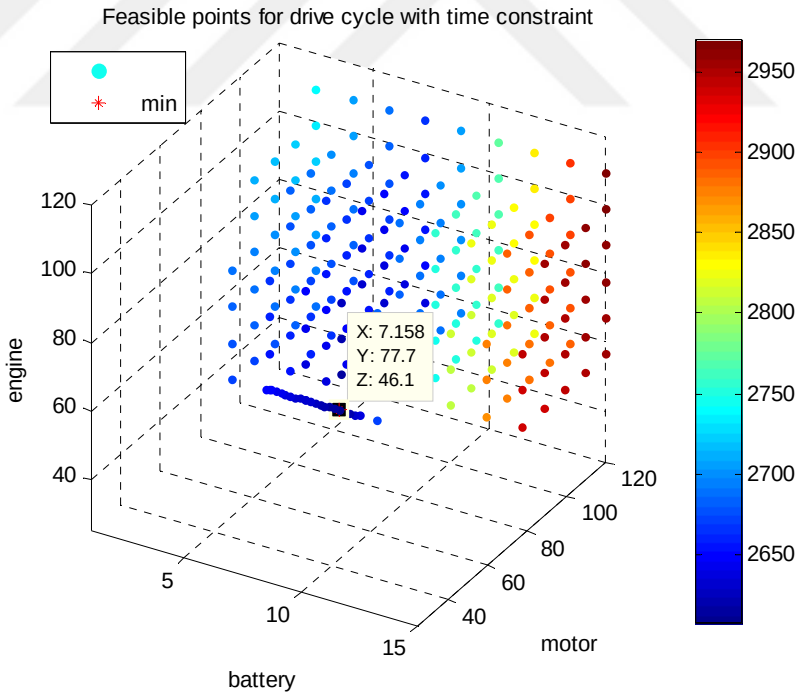

Figure 3-7 Co-design space with dynamic programming

Optimal co-design is found to be at x^*=[7.1 kWh, 77.7 kW, 46.1 kW]. It is seen that cost minimizing design is actively bounded by two design constraints: (1) CD mode acceleration time constraint which is the acceleration time from 0mph to 60mph being less than or equal to 11 seconds) and (2) engine needs to be sized to satisfy the max torque demand in CS mode.

Similarly, lifetime cost for the corresponding co-design space utilizing a rule based controller has been visualized in Figure 3-8. Discretization is kept the same with its counterpart space. Optimal co-design is found to be x=[7.5 kWh, 77.7 kW, 46.1, 272 Nm]. Although, the traction components stayed at the same size since they are actively constrained by the maximum road demand and the performance requirement, the battery is found to be 5% smaller. If one relaxes the constraints, since the battery mass is also reduced, smaller traction components might be obtained. Rule based control has only one engine threshold value for the whole drive cycle and whenever the road demand exceeds this value it turns the engine on. Battery downsizing is mainly achieved by better schedule of engine-on and off actions which translates to charge and discharge events for the battery via dynamic programming that explores the whole possible control actions to yield the globally optimal trajectory for battery state of charge.

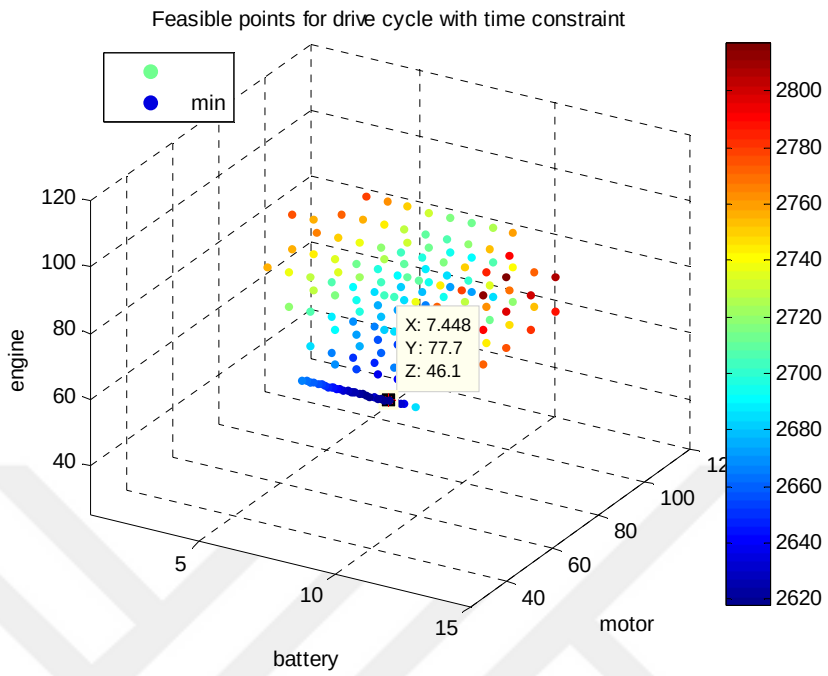

Figure 3-8 Co-design space with rule based control

When powertrain is optimized for a distribution of Kansas City driving patterns with distances of 5, 10, 20 and 30 miles where the operation cost is weighted for each drive cycle based on NHTS distribution, the optimal robust co-design is found to have a battery of 6.8kWh, a motor of 80 kW, and an engine of 50 kW (Figure 3-9 Robust co-design space with dynamic programming). Engine is constrained by CS mode torque requirement and motor is constrained by performance constrained which is 0-60mph acceleration time. Refining the resolution of this solution is left for future work.

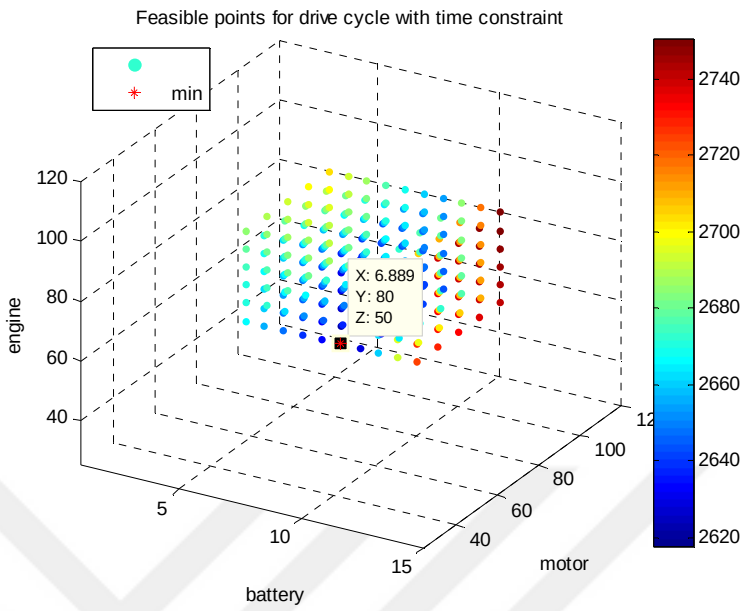

Figure 3-9 Robust co-design space with dynamic programming

3.5.2 Battery Downsizing

Intelligent energy management strategies might increase efficiency, thus reduce the need for bigger components. The effect of optimal control strategy versus rule based control on the vehicle battery is found to be up to 5% reduction.

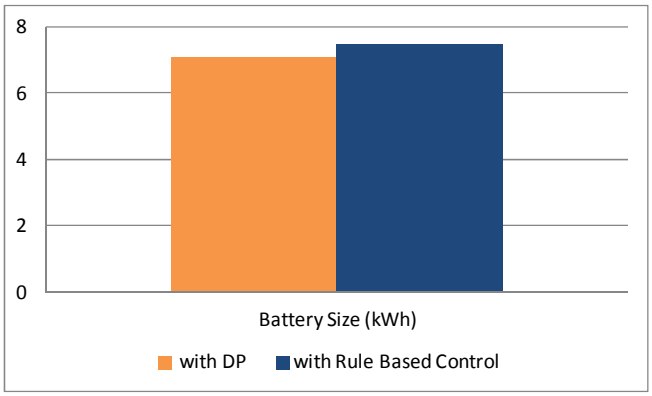

Figure 3-10 Implications of control strategy on vehicle design

Component Size	with DP	with Rule Based Control	% Reductions
Battery Size (kWh)	7.1	7.5	-5%

Table 3-3 Optimal component sizes for DP and Rule based control strategies.

3.5.3 Lifetime Cost Breakdown

Life cycle cost can be reduced up to via predictive controllers .4% which is not significant. However given the large scale of automotive industry and annual sales, these findings might lead to some considerable cost and environmental benefits.

3.6 Limitations and Future Work

We have showed the impact of intelligent control on the component downsizing and cost reductions for a parallel PHEV powertrain. In this work, have used a real world drive cycle which is randomly selected from the Kansas City driving data with the length of average NHTS daily driving distance which is 22 miles. Effect of terrain has not been accounted and left for future work where it is expected to further strengthen the impact of intelligent control on the battery downsizing and cost reductions when used with GPS assisted technologies in real world applications. If we relax the performance and CS maximum torque requirement for the engine, we might also see some downsizing in engine and motor sizes which could translate to mass reductions. This would have compound effect on battery downsizing since the road demand would reduce and it could be met with smaller traction and energy components. We have identified the upper bound for the cost and component downsizing potential of the intelligent controllers using a DP based approach. Predictive controllers may converge towards the benefits

suggested by DP as additional information improves predictive capabilities. This section only explores parallel hybrid electric powertrains which splits torque. Split and series architectures might yield more or less potential to downsize components. Control might be also important for self tuning capability for aging vehicles. Aging changes the dynamics of the powertrain and if a rule based control is employed, it might be no longer optimal for the aged powertrain. Sensitivity to gasoline, electricity, and battery prices is left for future work. These parameters might change the optimal-co design. We have only considered a small portion of NHTS distribution in this section due to computational burden. Optimizing for longer trips can change the cost minimizing co-design and might demonstrate more potential to downsize components via intelligent control.

3.7 Conclusions

In this chapter, we have demonstrated the potential benefits of predictive/smart controllers to reduce battery size and lifetime cost. We have investigated the design, control and economics interaction by adopting Dynamic Programming as the energy management strategy to determine the lower bound, and a rule-based control strategy to determine the upper bound of energy management capacity for a parallel PHEV powertrain. Performing a parametric study, we have identified the cost minimizing designs which meet the performance constraints for both type of control strategies. The effect of control strategy on the optimal design is found to be up to 5% reduction in battery size due to better state control of the battery and .4% in lifetime cost. Given the size of auto market and drivers, these numbers could may translate to some considerable savings.

3.8 References

[1] C. Samaras and K. Meisterling, “Life cycle assessment of greenhouse gas emissions from plug-in hybrid vehicles: implications for policy.,” *Environmental science technology*, vol. 42, no. 9, pp. 3170–3176, 2008.

[2] C.-S. N. Shiau, C. Samaras, R. Hauffe, and J. J. Michalek, “Impact of battery weight and charging patterns on the economic and environmental benefits of plug-in hybrid vehicles,” *Energy Policy*, vol. 37, no. 7, pp. 2653–2663, 2009.

[3] O. Karabasoglu and J. Michalek, “Influence of driving patterns on lifetime cost and life cycle benefits of hybrid and plug-in electric vehicle powertrains,” *In Press, Energy Policy*, 2013.

[4] P. Tulpule, V. Marano, and G. Rizzoni, “Effects of Different PHEV Control Strategies on Vehicle Performance,” *Control*, pp. 3950–3955, 2009.

[5] L. Fang and S. Qin, “Concurrent Optimization for Parameters of Powertrain and Control System of Hybrid Electric Vehicle Based on Multi-Objective Genetic Algorithms,” *2006 SICEICASE International Joint Conference*, pp. 2424–2429, 2006.

[6] J. W. Whitefoot, K. Ahn, and P. Y. Papalambros, “The Case for Urban Vehicles: Powertrain Optimization of a Power-Split Hybrid for Fuel Economy on Multiple Drive Cycles,” in *Volume 4: 12th International Conference on Advanced Vehicle and Tire Technologies; 4th International Conference on Micro- and Nanosystems*, 2010, vol. 2010, no. 44120, pp. 197–204.

[7] C.-S. Norman Shiau and J. J. Michalek, “Global Optimization of Plug-In Hybrid Vehicle Design and Allocation to Minimize Life Cycle Greenhouse Gas Emissions,” *Journal of Mechanical Design*, vol. 133, no. 8, p. 084502, 2011.

[8] J. J. Michalek, M. Chester, P. Jaramillo, C. Samaras, C.-S. N. Shiau, and L. B. Lave, “Valuation of plug-in vehicle life-cycle air emissions and oil displacement benefits.,” *Proceedings of the National Academy of Sciences of the United States of America*, vol. 108, no. 40, pp. 16554–8, 2011.

[9] O. Sundström, L. Guzzella, and P. Soltic, “Optimal hybridization in two parallel hybrid electric vehicles using dynamic programming,” in *Proceedings of the 17th World Congress The International Federation of Automatic Control*, 2008, pp. 4642–4647.

[10] R. Patil, B. Adornato, and Z. Filipi, “Impact of Naturalistic Driving Patterns on PHEV Performance and System Design,” *Society of Automotive Engineers Technical Paper*, pp. 01–2715, 2011.

[11] G. H. M Fellah G Singh A Rousseau S Pagerit E Nam, “Impact of Real-World Drive Cycles on PHEV Battery Requirements Mohammed Fellah , Gurhari Singh , Aymeric Rousseau and Sylvain Pagerit,” *SAE Technical Paper*, 2009.

[12] E. Traut, C. Hendrickson, E. Klampfl, Y. Liu, and J. J. Michalek, “Optimal design and allocation of electrified vehicles and dedicated charging infrastructure for minimum life cycle greenhouse gas emissions and cost,” *Energy Policy*, vol. 51, pp. 524–534, Dec. 2012.

[13] E. D. Tate and S. P. Boyd, “Finding Ultimate Limits of Performance for Hybrid Electric Vehicles,” *Society*, 1998.

[14] C.-C. L. C.-C. Lin, H. P. H. Peng, J. W. Grizzle, and J.-M. K. J.-M. Kang, *Power management strategy for a parallel hybrid electric truck*, vol. 11, no. 6. IEEE, 2003, pp. 839–849.

[15] C.-C. Lin, H. Peng, and J. W. Grizzle, “A stochastic control strategy for hybrid electric vehicles,” *Electrical Engineering*, vol. 5, pp. 4710–4715, 2004.

[16] S. J. Moura, D. S. Callaway, H. K. Fathy, and J. L. Stein, “Impact of Battery Sizing on Stochastic Optimal Power Management in Plug-in Hybrid Electric Vehicles,” in *IEEE International Conference on Vehicular Electronics and Safty*, 2008, no. 0160, pp. 96–102.

[17] S. J. Moura, D. S. Callaway, H. K. Fathy, and J. L. Stein, “Tradeoffs between battery energy capacity and stochastic optimal power management in plug-in hybrid electric vehicles,” *Journal of Power Sources*, vol. 195, no. 9, pp. 2979–2988, 2010.

[18] E. D. Tate, J. W. Grizzle, and H. Peng, “Shortest path stochastic control for hybrid electric vehicles,” *International Journal of Robust and Nonlinear Control*, vol. 18, no. 14, pp. 1409–1429, 2008.

[19] D. Opila, X. Wang, and R. McGee, “An Energy Management Controller to Optimally Trade Off Fuel Economy and Drivability for Hybrid Vehicles,” *Control Systems*, 2010.

[20] A. Sciarretta, M. Back, and L. Guzzella, *Optimal control of parallel hybrid electric vehicles*, vol. 12, no. 3. IEEE, 2004, pp. 352–363.

[21] R. Vijayagopal, J. Kwon, A. Rousseau, and P. Maloney, “Maximizing Net Present Value of a Series PHEV by Optimizing Battery Size and Vehicle Control Parameters,” *Energy*, 2010.

[22] C. N. Shiau, S. B. Peterson, and J. J. Michalek, “Optimal Plug-In Hybrid Vehicle Design and Allocation for Minimum Life Cycle Cost, Petroleum Consumption and Greenhouse Gas,” in *ASME 2010 International Design Engineering Technical Conferences Computers and Information in Engineering Conference IDETCCIE 2010*, 2010, pp. 1–13.

[23] L. Guzzella and A. Sciarretta, *Vehicle Propulsion Systems: Introduction to Modeling and Optimization*. Springer, 2007, p. 350.

[24] “Powertrain Systems Analysis Toolkit (PSAT).” Argonne National Laboratory, 2008.

[25] K. Koprubasi, “Modeling and Control of a Hybrid-Electric Vehicle for Drivability and Fuel Economy Improvements.,” *Mechanical Engineering*, no. December, pp. 2797–2802, 2008.

[26] L. Guzzella and A. Amstutz, “CAE tools for quasi-static modeling and optimization of hybrid powertrains,” *IEEE Transactions on Vehicular Technology*, vol. 48, no. 6, pp. 1762–1769, 1999.

[27] M. Plotkin, S Singh, “Multi-Path Transportation Futures Study : Vehicle Characterization and Scenario Analyses,” *Argonne National Lab*, 2009.

4 GLOBAL CONTROL OPTIMIZATION OF BATTERY-SUPERCAPACITOR ELECTRIC VEHICLES UNDER A SET OF REAL WORLD SPEED AND ELEVATION PROFILES VIA DYNAMIC PROGRAMMING

In the third chapter, we investigated the optimal co-design of PHEVs for real world driving cycles, and how much we can do better with software with perfect information. This chapters focuses on hardware implementation to minimize the impact of variation in driving patterns (Chapter 2) by integrating energy-dense batteries with power-dense supercapacitors in electric vehicles (EVs) to reduce battery stress and increase battery life. We globally optimize the energy management strategy of supercapacitor-battery systems in EVs for real world driving conditions. We minimize battery current squared as a degradation factor as peak-leveling and Joule heating accelerates battery degradation in EVs. Using dynamic programming to split power requirement between battery and supercapacitor for 72 real world trips from ChargeCar driving data, I achieve 63% reductions in current-squared losses by employing a 50 Wh supercapacitor. Increasing efficiency might help downsizing the expensive batteries by meeting the same electric range constraint, and reducing battery stress might extend battery life and reduce lifetime costs. Paul Kimball and Prof. Jeremy Michalek contributed to this work and we adopted ChargeCar`s vehicle model into our control framework coded in Matlab.

4.1 Introduction

As stricter fuel efficiency standards force automotive manufacturers to look towards alternative modes of power, electrified vehicles (EVs) are poised to become the successor to

internal-combustion vehicles. However, cost of batteries, battery life and all electric range are currently the biggest hurdles in the widespread adoption of EVs.

If there was a way to minimize the peak currents which are caused by high power demands during acceleration and deceleration, then we could minimize the stress in the battery, extend battery efficiency and electric range of the EVs. If electric range is extended by this method, then smaller batteries could be used to cover the same range. Extended battery life and smaller batteries which meets the same range could reduce the lifetime cost of the EVs.

Supercapacitors having high power density, fast charging and recharging capability, and long cycle life can help with the solution of the problem posed above. While battery powered EVs have long been the standard, the proper implementation of a super-capacitor can allow for great increases in energy discharge efficiency and therefore range extension. Combining batteries with supercapacitors for vehicle implementation might improve the fuel economy of electric vehicles up to 10-15% due to higher efficiency of capacitors compared to batteries. Supercapacitors has a lower impedance than batteries, as well as better surface are therefore the losses due to heating would be minimized. Consisting of a battery pack and supercapacitor bank, this architecture provides numerous advantages over traditional electric vehicles via increased power density and greatly improved cycle life (Figure 4-1)

Supercapacitors: High Power Density

Batteries: High Energy Density

Figure 4-1 Supercapacitor integration for EVs (photos from [16,17])

A simple means for extending effective battery lifetime is to reduce the current variability of the battery pack. By using an actively coupled ESS, with a battery as the main energy source (MES) and the supercapacitor acting as an auxiliary energy source (AES), the performance of a PHEV can be greatly increased. Peak-leveling of the battery current can be achieved and power regeneration via braking can be efficiently attained while minimizing deep-discharge of the battery [1]. Another benefit to using an actively coupled system is the reduction of Joule losses (I2R), as the lower impedance of supercapacitors is capable of more efficient operation at higher currents and temperatures and more surface area for enhanced cooling [2]. Since the heat is relocated outside the batteries, denser packing with thicker electrodes can be achieved for a higher overall density. Comparison of supercapacitors and batteries specifically optimized for energy and power is shown at Table 4-1.

A review of the current status of batteries and supercapacitors is essential for reasoning behind an actively coupled ESS. Depending on the chemical composition, batteries can hold 110-220 Wh/kg, while capacitors are limited to 12-20 Wh/kg. Batteries operate at 80%

efficiency with a life of 800-1500 cycles. Supercapacitors, on the other hand, are capable of thousands of W/kg, with efficiencies as high as 98%, and hundreds of thousands of cycles[7]. Batteries, while capable of holding much more energy than supercapacitors, cannot charge/discharge this energy at the same rates. An actively coupled ESS takes advantage of the benefits of both energy sources, allowing for maximum energy storage and performance with minimal losses. Supercapacitor has very low specific energy with very high specific power and allows same charge and discharge range [6][5]. Scientists at MIT have also manufactured a nanotube based capacitor capable of roughly 50% of the energy in a chemical battery of equivalent weight [4]. Furthermore, these new nanoengineered devices still retain all of the benefits that conventional capacitors have over batteries including higher efficiencies and increased lifespan. Today, integrating batteries and supercapacitors for their complementary benefits might offer more benefits rather than replacing supercapacitors with batteries. In the next section, we discuss the previous literature about the supercapacitor integration to EVs.

4.2 Literature Review

Smith et al. discusses the use of supercapacitors to improve battery performance for various applications in [5]. There are many loads that generate current pulses with small voltage droop, when a supercapacitor is employed, it can deliver the current pulse since it has enough energy storage with a small voltage droop since it`s internal resistance is small [5]. When used in parallel with the high energy density batteries, supercapacitors smoothes out the load, or stress, on the battery, while improving the source impedance experienced by the load. Sadoun et. al. [6] shows that addition of supercapacitor helps reduce the battery stress by ensuring high and short peaks of power and it helps in reducing the size of the batteries using a rule based algorithm.

Lajunen combined supercapacitors with batteries for a hybrid bus and found better breaking energy recovery efficiency and longer electric range compared to a bus without a supercapacitor [7]. Pay discusses the optimal usage of supercapacitors in EVs and mentions about the control challenges [8]. Styler et. al. [9] created a trajectory libraries based predictive control algorithm for battery-supercapacitor coupling by exploiting topographic information, traffic history, and specific driver performance. Jinrui et al. combined simulation and experimental data to quantify the benefits of a hybrid ESS containing both a battery and supercapacitor bank [11]. They found that an average supercapacitor-battery system could reduce total energy consumption for a given cycle an average of 23%, demonstrating an increase in the range of pure EVs.

	Battery (Li-ion)		**Supercapacitor**	
	Power	Energy	Power	Energy
Energy[Wh/kg]	70-130	110-220	3-5	12-20
Energy [Wh/l]	150-450	150-450	3-10	3-6
Power [W/kg]	600-3000	200-600	2000-10k	2000-10k
Number of cycles @80% DOD	800-1500	800-1500	500k-1M	500k-1M
Efficiency [%]	85-90	85-90	95-100	95-100
Temperature range [˚C]	-20, 60	-20,60	-20, 90	-20, 90

Table 4-1 Comparison of batteries and supercapacitors [7]

The two biggest issues impeding widespread PHEV adaptation are range and battery life. Range can be increased with larger battery and supercapacitor banks, but the added weight limits

vehicle performance, as well as increases cost. The other key factor when considering an electric vehicle is battery life. Current battery technology deteriorates greatly over the course of the design life. Any means of extending the effective battery lifetime greatly increases the commercial attractiveness of PHEVs [1]. Despite current progress, the cost feasibility of supercapacitor implementation in PHEVs is under debate amongst researchers. Studies show that if effective battery lifetime can be extended by 50% more than 2007 levels, then the use of supercapacitors will be justified.

HEVs are classified into three main types based on their peak power requirements for the electric motor. Micro hybrids attain 5-10 kW, charge-sustaining hybrids attain 25-35 kW, and PHEVs attain 50-70 kW. Supercapacitor-battery combinations in PHEVs are proven to be useful for vehicles with an electric range greater than 15 miles [10] .

4.2.1 Evaluating Control Strategies

Researchers are currently developing a wide variety of models and methods to provide the best electrified vehicle performance. Amongst these algorithms, three main families emerge. Heuristic methods utilize no a priori information and can be solved quickly and offline. While creating a control algorithm based solely on the speed of a vehicle will results in substantial current-squared losses, entire drive cycles must be taken into account for truly global optimums. Deterministic methods minimize analytical models of the losses, and require information about the driving pattern and numerous assumptions about the details of the electromechanical system. Methods such as equivalent consumption minimization strategy (ECMS) do not necessarily require an online system to be effective, but adaptable ECMS systems have shown to approach

the global optimum[14]. Finally, non-deterministic methods such as stochastic methods, dynamic programming and fuzzy logic achieve real time solutions of the non-closed form optimization problem, but with great computational cost [13].

This work will utilize dynamic programming methods to solve the actively coupled ESS management problem. Its use will be discussed in further detail in the next section.

4.2.2 Methodology and Experimentation

We have adopted a quasi-static backward looking electric vehicle modeling approach to conduct our energy management study since quasi-static vehicle models gives comparable results to that of dynamic models with much less computation burden. Efficiencies including drivetrain gears and joule losses in the motors have a varying effect on the output of the system. As it is our purpose to prove the potential improvements in applying dynamic programming methods to a battery-supercapacitor PHEV, many of the efficiencies have been simplified into constant values. The importance of the data is to show orders of magnitude, as opposed to precise changes in the output variables.

4.2.3 Data Processing

The drive cycle data used in simulating electric vehicles will have a great effect on the output of the optimization. While many studies use a single standard drive cycle without elevation profiles, we have used real world driving data collected by ChargeCar Research Group of CMU in the form of GPS points from various trips of an BEV driving around Pittsburgh [18]. We use these data to simulate our vehicle model and perform the energy management

optimization so that we can show the effect of an actively coupled supercapacitor-battery system might have in an environment with varying loads including high amounts of accelerating and braking.

The GPS data is gathered in the form of .GPX files from which times, latitudes, longitudes, and elevations are extracted, broken into individual trips based on the .trk markers inside the file. Each trip file is then traversed to check for accuracy and extract useful data.

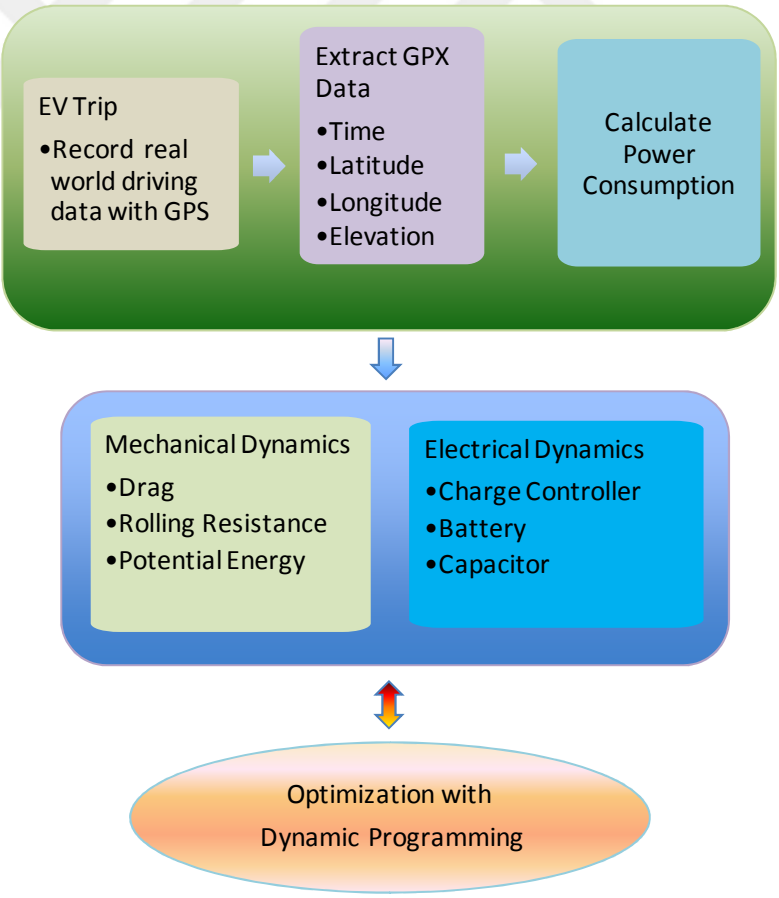

Figure 4-2 System Framework

Planar distance between two points on a sphere is computed with the haversine formula which is given below.

$$\begin{aligned}\text{haversin}\left(\frac{d}{r}\right) &= \text{haversin}\left(\phi_2 - \phi_1\right) + \ldots \\ &\cos\left(\phi_1\right)\cos\left(\phi_2\right)\text{haversin}\left(\psi_2 - \psi_1\right)\end{aligned} \tag{4-1}$$

where d is the distance between two points on the surface of a sphere in meters, r is the radius of the earth estimated as 6.371×10^6 meters, ϕ is the latitude of a point in radians, ψ is the longitude of a point in radians, and the trigonometric haversine function is given by:

$$\text{haversin}(\theta) = \sin\left(\frac{\theta}{2}\right)^2 \tag{4-2}$$

It then follows that the planar distance can be calculated between any two points *d*:

$$d = 2r \arcsin\sqrt{\begin{aligned}&\sin\left(\frac{\phi_2 - \phi_1}{2}\right)^2 + \ldots \\ &\cos\left(\phi_1\right)\cos\left(\phi_2\right)\sin\left(\frac{\psi_2 - \psi_1}{2}\right)^2\end{aligned}} \tag{4-3}$$

When the vehicle with a gps system passes through a tunnel, a period of time will exist during which data points will be recorded at regular intervals with no change in position, followed by a large change in position between two data points. Before any analysis can be

performed on the data, these anomalies must be corrected. For the data in our experiment, we assume a tunnel exists wherever a gap of 50 meters is found. These tunnel points are then deleted so that corrected points can be interpolated.

Interpolation has a two-fold purpose for our calculations. First, it fills in any gaps created during tunnel deletion. Secondly, it corrects for other missing data points somehow introduced into the .GPX file. For any two consecutive data points with a gap of greater than two seconds, additional points are linearly interpolated at one second intervals.

4.2.4 Vehicle Dynamics

Raw data points must be converted to power consumption through dynamic analysis of the vehicle. To make this transition, the motion of the vehicle, including displacements velocity, and acceleration, must be determined. These key characteristics can be found with the following calculations:

$$\begin{aligned}
&\delta Z = Z_2 - Z_1 \\
&d_p = \text{haversin}\left(\phi_1, \psi_1, \phi_2 \psi_2\right) \\
&d_a = \sqrt{\left(d_p\right)^2 + \left(dZ\right)^2} \\
&\delta t = t_2 - t_1 \\
&\text{v} = \frac{d_a}{\delta t} \\
&a = \frac{\text{v}_2 - \text{v}_1}{\delta t}
\end{aligned} \tag{4-4}$$

where Z is the vehicle elevation in meters, t is the time of data point in seconds, d_p is the planar distance between points in meters, d_a is the adjusted distance accounting for a change in elevation in meters, v is the velocity of the vehicle in m/s, and a is the net acceleration of the vehicle in m/s^2.

The forces on the car must be evaluated through the GPS data. The total motor force in N can be calculated by the summation of the net force and the resistive forces:

$$F_{motor} = F_{net} + F_{res} \tag{4-5}$$

where F_{net} is the force of the net vehicle acceleration in N, and F_{res} is the sum of the resistive forces on the car including both air drag and rolling resistance, as well as the change in potential energy due to changes in elevation. We will adopt the vehicle model in [9].

$$\begin{aligned} F_{res} &= F_{air} + F_{rolling} + mg\sin(\theta) \\ F_{air} &= C_{air}\mathrm{v}^2 \\ C_{air} &= .5\rho A_c C_{drag} \\ F_{rolling} &= C_{rolling} mg\cos(\theta) \end{aligned} \tag{4-6}$$

where F_{air} is the air drag in N, $F_{rolling}$ is the rolling resistance in N, m is the mass of the vehicle in kg, g is the gravitational constant of 9.81 m/s^2, θ is the incline of vehicle travel with respect to horizontal in radians, C_{air} is the coefficient of air resistance, ρ is the density of air in kg/m^3, A_c is the effective cross-sectional area of the vehicle in m^2, C_{drag} is the drag coefficient of

the vehicle, and $C_{rolling}$ is the coefficient of rolling resistance of the vehicle. The primary vehicle characteristics used in this simulation can be seen in Table 4-2 below.

Vehicle	**2001 Honda Civic**
Mass [kg]	1200
A_C [m^2]	1.98
C_{Drag}	0.31
$C_{Rolling}$	0.015

Table 4-2 Vehicle coefficients

Air pressure around the vehicle can be approximated as a function of temperature and height. As temperature data is not recorded via GPS, we must assume an average of 60 °F for the trip. Pressure is now a linear function of height, while density is still a function of both pressure and temperature.

$$p = 101,325\left(1 - \frac{.0065Z}{T}\right)^{\frac{.0289g}{8.314*.0065}}$$
$$\rho = \frac{.0289p}{8.314T} \qquad (4\text{-}7)$$

where p is the pressure in Pa, and T is the temperature in K. These values can then be substituted back in to (4-5) to determine F_{motor}. Total power consumption of the vehicle can then be concluded:

$$P_{tot} = \frac{F_{motor}v}{\eta_{drive}} \qquad (4\text{-}8)$$

where P_{tot} is the power consumption in W, F_{motor} is the total motor force in N, v is the velocity of the vehicle in m/s, and η_{drive} is the total drivetrain efficiency including the electric and mechanical efficiencies of the system.

For both the battery and the supercapacitor, the charge level of the battery can be determined through the following

$$Q_i = Q_{i-1} + \frac{P\delta t}{\eta}, \quad P<0$$
$$Q_i = Q_{i-1} + \eta P\delta t, \quad P>0 \tag{4-9}$$

where Q_i is the resulting charge level in Wh, Q_{i-1} is the previous charge level in Wh, P is the power consumption in W, η is the efficiency, and δt is the elapsed time in hours. Limits can be placed on state of charge depending on the desired operating characteristics of the battery and supercapacitor, as design life is greatly decreased when operated to extremes.

4.2.5 Power and Control Strategy

Electric motor is the only traction component in the electric powertrain and needs to be fed with electric power. With two power sources to choose from at each second during the trip, a control algorithm must be established to determine the power split between the battery and supercapacitor. Figure 4-3 shows the electrical power path in the vehicle drivetrain.

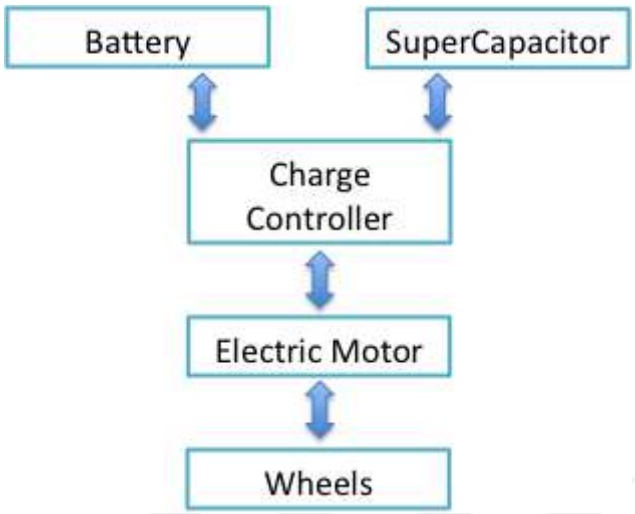

Figure 4-3 System level power flow

While many methods exist for choosing a charge controller, this work applies dynamic programming methods to determine the optimal control algorithm for a route with full a priori knowledge to evaluate the upper bounds for the benefits of supercapacitor-battery integration.

Dynamic programming operates by backward calculation [15]. The optimal state and decision for a given time k will lead to the optimal state at time k+1. The optimal control decision vector u can be calculated beginning with the final state, and only a discrete range of possibilities will lead to this state. The route is then traversed backwards through all data until the final optimal control vector is found. The route can then be traversed in a forward direction using this optimal control vector.

4.2.6 Battery- Supercapacitor Control Optimization through Dynamic Programming

$$c_{\mathrm{OP}}(s) = \min_{u_k \in U_s} \sum_{k=1}^{N_s} \left(i_k(u_k)\right)^2$$

$$i_k(u_k) = \frac{(1-u_k)P_k}{V_k}$$

$$U_s = \left\{ \begin{array}{c} \mathbf{u} \mid \mathbf{u} \in \mathbb{R}^{N_s-1};\ \ \mathbf{-1} \le \mathbf{u} \le \mathbf{1}; \\ P_{\mathrm{MIN}}^{\mathrm{CAP}} \le u_k P_k \le P_{\mathrm{MAX}}^{\mathrm{CAP}}; \\ P_{\mathrm{MIN}}^{\mathrm{BAT}} \le (1-u_k)P_k \le P_{\mathrm{MAX}}^{\mathrm{BAT}}; \\ x_{\mathrm{MIN}}^{\mathrm{CAP}} \le x_k^{\mathrm{CAP}} \le x_{\mathrm{MAX}}^{\mathrm{CAP}}; \\ x_{\mathrm{MIN}}^{\mathrm{BAT}} \le x_k^{\mathrm{BAT}} \le x_{\mathrm{MAX}}^{\mathrm{BAT}}; \\ x_{k+1}^{\mathrm{CAP}} = x_k^{\mathrm{CAP}} + \frac{u_k P_k \Delta t}{\kappa_{\mathrm{CAP}}} \eta_{\mathrm{CD}}; \\ x_{k+1}^{\mathrm{BAT}} = x_k^{\mathrm{BAT}} + \frac{(1-u_k)P_k \Delta t}{\kappa_{\mathrm{CAP}}} \eta_{\mathrm{CD}}; \\ \forall k \in \{1, 2, ..., N_s - 1\} \end{array} \right\}$$

$$\eta_{\mathrm{CD}} = \begin{cases} \eta_{\mathrm{CHG}}^{-1} & \text{if } P_k \ge 0 \\ \eta_{\mathrm{DISCHG}} & \text{if } P_k < 0 \end{cases}$$

Equation 4-10

where k is the time step, N is the total time steps in drive cycle indexed by s, $c_{op}(\mathbf{d}, s)$ is the operation cost for design $\mathbf{d}$ and drive cycle indexed by s. $\sum_{k=1}^{N_s}\left(i_k(u_k)\right)^2$ is the sum of the current squared losses during a single drive cycle to be minimized. u_k is the control action representing the portion of electrical power demand supplied by the supercapacitor vs. the battery at time step k; U is the set of feasible control actions; $x_k^{\mathrm{CAP}}(\mathbf{d}, u_k)$ is the supercapacitor state of charge at time step k, $x_k^{\mathrm{BAT}}(\mathbf{d}, u_k)$ is the battery state of charge at time step k,

$f_k^{\text{SIM}}(\mathbf{d}, x_k^{\text{CAP}}, u_k)$ is the electric vehicle simulation model which is described previously in this section (Eq1-10), $P_{\text{MAX}}^{\text{BAT}}(\mathbf{d})$ and $P_{\text{MIN}}^{\text{BAT}}(\mathbf{d})$ are the charging and discharging power limits for the battery power, $P_k^{\text{BAT}}(\mathbf{d}, u_k)$. $P_{\text{MAX}}^{\text{CAP}}(\mathbf{d})$ and $P_{\text{MIN}}^{\text{CAP}}(\mathbf{d})$ are the charging and discharging power limits for the battery power, $P_k^{\text{CAP}}(\mathbf{d}, u_k)$. V_k is the voltage of the battery at time step *k*. For simplicity, we assume that voltage is constant over time independently of the current drawn. If we were to account for the drop in voltage associated with high current draws, we expect the benefits of supercapacitor integration to increase.

4.3 Results and Conclusions

In this section, I discuss the implications of coupling the battery system of an electric vehicle with a supercapacitor system and using an intelligent control algorithm to manage the energy flow from supercapacitor and battery to the traction component of the electric vehicle which is motor, and vice versa.

We have used 72 different trips from Chargecar driving data for our study. Each trip was treated separately, with a fully charged capacitor at its inception. For each capacitor size, each trip was globally optimized with dynamic programming to reduce the total current-squared of the battery. Key results such as battery energy spent and net energy consumed were also recorded. A supercapacitor of 50 Watt-hours can reduce current squared by 63%, thereby extending the life of the battery.

A sample trip is selected and presented below for the ease of discussions. The speed and elevation profiles are given below in Figure 4-4 Real world speed and elevation profiles of a sample trip from the set used for the control optimization study.. Graphs also show the change in the state variable which is mainly the capacitor being charged and discharged. It is observed that the optimal actions depend on the current dynamics of the vehicle such as supercapacitor and battery state-of-charge, speed, acceleration and elevation at that instant of the trip and also the future conditions of the trip. Dynamic programming requires the perfect information about the trip, and generates a globally optimal trajectory for the state variable, which is supercapacitor state-of-charge. Supercapacitor system is especially used during acceleration and deceleration to reduce the current squared losses as well as before and during climbing hills and sliding downhill. Supercapacitor plays as a buffer zone for high levels of energy demand. After close examination of the vehicle dynamics, one can create a heuristic algorithm to be implemented in real world. The control rules can be based on the current state of the supercapacitor, and other vehicle dynamics and road information.

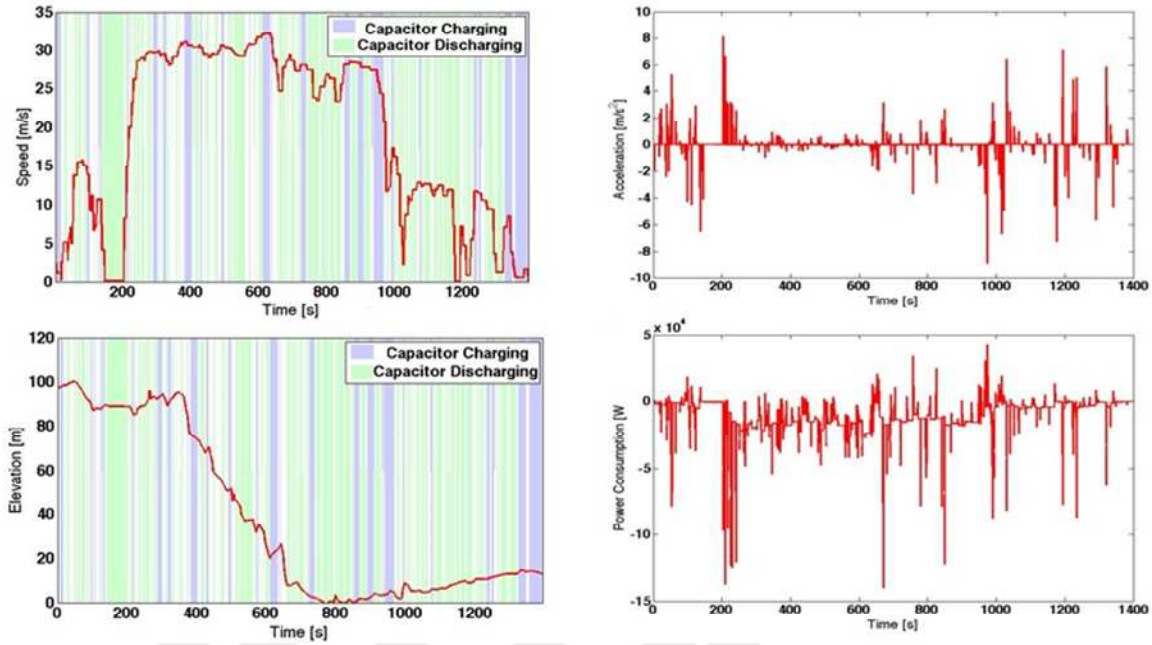

Figure 4-4 Real world speed and elevation profiles of a sample trip from the set used for the control optimization study.

Power consumption is a significant metric to size the battery optimally. In pure electric vehicle systems, battery should be sized to meet the power demand of the motor which is required to follow the drive cycle. Adding a supercapacitor, has the potential to reduce the size of the battery by smoothing the peaks of the power consumption graph in Figure 4-5. It is found that battery charge consumption is highly sensitive to the size of the capacitor used in the ESS. Even a small capacitor of 50 Watt-hours can reduce current squared by 63%, minimizing the battery stress.

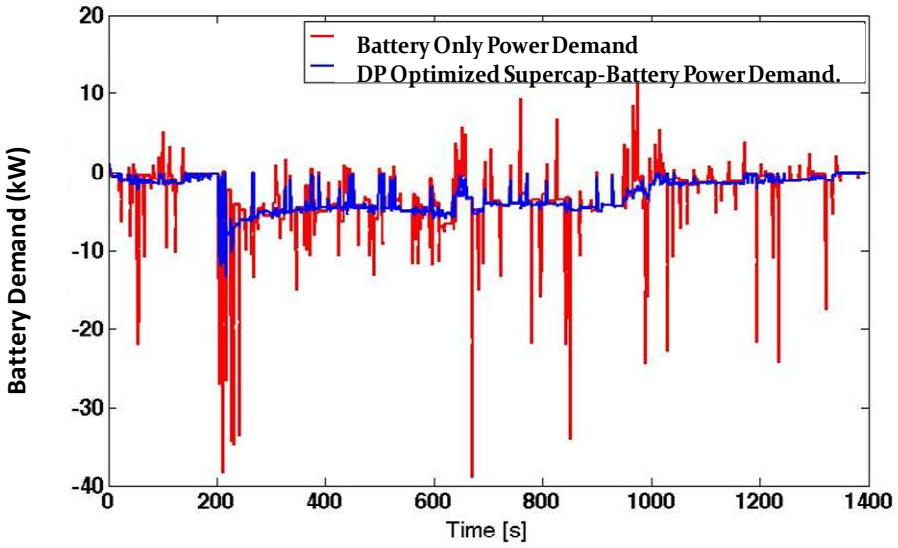

Figure 4-5 Comparison of the battery only power demand and the DP optimized supercapacitor-battery power demand.

Supercapacitor performs a buffering module and this fact is shown in Figure 8. It should be noted that supercapacitor state of charge is chosen as the state variable for the control optimization. It does deep charging and recharging over the entire drive cycle and if supercapacitor was not employed in the powertrain, the main battery system would be exposed to this kind of peak demands which has the potential to deteriorate the battery life. Battery cycle life is significantly smaller than the supercapacitor cycle life as shown in Table 4-1.

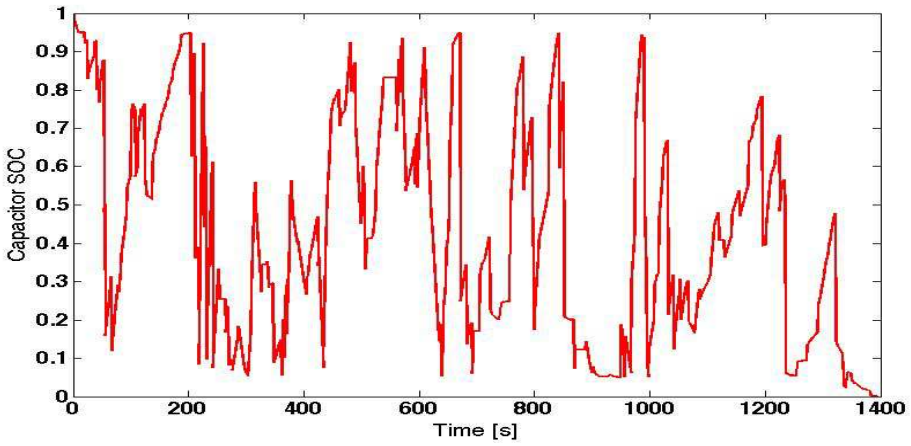

Figure 4-6 Supercapacitor state-of-charge dynamics over time.

Figure 4-6 shows the reduction in current squared for various capacitor sizes for the sample trip shown in Figure 4-4. The decrease in current squared follows a logarithmic trend.

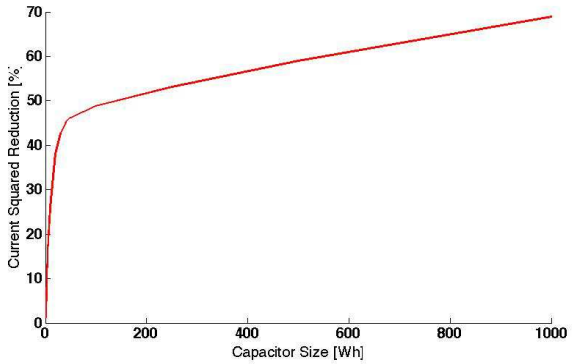

Figure 4-7 Sensitivity of cost function to supercapacitor size for a single drive cycle (Data points: 1, 5, 10, 20, 30, 40, 50, 100, 250, 500, 1000 Wh)

4.4 Conclusions

In this chapter, we have demonstrated the impact of supercapacitor-battery systems and intelligent energy management strategies on the reduction of peak power demand from the batteries to reduce battery stress. Integrating energy-dense batteries with power-dense supercapacitors in EVs might increase battery life. We globally optimized the control of supercapacitor-battery systems in EVs for real world driving conditions using dynamic programming algorithm. We minimized key degradation factors: battery current squared. We achieve 63% reductions in current-squared losses by employing a 50 Wh supercapacitor.

4.5 Future work and limitations

We have employed a dynamic programming approach to see the maximum potential of the current square reductions of the battery. One limitation of this method is that it requires perfect information about the trips. Real world results obtained by employing other types of control algorithms has the potential to converge towards the results we have presented in this work. A real world implementable control algorithm might be developed and results might be compared. Supercapacitor starting at fully charged and the possibility that it might end empty effectively makes the battery larger but estimated have minor impact on the results. The battery voltage is related to power and current. However we assumed that battery open circuit voltage is constant which has the potential to underestimate the results. Sensitivity analysis is performed for a single trip due to computational expense, however performing it across all 72 driving patterns might give different supercapacitor size probably with the same logarithmic trend. Future work includes developing a cost model for the supercapacitor system integration and

evaluating the integration from the lifetime cost point of view with the addition of a set of battery degradation models for a variety of chemistries. One can also choose different objective functions to minimize such as energy processed. It would be also interesting to see the potential of battery downsizing via the addition of a small supercapacitor. These are left as future work.

4.6 References

[1] R. Rizzo and P. Tricoli, "Power Flow Control Strategy for Electric Vehicles with Renewable Energy Sources," *Fuel Cells*, pp. 34–39, 2006.

[2] J. M. Miller, V. P. Systems, and T. Bohn, "Storage System and its Economic Viability," *Architecture*, pp. 190–198, 2009.

[3] Z. Juda, "Advanced Batteries and Supercapacitors for Electric Vehicle Propulsion Systems with Kinetic Energy Recovery," *Journal of KONES Powertrain and Transport*, vol. 18, no. 4, pp. 165–171, 2011.

[4] J. Schindall, "The Charge of the Ultra - Capacitors Nanotechnology takes energy storage beyond batteries," pp. 1–6, 2007.

[5] T. A. Smith, J. P. Mars, and G. A. Turner, *Using supercapacitors to improve battery performance*, vol. 1. 2002.

[6] R. Sadoun, N. Rizoug, P. Bartholomeus, B. Barbedette, and P. Le Moigne, *Optimal sizing of hybrid supply for electric vehicle using Li-ion battery and supercapacitor*. IEEE, 2011, pp. 1–8.

[7] A. Lajunen, *Evaluation of the benefits of using dual-source energy storage in hybrid electric vehicles*, no. April. IEEE, 2010, pp. 1–6.

[8] S. Pay and Y. Baghzouz, *Effectiveness of battery-supercapacitor combination in electric vehicles*, vol. 3, no. 1. Ieee, 2003, pp. 728–733.

[9] A. Styler, G. Podnar, P. Dille, M. Duescher, C. Bartley, and I. Nourbakhsh, "Active management of a heterogeneous energy store for electric vehicles," *IEEE Forum on Integrated and Sustainable Transportation Systems*, pp. 20–25, 2011.

[10] A. Burke and M. Miller, “Ultracapacitors and Batteries for Hybrid Vehicle Applications,” *23rd Electric Vehicle Symposium,*, 2007.

[11] N. Jinrui, W. Zhifu, and R. Qinglian, “Simulation and Analysis of Performance of a Pure Electric Vehicle with a Super-capacitor,” *2006 IEEE Vehicle Power and Propulsion Conference*, pp. 1–6, Sep. 2006.

[12] A. F. Burke, “Batteries and Ultracapacitors for Electric, Hybrid, and Fuel Cell Vehicles,” *Proceedings of the IEEE*, vol. 95, no. 4, pp. 806–820, 2007.

[13] G. Guidi, T. M. Undeland, and Y. Hori, “Effectiveness of Supercapacitors as Power-Assist in Pure EV Using a Sodium-Nickel Chloride Battery as Main Energy Storage,” *Fuel Cell*, pp. 1–9, 2009.

[14] P. Pisu and G. Rizzoni, “Strategies for Hybrid Electric Vehicles,” *Control*, vol. 15, no. 3, pp. 506–518, 2007.

[15] L. Sundström, O. and Guzzella, “A Generic Dynamic Programming Matlab Function,” in *Proceedings of the 18th IEEE International Conference on Control Applications*, p. pages 1625–1630.

[16] Supercapacitor image is adopted from http://allthingsembedded.com/?p=177

[17] Battery image is adopted from http://www.a123systems.com/

[18] http://www.chargecar.org/

5 CONCLUSIONS AND CONTRIBUTIONS

The work presented in this thesis aims to accomplish several interrelated novel contributions by considering the design, control, economics of plug-in hybrid electric vehicle powertrains *simultaneously* in an optimization setting for a real world driving pattern with the average NHTS distance. Bounds for the impact of predictive control on battery downsizing and lifetime cost is shown using a dynamic programming approach. Comparisons of alternative powertrains under different driving patterns from the point of life cycle benefits reveal useful information for policy makers. Influence of supercapacitor-battery integration on the battery stress is demonstrated. Research contributions can be categorized as follows:

5.1 Methodological contributions:

- Development of a robust co-design framework for multi-source energy systems where the energy demand significantly varies. Mathematical formulation is done specifically for the co-design of plug-in hybrid electric vehicle powertrains. Framework has the capacity to yield robust co-designs if multiple duty cycles are employed.

- Integration of design, control and life cycle economics to the design decision making of vehicles to achieve system optima.

- Development of a methodology for the comparison of advanced vehicle powertrains with comparable vehicle and performance metrics from the aspects of life cycle cost and emissions accounting for the variation in driving patterns.

- Development of a matlab based framework to investigate the effects of different control algorithms for supercapacitor-battery electric vehicles.

- Using the proposed co-design framework, impact of different control strategies on system design and various objectives can be investigated.

5.2 Applicative contributions:

- Potential for component downsizing via better control strategy is revealed: For a parallel PHEV powertrain, battery size might get reduced up to 5% for a static drive cycle which corresponds to $200/vehicle using a battery price of $550/kWh.

- Global control optimization of supercapacitor-battery systems has been done and 63% reduction in current squared losses is achieved by employing a 50 Wh supercapacitor.

- Optimal robust co-design of a parallel PHEV powertrain to minimize lifetime cost is determined for a distribution of real world driving patterns. Optimal robust co-design has a 6.8 kWh battery, 80kW motor and 50kW engine where the engine is bounded by torque constraint.

- Hybrid vehicles are found to be competitive on cost and emissions under all driving patterns, providing emissions-reduction at lower cost than plug-in vehicles.

- Policy designed based on standard EPA drive cycles might be misleading. Benefits of plug-ins depend on the driving conditions.

- City driving conditions with frequent stops can double life cycle emissions of conventional vehicles, increase cost up to 20% and reduce the all-electric range of plug-in vehicles by up to 45% compared to standard EPA test cycles.

- Under the urban NYC driving cycle, hybrid and plug-in vehicles can cut life cycle emissions by half and reduce costs up to 20% relative to conventional vehicles. In contrast, under highway conditions electrified vehicles have similar emissions to conventional vehicles (CVs) with up to 70% higher costs.

- Source of grid electricity might make electrified vehicles more beneficial at reducing GHG emissions compared to conventional vehicles even for highway conditions where for the base grid mix, HEVs offer comparable benefits.

- Driver heterogeneity matters, and efforts to encourage adoption of hybrid and plug-in vehicles will have greater impact if targeted to urban drivers vs. highway drivers.

6 APPENDIX

Mass Breakdown	Units	HEV	PHEV20	PHEV40	PHEV60	BEV100	CV
Vehicle glider/body mass	kg	815	815	815	815	815	815
Powertrain mass	kg	609	754	978	1212	1450	556
Vehicle curb mass	kg	1424	1569	1793	2027	2265	1371
Driver mass	kg	80	80	80	80	80	80
Total mass	kg	1504	1649	1873	2107	2345	1451
Engine							
Max. power	kW	73	73	73	73		110
Engine scale		1	1	1	1		1.5
Block mass	kg	108	108	108	108		166
Radiator mass	kg	6	6	6	6		6
Tank mass	kg	20	20	20	20		20
Fuel mass	kg	43	43	43	43		43
Total mass of engine block	kg	177	177	177	177		234
Motor							
Max. power	kW	60	78	88	98	120	
Motor scale		1.0	1.3	1.5	1.6	2.0	
Motor mass	kg	35	46	51	57	70	
Controller mass	kg	5	7	7	8	10	
Total mass of motor block	kg	40	52	59	65	80	
Motor 2							
Max. power	kW	30	30	30	30		
Motor mass	kg	20	20	20	20		
Controller mass	kg	5	5	5	5		
Total mass of motor 2	kg	25	25	25	25		
Battery							
Technology		NiMH	li-ion	li-ion	li-ion	li-ion	
Parallel cell array		1	5	10	14	25	
Number of cells in series		168	92	92	100	100	
Total # cells		168	460	920	1400	2500	
Cell capacity	Ah	7	6	6	6	6	
Nominal output voltage	V	1.2	3.6	3.6	3.6	3.6	
Output voltage	V	202	331	331	360	360	
Energy capacity	kWh	1.3	9.9	19.9	30.2	54.0	
Packaging factor		1.3	1.3	1.3	1.3	1.3	
SOC min	%	30	30	30	30	30	
SOC max	%	90	90	90	90	90	
SOC init	%	60	90/30	90/30	90/30	90/30	
SOC target	%	60	30	30	30	30	
Battery swing	%		0.6	0.6	0.6	0.6	
Mass of each cell	kg	0.4	0.4	0.4	0.4	0.4	
Total mass of battery block	kg	84	217	435	662	1182	22
Other Components							
Electrical accessories	kg	18	18	18	18	18	18
Exhaust mass	kg	30	30	30	30		30
Planetary gear mass/gear mass	kg	40	40	40	40		75
Mechanical accessories	kg	35	35	35	35		0
Wheel mass	kg	140	140	140	140	140	140
Final drive mass	kg	20	20	20	20	20	20
Torque coupling	kg					10	10
Alternator and controller	kg						7

Table A1: Vehicle component specifications

	Acceleration Time (sec)	
CV		10.2
HEV		10.3
PHEV20	CD mode	10.2
	CS mode	9.3
PHEV40	CD mode	10.1
	CS mode	8.1
PHEV60	CD mode	10.1
	CS mode	8.3
BEV100	CD mode	10.1

Table A2: Performance of vehicles

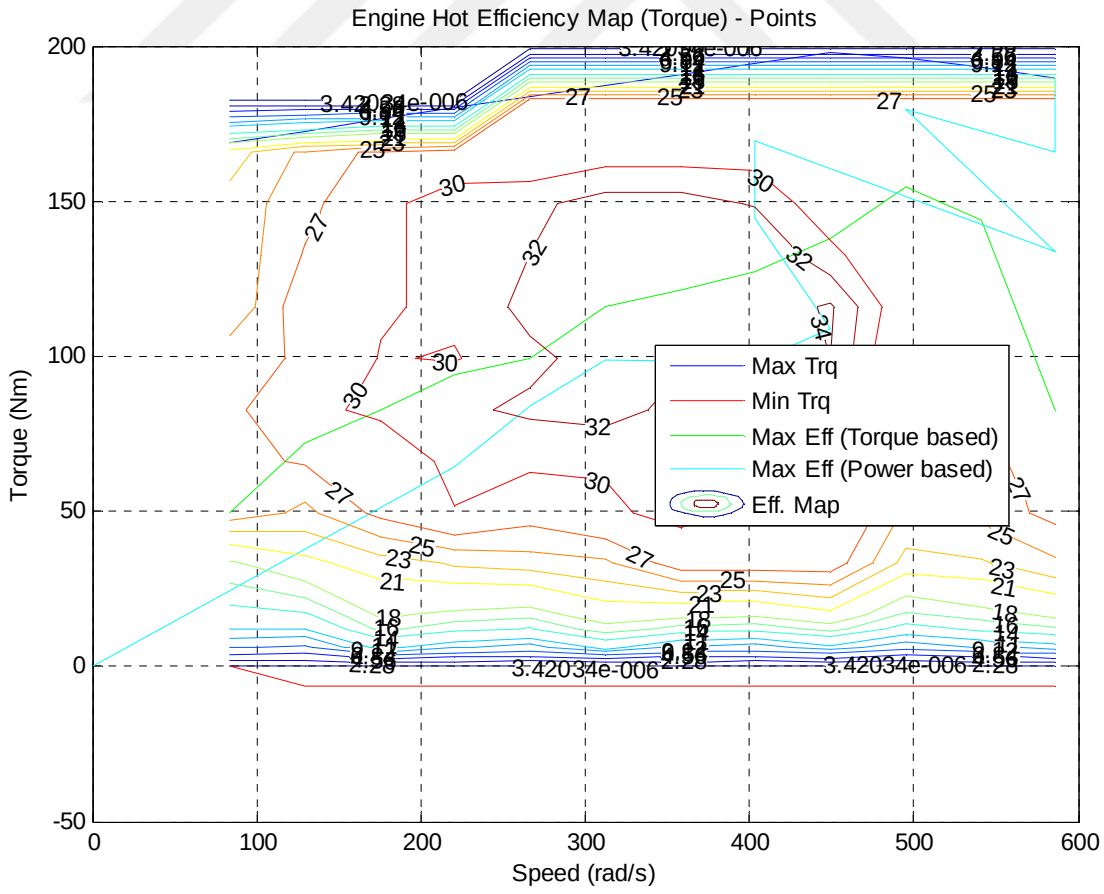

Figure A1: Engine efficiency map of CV (%) [32]

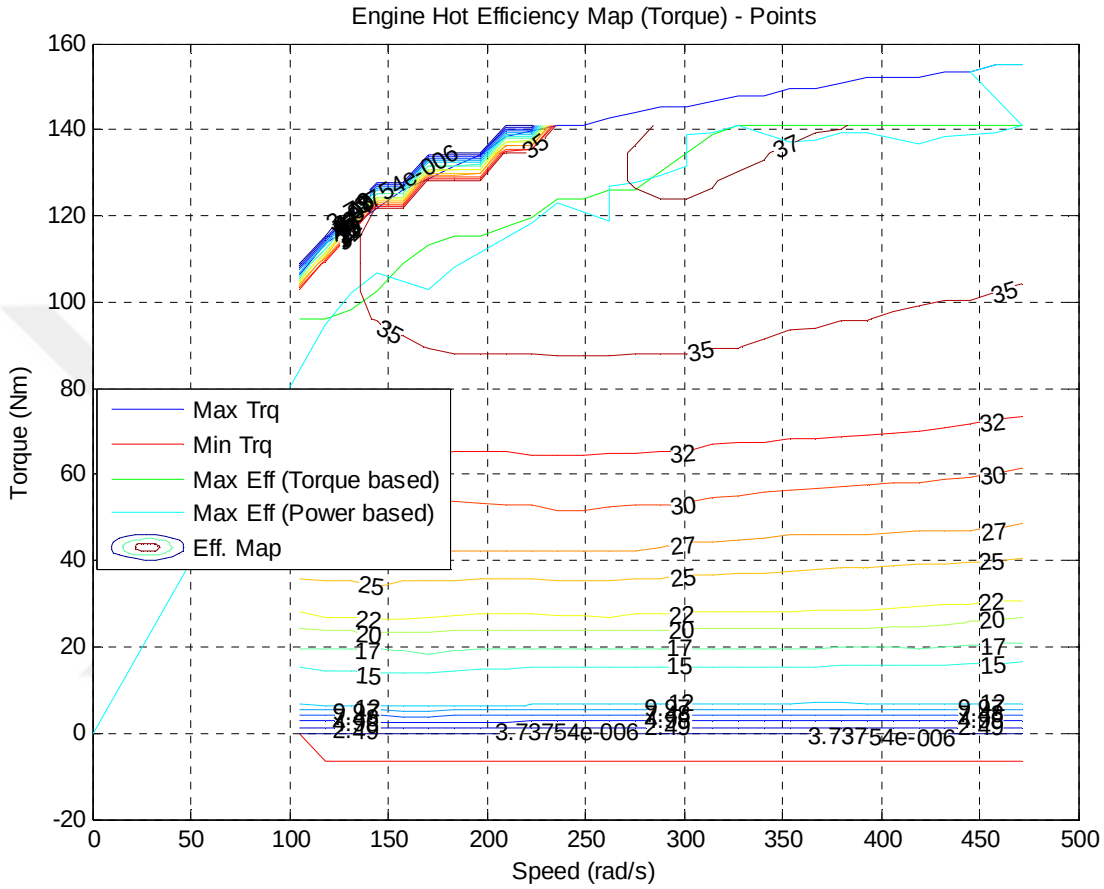

Figure A2: Engine efficiency map of HEV (%) [32]

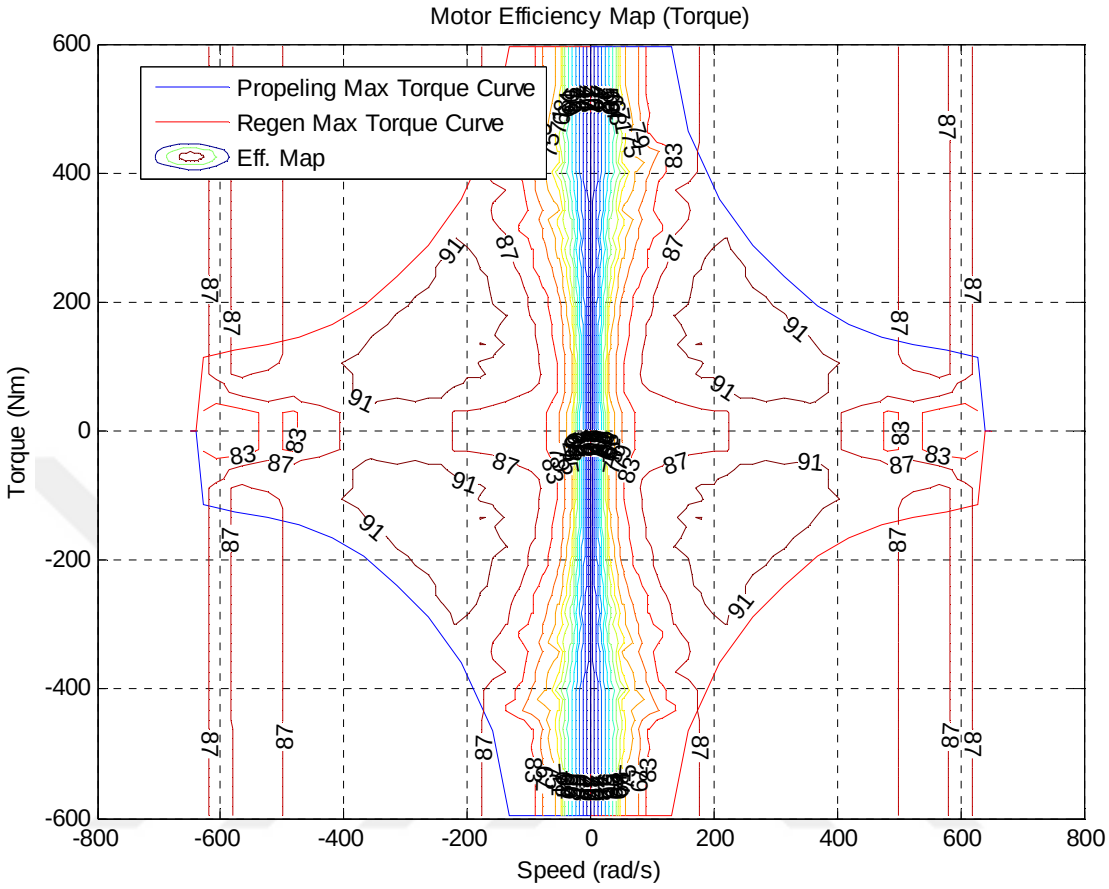

Figure A3: Motor efficiency map of HEV and PHEVs (%) [32]

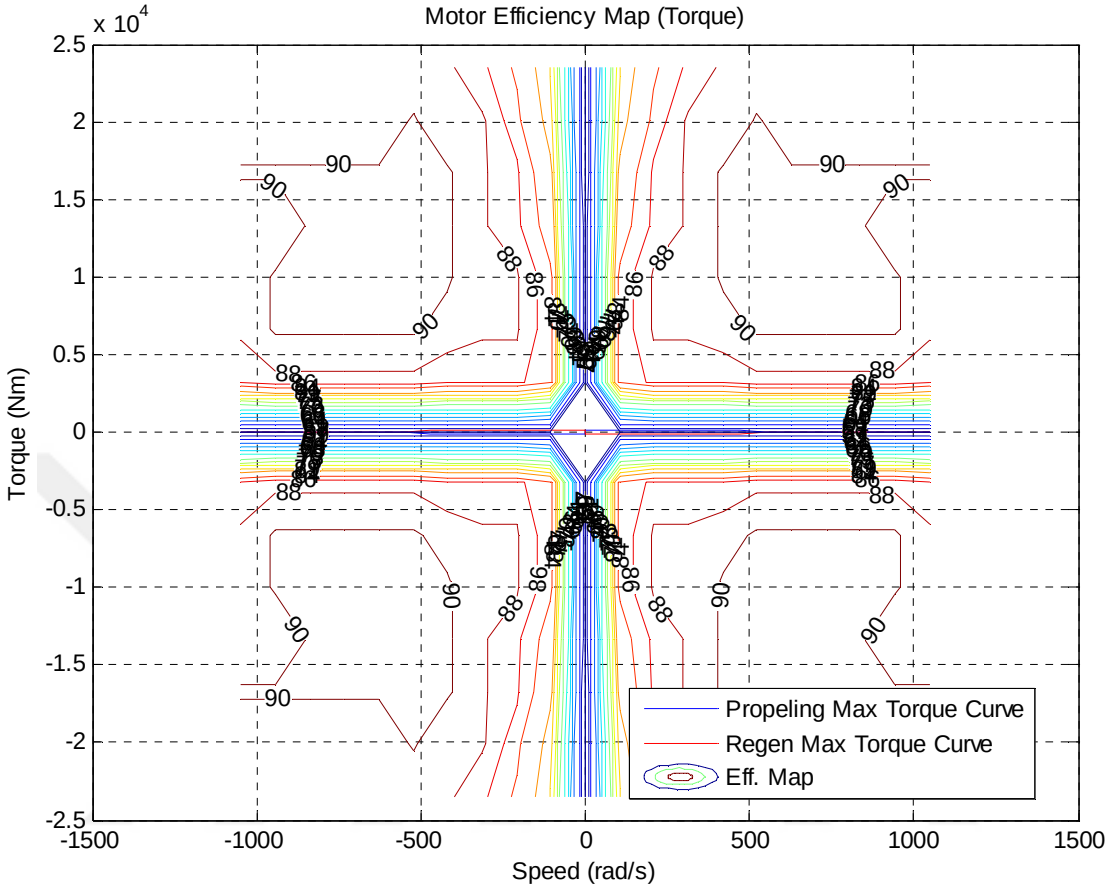

Figure A4: Motor 2 (generator) efficiency map of HEV and PHEVs (%)

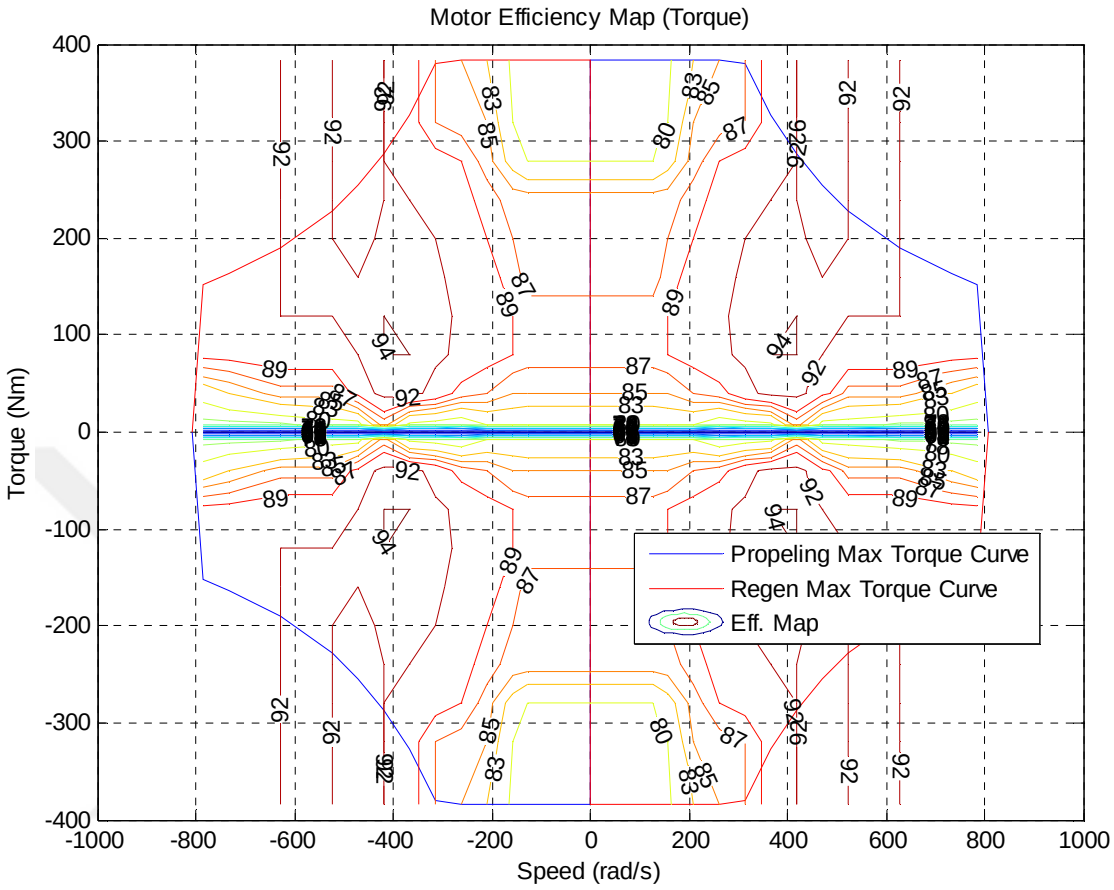

Figure A5: Motor efficiency map of BEV (%) [32]